Universidade do Minho
Escola de Engenharia

Temitayo Afolabi

Durability assessment and prediction using artificial intelligence of relatively thick FRP composites under water immersion

FRP++
Advanced structural analysis and design using composite materials

Funded by the European Union

September 2026

Durability assessment and prediction using artificial intelligence of relatively thick FRP composites under water immersion

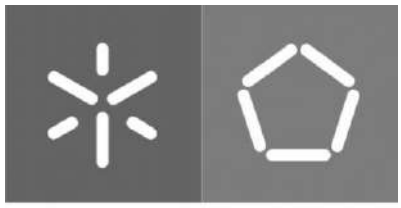
Temitayo Afolabi

FRP++

UMinho | 2026

The European Master in Advanced Structural Analysis and Design using Composite Materials is a join initiative of:

Universidade do Minho · Universitat de Girona · University of Naples Federico II · INSA Institut National des Sciences Appliquées Toulouse · Université de Toulouse



Universidade do Minho
Escola de Engenharia

Temitayo Afolabi

Durability assessment and prediction using artificial intelligence of relatively thick FRP composites under water immersion



FRP++
Advanced structural analysis and design using composite materials

Master Dissertation
European Master Advanced Structural Analysis and Design using Composite Materials

Work developed under the supervision of
Doctor Amirhossein Mohammadi
Professor Doctor José Sena Cruz
September 2026



Funded by
the European Union

DIREITOS DE AUTOR E CONDIÇÕES DE UTILIZAÇÃO DO TRABALHO POR TERCEIROS

Este é um trabalho académico que pode ser utilizado por terceiros desde que respeitadas as regras e boas práticas internacionalmente aceites, no que concerne aos direitos de autor e direitos conexos.

Assim, o presente trabalho pode ser utilizado nos termos previstos na licença abaixo indicada.

Caso o utilizador necessite de permissão para poder fazer um uso do trabalho em condições não previstas no licenciamento indicado, deverá contactar o autor, através do RepositóriUM da Universidade do Minho.

Licença concedida aos utilizadores deste trabalho



Atribuição CC BY

https://creativecommons.org/licenses/by/4.0/

ACKNOWLEDGEMENTS

I would like to express my sincere gratitude to my supervisors, Doctor Amirhossein Mohammadi and Professor Doctor José Sena Cruz, for their invaluable guidance, encouragement, constructive feedback, and continuous support throughout the development of this dissertation. Their expertise and dedication contributed significantly to the successful completion of this work.

I am also grateful to the academic and technical staff of the University of Minho for their assistance during the experimental programme and laboratory testing. My sincere appreciation also goes to the University of Naples Federico II, Italy, where I completed the coursework component of the Erasmus Mundus FRP++ programme. I am thankful to the lecturers and staff for the knowledge, training, and academic support provided during this stage of my studies.

I would also like to thank the coordinators, lecturers, and colleagues of the Erasmus Mundus FRP++ programme for their support and for the valuable knowledge and experiences shared throughout the programme. Finally, I am deeply grateful to my family and friends for their continuous encouragement, patience, and support during my studies.

I would like to gratefully acknowledge the financial support provided by the European Union for participation in the Erasmus Mundus FRP++ European Master Course in Advanced Structural Analysis and Design using Composite Materials (Project no. 101048961).

This work was supported by the R&D Project "CirWind—Development of innovative sustainable urban furniture and equipment in composites from waste produced by the wind energy industry for circularity", project no. 15232, operation code COMPETE2030-FEDER-00889600, cofounded by Innovation and Digital Transition Program (COMPETE 2030), by the Portugal 2030 and by the European Union, in its FEDER component. This work was also supported by FCT/MCTES under the R&D Unit Institute for Sustainability and Innovation in Structural Engineering (ISISE) under the references UID/4029/2025 (DOI: 10.54499/UID/04029/2025), UID/PRR/04029/2025 (DOI: 10.54499/UID/PRR/04029/2025) and UID/PRR2/04029/2025 (DOI: 10.54499/UID/PRR2/04029/2025), and under the Associate Laboratory Advanced Production and Intelligent Systems ARISE under reference LA/P/0112/2020 (DOI: 10.54499/LA/P/0112/2020).

STATEMENT OF INTEGRITY

I hereby declare having conducted this academic work with integrity. I confirm that I have not used plagiarism or any form of undue use of information or falsification of results along the process leading to its elaboration.

I further declare that I have fully acknowledged the Code of Ethics and Conduct of the University of Minho.

DECLARATION ON THE USE OF ARTIFICIAL INTELLIGENCE (AI) TOOLS

I hereby declare having acted on this academic work with integrity and confirm that I have not resorted to any form of undue use of AI tools, nor to the falsification or omission of information, sources, data, results or processes in any of the stages leading to its elaboration.

I further declare that any use of AI tools was done in a transparent and responsible manner, being duly noted in the work, and that I critically verified the accuracy of the content produced with their support, assuming full responsibility for what I submit.

I further declare that I have fully acknowledged the Code of Ethics and Conduct of the University of Minho, as well as the applicable standards of academic integrity and data protection.

Avaliação da Durabilidade e Previsão através de Inteligência Artificial de Compósitos de FRP Relativamente Espessos sob Imersão em Água

RESUMO

Os compósitos de polímero reforçado com fibras (FRP) são amplamente utilizados na engenharia civil devido à sua elevada relação resistência-peso, resistência à corrosão e durabilidade. No entanto, a exposição prolongada à humidade e a temperaturas elevadas pode reduzir o seu desempenho mecânico. Esta dissertação investiga a durabilidade de compósitos pultrudidos relativamente espessos de polímero reforçado com fibra de vidro (GFRP), fabricados com resinas de poliéster insaturado (P-UP) e vinil éster (P-VE), sujeitos à imersão em água e ao envelhecimento higrotérmico acelerado. Foram realizados ensaios de tração, compressão, flexão, corte no plano e corte interlaminar, sendo a retenção das propriedades avaliada relativamente a provetes de referência não envelhecidos.

Os resultados experimentais mostraram uma degradação dependente do tipo de resina, condição de exposição, temperatura, duração e propriedade mecânica. De forma geral, os provetes de P-VE apresentaram melhor durabilidade do que os de P-UP sob exposição prolongada à água.

Para a modelação preditiva, a análise foi limitada à resistência à tração devido à maior consistência dos dados disponíveis. Foi desenvolvida uma rede neuronal bayesiana informada pela física, incorporando uma relação de degradação de Arrhenius–Weibull, e avaliada através de validação leave-one-temperature-out, obtendo um RMSE médio de 9,58 pontos percentuais e um MAE de 7,80 pontos percentuais. A abordagem permitiu quantificar a incerteza e impor restrições físicas, apresentando desempenho comparável ao modelo determinístico de Arrhenius–Weibull. As previsões a longo prazo foram consideradas extrapolações baseadas no modelo, evidenciando o potencial desta abordagem para avaliação da durabilidade de compósitos GFRP, embora sejam necessárias condições de exposição adicionais e validação experimental prolongada.

PALAVRAS-CHAVE: Compósitos GFRP; Durabilidade a longo prazo; Envelhecimento higrotérmico; Imersão em água; Modelação de Arrhenius; Retenção da resistência à tração.

Durability Assessment and Prediction Using Artificial Intelligence of Relatively Thick FRP Composites under Water Immersion

ABSTRACT

Fibre-reinforced polymer (FRP) composites are widely used in civil engineering because of their high strength-to-weight ratio, corrosion resistance, and durability. However, prolonged exposure to moisture and elevated temperatures can reduce their mechanical performance.

This dissertation investigates the durability of relatively thick pultruded glass fibre-reinforced polymer (GFRP) composites manufactured with unsaturated polyester (P-UP) and vinyl ester (P-VE) resins under water immersion and accelerated hygrothermal ageing. Tensile, compression, flexural, in-plane shear, and interlaminar shear tests were conducted, and property retention was evaluated relative to unaged reference specimens.

The experimental results showed degradation that depended on resin type, conditioning state, temperature, duration, and mechanical property. P-VE generally showed better durability than P-UP under prolonged water exposure.

For predictive modelling, the analysis was limited to tensile strength due to its more complete and consistent dataset. A Bayesian physics-informed neural network incorporating an Arrhenius–Weibull degradation relationship was developed to predict tensile-strength retention under environmental ageing. The model was evaluated using leave-one-temperature-out validation, achieving a mean fold RMSE of 9.58 percentage points and MAE of 7.80 percentage points. The Bayesian approach provided uncertainty quantification and physical consistency while achieving comparable predictive performance to a deterministic Arrhenius–Weibull model.

Long-term tensile-strength retention was further investigated, but the predictions beyond the experimental duration were considered model-based extrapolations rather than validated service-life predictions. The study highlights the influence of hygrothermal ageing on thick pultruded GFRP composites and demonstrates the potential of physics-informed Bayesian modelling for durability assessment, while emphasising the need for additional independent exposure conditions and longer-term validation.

KEYWORDS: GFRP composites; Long-term durability; Hygrothermal ageing; Water immersion; Bayesian physics-informed neural network; Tensile-strength retention.

Table of Contents

Acknowledgements iii
Resumo v
Abstract vi
List of Figures x
List of Tables xiii
List of Abbreviations and Symbols xv
1. Introduction 1
1.1. Context and Motivation 1
1.2. Research Objectives 2
1.3. Research Methodology 2
1.4. Structure of Dissertation 3
2. Literature Review 5
2.1. Introduction to FRP Composites 5
2.2. Durability of FRP Composites 6
2.2.1. Effect of temperature on FRP composites 6
2.2.2. Effect of moisture on FRP composites 7
2.2.3. Effect of chemicals on FRP composites 8
2.2.4. Effect of UV radiation on FRP composites 9
2.3. Role of Artificial Intelligence in Durability Prediction 10
2.4. Conventional Machine Learning Models 10
2.5. Physics-Informed Machine Learning for Durability Prediction 11
2.6. CEN/TS 19101:2022 – Overview and How Durability is Addressed 13
2.7. Summary and Research Gaps 15
3. Experimental Characterization of Unaged and Aged GFRP Composites 17
3.1. DURABLE-FRP Project 17
3.2. Materials 19
3.3. Experimental Campaign 20
3.4. Mechanical Characterization Tests 22
3.4.1. Testing equipment 22

3.4.2. Tensile test at 0° and 90° 24
3.4.3. In-plane shear test 26
3.4.4. Uniaxial compression test 29
3.4.5. Flexural test 31
3.4.6. Interlaminar shear test 32
3.5. Results and Analysis 33
3.5.1. Uniaxial tension with fibres oriented at 0° 34
3.5.2. Uniaxial tension with fibres oriented at 90° 37
3.5.3. In-plane shear tests 40
3.5.4. Uniaxial compression 44
3.5.5. Flexural tests 47
3.5.6. Interlaminar shear test (short beam) 50
4. Physics-Informed Neural Network Study 55
4.1. Introduction and Modelling Rationale 55
4.2. Dataset 56
4.2.1. Composition and response variable 56
4.2.2. Reference populations 57
4.2.3. Exposure settings and replicate balancing 58
4.3. Methodology 59
4.3.1. Overview 59
4.3.2. Bayesian neural network and variational inference 60
4.3.3. Governing degradation relation 60
4.3.4. Hard constraints 61
4.3.5. Training objective 62
4.3.6. Predictive quantities 63
4.3.7. Model configuration 64
4.3.8. Deterministic reference model 65
4.4. Ensemble Fitting Strategy 65
4.5. Training Behaviour 66
4.6. Inferred Physical Parameters 66

4.7. Physics-Constraint Audit 68
4.8. In-Sample Posterior Diagnostics 69
4.9. Posterior Degradation Curves 71
4.10. Predictive Validation 72
4.10.1. Validation protocol and metrics 72
4.10.2. Held-out results 73
4.10.3. 333.15 K fold 74
4.10.4. Interpretation of negative R^2 75
4.11. Uncertainty Calibration and Reproducibility 75
4.11.1. Interval calibration 76
4.11.2. Reproducibility across random seeds 77
4.12. Comparison with the Deterministic Reference Model 79
4.13. Long-Term Retention Projection 81
4.14. Limitations 83
4.15. Summary 84
5. Conclusions and Future Development 85
5.1. Conclusions 85
5.2. Future Developments 87

LIST OF FIGURES

Figure 3.1: Materials and conditioning facilities used in the experimental programme. 18
Figure 3.2: Specimen extraction layout for mechanical characterisation and DMA testing of the pultruded GFRP plate. 19
Figure 3.3: CNC BETA MINI 6010 cutting machine and use of UCCNC software. 22
Figure 3.4: Test equipment used in the experimental programme. 23
Figure 3.5: Type 2 geometry of the specimen used for uniaxial tensile tests with fibres oriented at 0° and 90° (adapted from 'EN ISO 527-4', 1997). 24
Figure 3.6: Type 1b geometry of the specimen used for uniaxial tensile tests 25
Figure 3.7: Reference lines marked on specimens for precise strain measurement in the gauge section. 25
Figure 3.8: Specimen preparation and tensile test setup. 26
Figure 3.9: Geometry of the specimen used for in-plane shear tests 27
Figure 3.10: In-plane shear test setup (adapted from 'ASTM D5379', 2005). 27
Figure 3.11: In-plane shear strain measurement. 28
Figure 3.12: In-plane shear test. 28
Figure 3.13: Specimen geometry used for compression tests (adapted from 'EN ISO 14126', 1999). 29
Figure 3.14: Compression strain measurement procedure. 30
Figure 3.15: Compression test setups. 30
Figure 3.16: Setup used in the flexural tests and geometry of the corresponding specimen 31
Figure 3.17: Flexural test preparation and setup. 32
Figure 3.18: Configuration used for the interlaminar shear tests and geometry of the respective specimen (adapted from 'EN ISO 14130', 1997). 32
Figure 3.19: Interlaminar shear test preparation and setup. 33
Figure 3.20: Average tensile stress–strain curves of pultruded GFRP specimens in the 0° direction under different conditioning states. 35
Figure 3.21: Normalised retention of the 0° tensile properties of P-UP and P-VE specimens under different conditioning states. n.a = not available 36
Figure 3.22: Failure modes observed during tensile tests (adapted from ASTM D3039/D3039M:2002). 37

Figure 3.23: Average tensile stress–strain curves of pultruded GFRP specimens in the 90° direction under different conditioning states. 39
Figure 3.24: Normalised retention of the 90° tensile properties of P-UP and P-VE specimens under different conditioning states. n.a = not available 40
Figure 3.25: Average in-plane shear stress–strain curves of pultruded GFRP specimens under different conditioning states. 42
Figure 3.26: Normalised retention of the in-plane shear properties of P-UP and P-VE specimens under different conditioning states. 43
Figure 3.27: V-Notched Beam Shear Test Failure Codes and Typical Modes (adapted from ASTM D5379/D5379M-12). 44
Figure 3.28: Average compressive stress–displacement curves of the pultruded GFRP specimens under different conditioning states. 46
Figure 3.29: Normalised compressive strength retention of P-UP and P-VE specimens under dry and wet conditioning states relative to their respective reference series. 46
Figure 3.30: Failure modes observed during uniaxial compression tests (adapted from EN ISO 14126:2000). 47
Figure 3.31: Average flexural stress–displacement curves of the pultruded GFRP specimens under different conditioning states: (a) P-UP specimens and (b) P-VE specimens. 48
Figure 3.32: Normalised flexural strength retention of P-UP and P-VE specimens under dry and wet conditioning states relative to their respective reference series. 49
Figure 3.33: Failure modes observed during flexural tests (adapted from EN ISO 14125:1998). 49
Figure 3.34: Average interlaminar shear stress–displacement curves of the pultruded GFRP specimens under different conditioning states. 51
Figure 3.35: Normalised interlaminar shear strength retention of P-UP and P-VE specimens under dry and wet conditioning states relative to their respective reference series. 52
Figure 3.36: Classification of failure modes observed during interlaminar shear testing (adapted from ASTM D2344/D2344M). 53
Figure 4.1: Schematic representation of the variational Bayesian physics-informed neural network (BPINN), showing the neural network prediction pathway, embedded Arrhenius–Weibull degradation relation, imposed physical constraints and combined training objective. 59
Figure 4.2: Evolution of the training objective: (a) data negative log-likelihood, (b) physics-residual negative log-likelihood on a logarithmic axis, and (c) the learned coupon scatter. 66

Figure 4.3: Posterior physical parameters with 90% credible intervals: (a) degradation rate q by cell, (b) shape exponent p by cell, and (c) the global apparent activation energy, comparing the ensemble-pooled posterior with a single variational fit. 68
Figure 4.4: In-sample agreement between predicted and observed group-mean retention, with 90% group-mean credible intervals, coloured by exposure temperature. 70
Figure 4.5: Residual diagnostics: (a) residual against predicted retention, (b) residual against exposure duration, and (c) residual distribution by exposure temperature. Positive residuals indicate that the model under-predicts retention. 70
Figure 4.6: Posterior tensile-strength retention curves with 90% credible bands for all eight material-condition cells at the three exposure temperatures. Filled markers are measured group means. 72
Figure 4.7: Leave-one-temperature-out validation: (a) held-temperature error against a constant-mean baseline, (b) single variational fit compared with the ensemble, and (c) empirical coverage of the nominal 90% intervals. 74
Figure 4.8: Calibration curve: empirical coverage against nominal interval level for a single variational fit and for the pooled ensemble. Points below the diagonal indicate over-confident intervals. 76
Figure 4.9: Whole-temperature-out predictive error of the deterministic reference model and the Bayesian physics-informed neural network: (a) pooled across folds and (b) by held-out temperature. 80
Figure 4.10: Fifty-year tensile-strength retention projection for PUP, 0°, Wet conditioning at 293.15 K (20 °C), on (a) linear and (b) logarithmic time axes. The dashed line marks the last measurement available for this condition. 82

LIST OF TABLES

Table 3.1: Identification and geometry of the specimens used for mechanical and DMA testing..... 20

Table 3.2: Test matrix and number of specimens for each mechanical test..... 21

Table 3.3: Mean results of the 0° uniaxial tensile tests for P-UP and P-VE specimens under different conditioning conditions 34

Table 3.4: Mean results of the 90° uniaxial tensile tests for P-UP and P-VE specimens under reference and conditioned states..... 38

Table 3.5: Mean results of uniaxial in-plane shear tests for P-UP and P-VE specimens under reference and conditioned states..... 41

Table 3.6: Mean results of the uniaxial compression tests for P-UP and P-VE specimens under different conditioning conditions. 45

Table 3.7: Mean results of the three-point flexural tests for P-UP and P-VE specimens under different conditioning conditions. 48

Table 3.8: Mean apparent interlaminar shear strength results from short-beam tests for P-UP and P-VE specimens under different conditioning conditions..... 50

Table 4.1: Composition of the tensile modelling dataset. 57

Table 4.2: Reference tensile-strength statistics by resin and fibre orientation..... 57

Table 4.3: Exposure design by temperature, with the error of a constant-mean predictor for reference. 58

Table 4.4: The three predictive intervals reported by the model. 63

Table 4.5: Model configuration used for all reported results 64

Table 4.6: Parameter counts of the Bayesian model 64

Table 4.7: Posterior degradation-rate and shape parameters by material-condition cell (ensemble-pooled draws)..... 67

Table 4.8: Apparent activation energy: ensemble-pooled posterior versus a single variational fit..... 67

Table 4.9: Numerical audit of the embedded physical constraints..... 68

Table 4.10: In-sample posterior diagnostics (not an unbiased estimate of predictive accuracy) 69

Table 4.11: In-sample residuals by exposure temperature (observed minus predicted retention). 71

Table 4.12: Leave-one-temperature-out validation results (ensemble). The baseline predicts the mean retention of the training folds. 73

Table 4.13: Interval calibration on in-sample group means. 76

Table 4.14: Effect of the initial posterior spread and training length on held-out accuracy and interval calibration (nominal level 0.90 throughout). 77
Table 4.15: Sensitivity of the complete validation result to the random seed (single variational fits). ... 78
Table 4.16: Reported uncertainty in the apparent activation energy compared with its reproducibility across random seeds. 78
Table 4.17: Comparison of the deterministic reference model and the Bayesian physics-informed neural network. 79
Table 4.18:Projected tensile-strength retention for PUP, 0°, Wet conditioning at 293.15 K (20 °C). ... 81
Table 4.19: Summary of principal results. 84

List of Abbreviations and Symbols

Abbreviations

Abbreviation	Meaning
AI	Artificial Intelligence
ASTM	ASTM International
BPINN	Bayesian Physics-Informed Neural Network
CNC	Computer Numerical Control
CoV	Coefficient of Variation
CSM	Chopped Strand Mat
DIC	Digital Image Correlation
DMA	Dynamic Mechanical Analysis
EN	European Standard
FRP	Fibre-Reinforced Polymer
GFRP	Glass Fibre-Reinforced Polymer
ILSS	Interlaminar Shear Strength
ISO	International Organization for Standardization
LOTO	Leave-One-Temperature-Out
MAE	Mean Absolute Error
ML	Machine Learning
MSE	Mean Squared Error
P-UP	Pultruded Unsaturated Polyester GFRP
P-VE	Pultruded Vinyl Ester GFRP
REF	Reference condition/specimen
RMSE	Root Mean Squared Error
SEM	Scanning Electron Microscopy
UD	Unidirectional

Abbreviation	Meaning
UP	Unsaturated Polyester
VE	Vinyl Ester
W60-24M-D	Water immersion at 60 °C for 24 months followed by drying before testing
W60-24M-W	Water immersion at 60 °C for 24 months, tested in wet condition

Symbols

Symbol	Meaning
$A_f(T)$	Arrhenius acceleration factor at temperature (T)
b	Specimen width
D	Diffusion coefficient
E	Elastic modulus
E_a	Apparent activation energy
E_1	Longitudinal elastic modulus
E_2	Transverse elastic modulus
F	Applied force
f_{cu}	Ultimate compressive strength
f_{tu}	Ultimate tensile strength

Symbol	Meaning
G_s	Shear modulus
h	Specimen thickness
k	Material constant associated with degradation/diffusion
L	Specimen length
L_{data}	Data loss term
$L_{\mathbf{physics}}$	Physics-based loss term
$L_{\mathbf{total}}$	Total loss function
M_t	Moisture absorbed at time (t)
M_∞	Equilibrium moisture absorption
n	Number of observations
P	Applied load
R	Universal gas constant
R^2	Coefficient of determination
T	Absolute exposure temperature
T_g	Glass transition temperature

Symbol	Meaning
$\boldsymbol{T_{\mathrm{ref}}}$	Reference temperature
$\boldsymbol{t}$	Exposure duration
$\boldsymbol{t_s}$	Time-scaling parameter
$\mathbf{w}$	Neural network weight
$\mathbf{x_i}$	Input feature vector for observation
$\boldsymbol{y_i}$	Experimental measured value for observation
$\boldsymbol{\hat{y}_i}$	Predicted value for observation
$\boldsymbol{\bar{y}}$	Mean experimental value
$\boldsymbol{\varepsilon}$	Strain
$\boldsymbol{\varepsilon_{tu}}$	Ultimate tensile strain
$\boldsymbol{\gamma}$	Shear strain
$\boldsymbol{\lambda}$	Weighting coefficient for physics loss
$\boldsymbol{\sigma}$	Normal stress
$\boldsymbol{\sigma_c}$	Compressive stress
$\boldsymbol{\sigma_t}$	Tensile stress

Symbol	Meaning
τ	Shear stress

1. Introduction

1.1. Context and Motivation

The use of Glass Fiber-Reinforced Polymers (GFRP) has gained rapid popularity and adoption in the civil and structural engineering sector. Their unique properties include corrosion resistance, lightweight, and the ability to withstand adverse environmental conditions [1], [2], [3]. These materials have been used in the construction and rehabilitation of civil and marine infrastructure, especially in areas where materials such as steel are susceptible to corrosion and environmental deterioration [4]. Despite their many advantages over traditional materials such as steel, long-term durability under environmental and mechanical stresses remains a major concern for researchers and engineers [3].

Hygrothermal ageing, an important environmental factor responsible for degradation, has been well discussed and documented. Several studies have shown that exposure of pultruded GFRP to moisture can significantly affect its mechanical properties, leading to damage mechanisms such as matrix softening, fibre-matrix interfacial weakening, and delamination [5] [6]. In addition, the type of resin used in the production of pultruded GFRP has been shown to play an important role in GFRP absorption rate and degradation properties [1], [7].

Although extensive high-quality research has investigated the effects of environmental factors on the degradation of FRP composites, assessing their long-term durability remains challenging. Fickian diffusion and Arrhenius physically based approaches formulations are widely used for describing moisture uptake and temperature-dependent degradation processes, respectively [8], [9]. These models can provide meaningful predictions when their underlying assumptions are satisfied. However, for relatively thick FRP composites subjected to prolonged water immersion, the degradation response may involve coupled, non-linear interactions among moisture diffusion, temperature, resin degradation, fibre–matrix interfacial deterioration, and changes in mechanical properties. These interacting mechanisms may not be fully represented by simplified diffusion assumptions or by a single temperature-dependent degradation relationship[6]. This limitation therefore motivates the use of data-driven approaches, including machine learning techniques, to capture more complex relationships among environmental exposure conditions, material characteristics, and degradation behaviour when sufficient experimental data are available

[10] demonstrated the potential of machine learning approaches for predicting the mechanical properties of FRP composites subjected to harsh environmental conditions. These models are particularly useful for

analysing complex, multi-parameter systems and identifying non-linear relationships among material properties, environmental exposure conditions, and degradation behaviour that may be difficult to represent using simplified analytical formulations. This research, therefore, aims to address the limitations in current FRP durability studies by combining experimental characterisation with a physics-informed predictive framework for tensile-strength degradation of relatively thick pultruded GFRP composites subjected to hygrothermal ageing. The study focuses on the development and evaluation of a hierarchical Arrhenius-informed model based on experimental tensile-strength data, considering the effects of resin system, fibre orientation, conditioning state, exposure temperature, and duration. The integration of experimental testing with physics-informed artificial intelligence provides a reliable approach for predicting long-term tensile-strength retention and assessing the degradation behaviour of pultruded GFRP composites under water immersion conditions.

1.2. Research Objectives

This master's dissertation was developed within the context of the DURABLE-FRP and CirWind projects. The former initiated the research, while the latter provided continuity to the investigation. The main aim is to assess the long-term durability of relatively thick pultruded GFRP composites exposed to water and to develop a predictive framework for tensile-strength degradation. The following objectives were established:

1. To assess the effects of hygrothermal ageing on the mechanical properties of relatively thick pultruded GFRP composites through experimental testing of reference and aged specimens.
2. To investigate the influence of resin type on the durability of GFRP composites by comparing unsaturated polyester and vinyl ester resin systems under water exposure.
3. To develop and validate a hierarchical Arrhenius-informed model for predicting tensile-strength degradation using complete leave-one-temperature-out validation.
4. To evaluate the long-term tensile-strength retention behaviour predicted by the developed model and assess the limitations associated with the available experimental dataset.

1.3. Research Methodology

To achieve the research objectives, a comprehensive literature review was conducted on the effects of hygrothermal ageing and long-term performance of FRP composites, with particular attention to durability

assessment and prediction approaches. Subsequently, laboratory tests were conducted to characterise the physical and mechanical properties of the composites under accelerated ageing. The mechanical programme included tensile tests at 0° and 90°, compression, flexural, interlaminar shear, and in-plane shear tests on reference and aged specimens. The resulting experimental data were processed and statistically analysed to evaluate degradation trends and material durability behaviour.

For the predictive analysis, the modelling scope was restricted to tensile strength degradation because this property provided the most complete and internally consistent dataset across resin system, fibre orientation, conditioning state, exposure temperature, and duration. A Bayesian Physics-Informed Neural Network (BPINN) framework incorporating Arrhenius-based temperature dependence was developed and evaluated using complete leave-one-temperature-out validation. Model performance was assessed using the coefficient of determination (R^2), mean absolute error (MAE), and root mean squared error (RMSE).

Following validation, the developed model was used to estimate long-term tensile-strength retention under extended exposure conditions. These projections were considered model-based extrapolations rather than validated service-life predictions, and the limitations associated with the available experimental dataset and exposure conditions were acknowledged.

1.4. Structure of Dissertation

The dissertation is organised into five main chapters. **Chapter 1** provides the general framework of the study, including the research background, objectives, methodology, and dissertation structure.

Chapter 2 presents the literature review on FRP composites and their durability under environmental exposure. It discusses key degradation mechanisms associated with temperature, moisture, chemicals, and ultraviolet radiation, together with approaches for long-term durability assessment and prediction. The chapter also introduces Arrhenius-based modelling, physics-informed machine learning approaches, relevant durability standards, and identifies the main research gaps addressed in this study.

Chapter 3 describes the DURABLE-FRP project on which this dissertation is based. It presents the materials, specimen preparation, conditioning procedures, and experimental test methods. The chapter also reports and discusses the physical and mechanical results obtained from the tensile, flexural, compression, in-plane shear, and interlaminar shear tests.

Chapter 4 presents the physics-informed predictive modelling framework developed for tensile-strength degradation. It describes the preparation of the tensile dataset, development of the Bayesian Physics-Informed Neural Network (BPINN) framework incorporating Arrhenius-based temperature dependence,

complete leave-one-temperature-out validation, long-term tensile-strength retention extrapolation, and the limitations associated with the available experimental data.

Chapter 5 summarises the principal findings of the study, combining the conclusions from the experimental durability assessment and tensile predictive modelling. It also discusses the main limitations of the work and proposes future research directions aimed at expanding the experimental database, improving long-term prediction, and independently validating the developed modelling framework.

2. Literature Review

2.1. Introduction to FRP Composites

Fibre-Reinforced Polymer (FRP) materials in general, and glass-fibre-reinforced polymer (GFRP) pultruded profiles in particular, are being used increasingly in civil engineering applications as an alternative to traditional materials, such as steel, reinforced concrete and timber [11]. This is due to the different benefits they offer, such as high strength-to-weight ratio, low self-weight, electromagnetic transparency, ease of installation, low maintenance, and improved durability in adverse environmental conditions [12]. GFRP composites are primarily composed of reinforcing fibres, a polymer matrix, and a fibre–matrix interface, while fillers and additives may also be incorporated to enhance specific properties. The reinforcing fibres primarily provide stiffness and strength to the composite due to their relatively high elastic modulus, while the polymer matrix binds the fibres together, transfers and distributes stresses between them, and protects them from mechanical and environmental damage [13]. The polymer matrices used in FRP composites may be classified as either thermosetting or thermoplastic. Common thermosetting matrices used in structural composite applications include vinyl ester, epoxy, and polyester resins. These materials form cross-linked polymer networks during curing and once fully cured, do not melt or soften upon reheating in the same manner as thermoplastics. Thermosetting resins are generally produced through polymerisation reactions that create a three-dimensional cross-linked molecular structure [14].

In many civil engineering applications, the composite processing method is pultrusion since it is cost-efficient in producing continuous lengths of constant cross-section shapes, having fibre volume fractions of 40–60% [15]. Pultrusion is a continuous manufacturing process that offers a systematic method for creating high-strength and lightweight materials with consistent cross-sectional shapes, making it particularly suitable for producing structural components [16].

The favourable properties of pultruded GFRP composites have enabled their application in a wide range of civil engineering structures. Typical applications include handrails, gratings, bridge decks, pedestrian bridges, buildings, pipelines, storage tanks, and chemical-resistant equipment operating in aggressive environments [11], [15], [17]. Their low weight further facilitates transportation and installation, providing additional economic benefits during construction.

Despite the numerous advantages of FRP materials compared to traditional construction materials like steel and concrete, their long-term durability continues to be a subject of ongoing research in the scientific community. This section examines the primary factors influencing the durability of FRP composites, namely the impacts of temperature, moisture, chemical agents, and ultraviolet (UV) radiation.

2.2. Durability of FRP Composites

During their service life, FRP materials may be exposed to a range of environmental conditions arising from natural or artificial sources. These include variations in temperature and humidity, energetic radiation such as ultraviolet (UV) radiation from sunlight or artificial sources, and chemical agents such as liquids contained in storage tanks and pipes, as well as atmospheric oxygen and ozone [14]. In addition, ageing mechanisms such as microcracking, fibre–matrix debonding, creep, fatigue, and fibre deterioration may contribute to the gradual degradation of material properties [18]. Environmental actions may occur individually or in combination, and their effects can accumulate over time depending on the exposure conditions and material characteristics. In many cases, environmental degradation develops gradually over extended periods before significant changes in material performance become apparent[19]. In this dissertation, particular attention is given to the effects of temperature and moisture exposure on the durability of FRP composites. The following sections therefore discuss the principal considerations associated with these environmental degradation mechanisms.

2.2.1. Effect of temperature on FRP composites

One of the main concerns regarding the use of fibre-reinforced polymer (FRP) materials in civil engineering structures is the potential reduction in their stiffness and strength when exposed to elevated temperatures [17]. In the natural environment, FRP materials may be subjected to temperatures ranging from −30°C to 60°C, depending on the geographical region, climatic season, and time of day [19]. As temperature increases, particularly near the glass transition temperature (Tg) of the polymer matrix, the stiffness and mechanical strength of the FRP composite decrease significantly. According to [20] the glass transition temperature (Tg) of a polymer resin is the temperature at which an amorphous polymer moves from a hard or glassy state to a softer, often rubbery, or viscous or sticky state.

Several factors, such as the type of resin used, particularly its Tg, the type and arrangement of fibres, and the manufacturing process, determine the extent of this reduction in load-bearing capacity [17].

Temperature is also responsible for the development of residual stresses within FRP laminates. One of the well-known deleterious effects results from thermal cycling. Prolonged exposure to sunlight increases the material temperature [14]. Thermal cycling can weaken the bond between the reinforcing fibres and the polymer matrix due to differences in their coefficients of thermal expansion (CTE). E-glass fibres exhibit a coefficient of thermal expansion of approximately 5×10^{-6} K^{-1}, whereas unsaturated polyester and vinyl ester resins exhibit significantly higher values of 30–200 $\times$ 10^{-6} K^{-1} and 30–50 $\times$ 10^{-6} K^{-1}, respectively. This mismatch can generate internal stresses during repeated heating and cooling cycles, potentially leading to interfacial degradation [21]. Additionally, freeze–thaw cycles in the presence of salts may further accelerate degradation through moisture ingress and associated physical and interfacial damage. At moderately elevated temperatures, the mechanical response of GFRP composites is generally more strongly influenced by the polymer matrix and fibre–matrix interface than by significant degradation of the glass fibres themselves. As the temperature increases towards the glass transition temperature (Tg) of the polymer matrix, matrix softening and reduced stress-transfer efficiency may lead to deterioration in the mechanical properties of the composite [22], [23].

2.2.2. Effect of moisture on FRP composites

Moisture and humidity can significantly influence the physical and mechanical behaviour of FRP composites. Moisture absorption may induce changes in the polymer matrix and fibre–matrix interface, contributing to swelling, interfacial deterioration and debonding. These changes can reduce the efficiency of stress transfer between the fibres and matrix and consequently lead to reductions in stiffness and strength. When moisture exposure is combined with elevated temperature, the resulting hygrothermal ageing may further accelerate degradation and adversely affect the long-term durability of FRP composites [18].

Plasticization in FRP composites is a reversible physical degradation caused by moisture absorption into the polymer matrix, which increases polymer chain mobility and reduces matrix stiffness. It lowers the glass transition temperature (Tg), alters viscoelastic behaviour, and can temporarily affect mechanical performance by promoting stress relaxation, particularly in hydrophilic resins such as bio-epoxy [24].
Moisture absorption of the matrix results in swelling of the composite. Since swelling of the composite lamina is restrained in the fibre direction, significant residual stresses are induced in the multidirectional laminate by moisture absorption [25].

Recent research on moisture-induced chemical degradation of FRP composites shows that hydrolytic reactions, molecular chain scission, interfacial weakening, and leaching of low-molecular-weight species are key irreversible mechanisms. Long-term hygrothermal exposure drives hydrolysis of polymer chains, producing hydroxyl and other hydrophilic groups that reduce molecular weight and embrittle the matrix, which in turn diminishes mechanical properties such as tensile strength and interlaminar shear strength [26], [27]. In addition to hydrolysis, moisture-driven interfacial debonding reduces stress transfer efficiency between fibre and matrix, further degrading composite performance [26], [27]. Complementary evidence from recent studies also shows that leaching of low-molecular-weight polymer species and ions (e.g., from glass fibres) into the surrounding medium occurs during moisture uptake, contributing to permanent mass loss and matrix weakening [28]. Collectively, these chemical degradation processes are significant contributors to the long-term durability decline of FRP composites in humid and hygrothermal environments.

In summary, moisture exposure induces a combination of reversible physical changes, such as plasticization and swelling, and irreversible chemical degradations, including hydrolysis, interfacial debonding, and leaching of low-molecular-weight species. These mechanisms collectively compromise the mechanical integrity of FRP composites by reducing stiffness, strength, and load-transfer efficiency, highlighting the critical role of moisture management in ensuring long-term durability in humid and hygrothermal environments.

2.2.3. Effect of chemicals on FRP composites

The chemical durability of the polymer matrix depends strongly on the resin type. Unsaturated polyester (UP) resins generally exhibit good resistance to acidic environments, although their performance varies with resin formulation; isophthalic polyester resins typically provide better chemical resistance than orthophthalic grades [29], [30].

Vinyl ester (VE) resins generally offer improved resistance to moisture, organic solvents, and alkaline environments compared with conventional polyester systems and have shown that unsaturated polyester (UP) resins show better acid resistance, with isophthalic variants showing superior performance compared to Orthophthalic ones, and they can be adopted for moderate alkaline resistance [31], [32]. Vinyl ester (VE) resins combine the properties of epoxy and polyester systems to offer excellent resistance to water, organic solvents, and alkaline solutions [29], [33], [34]. In the study reported in [35], epoxy- and vinyl-ester-based GFRP bars exhibited better retention of flexural and interlaminar shear properties than polyester-based bars. After 5000 h of exposure at 60 °C, the reported reductions in flexural strength

were approximately 25% for polyester, 17% for vinyl ester and 23% for epoxy specimens. Lower moisture uptake and less severe fibre–matrix interfacial deterioration were also observed in the vinyl-ester and epoxy systems, indicating improved resistance to alkaline ageing relative to polyester [35].

Glass fibres used in FRP composites are formulated with different chemical compositions to improve their resistance to specific environmental conditions. Common glass fibre types include E-glass, C-glass, AR-glass, and E-CR glass, each offering different levels of chemical resistance depending on their intended application. E-glass fibres are widely used in structural FRP composites due to their good mechanical performance and cost-effectiveness; however, their resistance to highly alkaline environments is lower compared with specially formulated glass types. AR-glass fibres are designed to provide improved resistance to alkaline conditions, while E-CR glass fibres exhibit enhanced chemical durability, particularly in acidic environments[36]. Experimental results by [37] indicate significant differences in chemical resistance among commonly used glass fibre types. Carbon fibres generally exhibit the highest chemical resistance, maintaining structural integrity with negligible mass loss across acidic, alkaline, and saline environments. Basalt fibres show good resistance in acidic conditions but may be more susceptible to chemical reactions under alkaline exposure.

2.2.4. Effect of UV radiation on FRP composites

Fiber-reinforced polymer (FRP) composites are increasingly used outdoors, but their polymer matrices are vulnerable to degradation from UV radiation, thermal cycling, moisture, and environmental pollutants—a process known as weathering. UV radiation is particularly critical, as it triggers photochemical reactions that can irreversibly damage the matrix, compromising the load transfer to fibers and reducing the composite's mechanical performance and service life [38].

Exposure to UV radiation significantly affects the bulk tensile properties of vinyl ester resin matrices. Ultimate tensile properties, including ultimate strain and specific toughness, were particularly sensitive, showing up to a 40% reduction in ultimate strain and a 60% reduction in specific toughness after 4000 hours of exposure in an integrating-sphere-based UV chamber. Hardness and modulus, measured via atomic force microscopy indentation, increased after 1000 hours of exposure, but no notable change was observed between 1000 and 4000 hours, indicating an early plateau in these surface mechanical changes [39].

UV-induced degradation of polymers can be slowed or prevented by adding stabilizers to the polymer matrix or a surface coating. Typical stabilizer concentrations range from 0.05–2% by mass, which can significantly extend polymer lifespan. Effective stabilizers must be photostable, compatible with the

polymer, and non-leaching. Often, combinations are used—for example, UV absorbers work best when paired with hindered amine light stabilizers (HALS). Stabilizers act by: (i) absorbing or blocking UV radiation before it reaches the polymer, (ii) deactivating excited species generated by UV exposure, and (iii) scavenging free radicals to convert them into stable, non-reactive forms [38].

2.3. Role of Artificial Intelligence in Durability Prediction

Artificial Intelligence (AI) and its subset, Machine Learning (ML), have emerged as powerful tools for engineering applications due to their ability to process large volumes of data, identify complex patterns, and model nonlinear relationships between material parameters and performance. In civil engineering and materials science, AI has been increasingly applied to material property prediction, structural monitoring, defect detection, and durability assessment, providing improved predictive capabilities compared with many conventional approaches [40], [41].

Traditional durability prediction methods, including Arrhenius- and diffusion-based models, have been widely used for FRP durability assessment. However, these approaches often rely on simplifying assumptions and may struggle to represent the multiple interconnected degradation mechanisms involving fibres, matrices, interfaces, and moisture diffusion in FRP composites [41].

Consequently, ML techniques have gained attention as data-driven approaches capable of analysing multidimensional datasets and modelling complex, non-linear relationships associated with FRP degradation [41]. Algorithms such as Artificial Neural Networks (ANN), Support Vector Machines (SVM), Random Forest (RF), and Extreme Gradient Boosting (XGBoost) have been investigated for FRP-related applications due to their ability to identify relationships between multiple input variables and material responses [42]. Therefore, ML approaches are increasingly being explored as potential tools for supporting durability prediction of FRP composites by complementing traditional analytical and empirical models [41].

2.4. Conventional Machine Learning Models

Artificial Neural Networks (ANNs) are among the most widely used machine learning techniques in materials engineering because of their ability to learn complex nonlinear relationships from data. Consisting of interconnected input, hidden, and output layers, ANNs can identify patterns and predict material behaviour with high accuracy [43]. In FRP research, they have been successfully applied to predict mechanical properties, degradation behaviour, and long-term durability performance under

different environmental conditions [41]. Their ability to capture complex interactions among multiple variables makes them particularly valuable for durability prediction, where conventional models often face limitations [41], [43].

Support Vector Machines (SVMs) are supervised learning algorithms widely used for regression and classification problems. Their regression form, Support Vector Regression (SVR), has shown strong predictive performance for composite materials due to its ability to model complex nonlinear relationships while maintaining good generalization, particularly with limited datasets. SVMs have been successfully applied to predict mechanical properties and durability-related responses of FRP composites, making them a valuable tool for long-term durability prediction [43].

Random Forest (RF) is an ensemble machine learning algorithm that combines multiple decision trees to improve prediction accuracy and robustness. By analysing complex nonlinear relationships among variables, RF can effectively model material behaviour and reduce the risk of overfitting [44]. In composite materials research, RF has been successfully applied to predict mechanical properties, bond strength, and durability-related performance. Recent studies have identified RF as a promising tool for FRP durability prediction due to its ability to process multidimensional datasets and capture the complex degradation mechanisms associated with environmental exposure [43].

Extreme Gradient Boosting (XGBoost) is a powerful ensemble machine learning algorithm that builds sequential decision trees to improve prediction accuracy and reduce modelling errors. Due to its ability to capture complex nonlinear relationships and analyse multidimensional datasets, XGBoost has been widely applied in materials engineering. [45] demonstrated its effectiveness in predicting the compressive strength of FRP-confined concrete, while [11] identified it as a promising technique for FRP durability prediction. Its high predictive accuracy and ability to model complex material behaviour make it well suited for long-term durability assessment of FRP composites.

2.5. Physics-Informed Machine Learning for Durability Prediction

Conventional machine learning has demonstrated considerable potential for predicting the long-term durability of fibre-reinforced polymer (FRP) composites. However, these models primarily learn statistical relationships from data and do not explicitly represent the physical mechanisms governing material degradation. This limitation has driven the development of physics-informed machine learning, which integrates engineering knowledge into artificial intelligence to improve prediction accuracy and model interpretability.

The importance of incorporating physical knowledge is evident from the degradation behaviour of FRP composites. [46] It was shown that long-term deterioration results from the combined degradation of the glass fibres, resin matrix and fibre-matrix interface through mechanisms such as water ingress, hydrolysis, swelling and interfacial debonding. These processes are further accelerated by elevated temperature, alkaline environments and high relative humidity, demonstrating that durability prediction should account for the underlying physics governing material degradation.

To describe these mechanisms, traditional durability models commonly employ the Arrhenius relationship, which links degradation rate to temperature. [46] further incorporated a time shift factor and a humidity correction factor to account for environmental effects. Although these analytical models are physically meaningful, the authors showed that conventional logarithmic degradation models cannot accurately represent the early stages of degradation and may produce unrealistic long-term predictions, motivating the need for more robust predictive approaches.

Machine learning offers an alternative by capturing complex nonlinear relationships that are difficult to model analytically. [47] developed an XGBoost framework to predict the residual tensile strength and modulus of pultruded FRP composites using variables describing material properties, exposure conditions, and specimen geometry. While the model demonstrated strong predictive capability, it remained fundamentally data-driven because physical principles were not explicitly incorporated into the learning process.

To address this limitation, [48] proposed a physics-guided machine learning framework that embedded engineering knowledge into both the input features and the neural network architecture. The authors introduced an early-age durability fingerprint and transformed variables using physically meaningful relationships, including logarithmic exposure time, an Arrhenius-inspired temperature function, and pH transformation. They further organised the neural network into material, environmental, and temporal modules, allowing each subnetwork to learn degradation patterns associated with a specific physical aspect of the problem before combining them to produce the final prediction.

These studies illustrate the progression of durability prediction from traditional physics-based models to data-driven machine learning and, more recently, to physics-informed machine learning approaches. Collectively, they suggest that integrating engineering principles with machine learning can provide a more physically consistent framework for modelling the long-term durability of FRP composites, while retaining the ability of data-driven methods to capture complex relationships. However, the predictive performance of such approaches remains dependent on the quality and quantity of the available data, the selected model structure, and the validity of the incorporated physical assumptions.

2.6. CEN/TS 19101:2022 – Overview and How Durability is Addressed

As the use of FRP composites in civil engineering continues to increase, design provisions are required to address both their short-term mechanical performance and long-term durability. An important European technical specification for the structural design of FRP composite structures is CEN/TS 19101:2022, *Design of Fibre-Polymer Composite Structures*. This document follows the general design philosophy of the Eurocodes and guides the use of fibre-polymer composites in buildings, bridges, and other civil engineering structures, including both all-composite and hybrid structural systems [49].

One important consideration in CEN/TS 19101:2022 is that the properties of FRP composites may change throughout the service life of a structure. These properties depend on several factors, including fibre type, resin matrix, fibre architecture, manufacturing process, fibre volume fraction, and quality control during production. In addition, exposure to environmental conditions may gradually reduce the stiffness and strength of FRP composites, particularly under elevated temperature, moisture, or combined hygrothermal exposure [49].

CEN/TS 19101:2022 addresses durability considerations using environmental conversion factors, which are applied to material properties to account for reductions caused by environmental exposure. For temperature and moisture effects, the total environmental conversion factor is expressed as:

$$\eta_c = \eta_{ct} \cdot \eta_{cm} \tag{2.1}$$

where η_c is the total environmental conversion factor, η_{ct} represents the conversion factor for temperature effects, and η_{cm}represents the conversion factor for moisture effects[45].

This approach is relevant to durability design because it recognises that mechanical properties measured under reference laboratory conditions may not represent the long-term performance of FRP composites exposed to environmental conditions during service.

CEN/TS 19101:2022 accounts for the influence of service temperature on the mechanical properties of FRP composites through the temperature conversion factor, (η_{ct}). The factor depends on the maximum material temperature in service conditions (T_s) and the glass transition temperature $\left(T_g\right)$ of the composite material. The standard is applicable when the service temperature is higher than $(-40,^\circ\mathrm{C})$ and lower than $\left(T_g - 20,^\circ\mathrm{C}\right)$, thereby maintaining a minimum temperature margin below the glass transition temperature [51]. For composite materials comprising glass, carbon or basalt fibres with thermoset unsaturated polyester, vinyl ester or epoxy matrices, (η_{ct}) is defined separately for fibre-dominated and matrix-dominated properties as follows:

$$\eta_{ct} = \min\left\{1 - \alpha\left(\frac{T_s - 20\,°C}{T_g - 20\,°C}\right); 1.0\right\} \tag{2.2}$$

where (T_s) is the maximum service temperature of the material and α is a parameter that depends on whether the property is fibre-dominated or matrix-dominated. According to [18] α = 0.25 is used for fibre-dominated properties, while α = 0.80 is used for matrix-dominated properties. Fibre-dominated properties include longitudinal tensile strength and stiffness, as well as longitudinal compressive stiffness, where the load-carrying contribution of the fibres is predominant. Matrix-dominated properties are those strongly influenced by the polymer matrix and fibre–matrix interface, such as shear or interlaminar properties [49].

This distinction is particularly important for the present dissertation because the experimental programme includes both fibre-dominated and matrix-dominated mechanical properties. Tensile behaviour in the pultrusion direction is strongly influenced by the glass fibres, whereas interlaminar shear strength and in-plane shear behaviour are more dependent on the polymer matrix and the fibre–matrix interface. These matrix-dominated properties are generally more sensitive to moisture absorption and temperature effects, making them important indicators of hygrothermal degradation.

The moisture conversion factor, η_{cm}, accounts for changes in the mechanical properties of FRP composites caused by moisture absorption and long-term exposure to humid or immersed environments. CEN/TS 19101:2022 defines three moisture exposure classes: Class I for indoor exposure, Class II for outdoor exposure without continuous water contact, and Class III for continuous exposure to water or seawater, permanent immersion, or sustained relative humidity above 80% [49]. For unprotected composite materials consisting of glass, carbon, or basalt fibres combined with thermoset unsaturated polyester, vinyl ester, or epoxy matrices, the moisture conversion factor is assigned according to the relevant exposure class:

$$\eta_{cm} = \begin{cases} 1.00, & \text{for Class I} \\ 0.85, & \text{for Class II} \\ 0.60, & \text{for Class III} \end{cases} \tag{2.3}$$

These values indicate that continuous moisture exposure can significantly reduce the design mechanical properties of FRP composites. The Class III condition is especially relevant to this dissertation because the investigated pultruded GFRP composites were subjected to long-term water immersion under hygrothermal conditions.

The basis for the moisture conversion factor has been supported by experimental and analytical studies on pultruded GFRP materials. [50] investigated pultruded GFRP profiles manufactured with unsaturated

polyester and vinyl ester resin systems and exposed them to water and salt-water immersion at 20°C, 40°C, and 60°C for up to two years. Their study developed Arrhenius-type prediction models for the long-term retention of tensile, flexural, in-plane shear, and interlaminar shear properties. Based on these predictions and a wider literature survey of moisture-exposed GFRP materials, they proposed a 50-year moisture conversion factor of η_{cm}= 0.60 for GFRP composites subjected to high-moisture or continuous-moisture exposure [50].

The relevance of CEN/TS 19101:2022 to the present dissertation lies in its recognition that environmental degradation must be explicitly considered in the structural use of FRP composites. The standard shows that the durability of FRP materials is strongly connected to the effects of temperature and moisture, particularly for properties governed by the polymer matrix and fibre–matrix interface. Therefore, experimental evaluation of mechanical property retention after hygrothermal exposure is necessary for understanding the long-term performance of pultruded GFRP composites.

In this dissertation, relatively thick pultruded GFRP composites manufactured with unsaturated polyester and vinyl ester resin systems are investigated. The study compares unconditioned specimens with specimens conditioned by water immersion at 60°C for two years. By evaluating tensile, compression, flexural, interlaminar shear, and in-plane shear properties, the work provides experimental evidence on the effects of severe hygrothermal exposure on mechanical property retention. This contributes to the broader need for reliable durability data and long-term performance prediction methods for FRP composites used in civil engineering structures.

2.7. Summary and Research Gaps

Although considerable research has been conducted on the durability of pultruded glass fibre-reinforced polymer (GFRP) composites, relatively few studies have investigated relatively thick pultruded laminates using a comprehensive and internally consistent experimental programme that evaluates multiple mechanical properties under identical conditioning conditions. Such datasets are important for understanding how degradation affects fibre-dominated, matrix-dominated and interface-dominated responses.

Another limitation concerns the assessment of moisture-induced degradation. Most published studies focus on specimens tested immediately after environmental conditioning, while comparatively less attention has been given to specimens tested after drying. Evaluating both wet and dried conditions is important for distinguishing potentially reversible effects, such as matrix plasticisation, from irreversible

degradation associated with hydrolysis and deterioration of the fibre–matrix interface. Consequently, the long-term influence of hygrothermal ageing on the different mechanical properties of relatively thick pultruded laminates remains insufficiently established.

More recently, data-driven and machine-learning approaches have shown potential for modelling complex degradation behaviour. However, purely data-driven methods may provide limited physical interpretability, while predictive approaches incorporating physical principles still require validation against comprehensive and internally consistent experimental datasets covering different resin systems, conditioning states, temperatures and mechanical properties. The limited availability of such datasets also creates challenges for the reliable application of machine-learning methods.

To address these gaps, this dissertation investigates the durability of relatively thick pultruded GFRP laminates manufactured with unsaturated polyester and vinyl ester resin systems through a comprehensive experimental programme involving tensile, compression, flexural, in-plane shear, and interlaminar shear testing of reference, wet-aged, and dried specimens. The resulting experimental data provide the basis for developing and validating a Bayesian Physics-Informed Neural Network (BPINN) framework for predicting tensile-strength degradation. The developed framework incorporates Arrhenius-based temperature dependence and is evaluated using complete leave-one-temperature-out validation. Where supported by validation, the model is further used to estimate long-term tensile-strength retention, while considering the limitations associated with the available experimental dataset.

3. Experimental Characterization of Unaged and Aged GFRP Composites

3.1. DURABLE-FRP Project

This dissertation was carried out within the framework of the DURABLE-FRP and CirWind projects, a research initiative focused on evaluating the long-term durability of Fibre-Reinforced Polymer (FRP) composites for civil engineering applications. The project DURABLE-FRP involves the collaboration of the University of Minho (UMinho), the National Laboratory for Civil Engineering (LNEC), and the Instituto Superior Técnico (IST), and aims to improve the understanding of the degradation mechanisms affecting FRP composites when exposed to different environmental conditions.

The DURABLE-FRP project comprises an extensive experimental programme involving both laboratory conditioning and natural environmental exposure. Various environmental factors, including moisture, temperature, ultraviolet radiation, and mechanical stress, are investigated to assess their influence on the mechanical performance and long-term durability of FRP composites. The outcomes of the project are expected to contribute to the development of degradation models, durability assessment methodologies, and design recommendations for FRP structures used in civil engineering.

The present dissertation focuses on a specific component of the project related to the durability assessment of relatively thick pultruded glass fibre-reinforced polymer (GFRP) composites subjected to water immersion under hygrothermal conditions. The investigated material consisted of pultruded GFRP laminates manufactured using unsaturated polyester and vinyl ester resin systems. The study considered both unconditioned specimens and specimens conditioned through immersion in water at 60°C for a period of two years. Following the conditioning period, the mechanical performance of the materials was evaluated through an experimental testing campaign. The programme included tensile tests, compression tests, flexural tests, interlaminar shear strength (ILSS) tests, and in-plane shear tests.

The experimental data generated in this study provide the primary basis for the development and evaluation of artificial intelligence (AI)-based predictive models aimed at estimating the long-term durability and mechanical property retention of pultruded GFRP composites exposed to water immersion. In addition, complementary data from previous investigations (MSc Projects) are incorporated into the modelling dataset, particularly for tensile property prediction, to enhance the diversity of the available data. This approach contributes to the broader objectives of the DURABLE-FRP project regarding durability

assessment and long-term performance prediction of FRP composites. Figure 3.1 illustrates the pultruded GFRP laminates used in the study together with the laboratory facilities employed for specimen conditioning and environmental exposure.



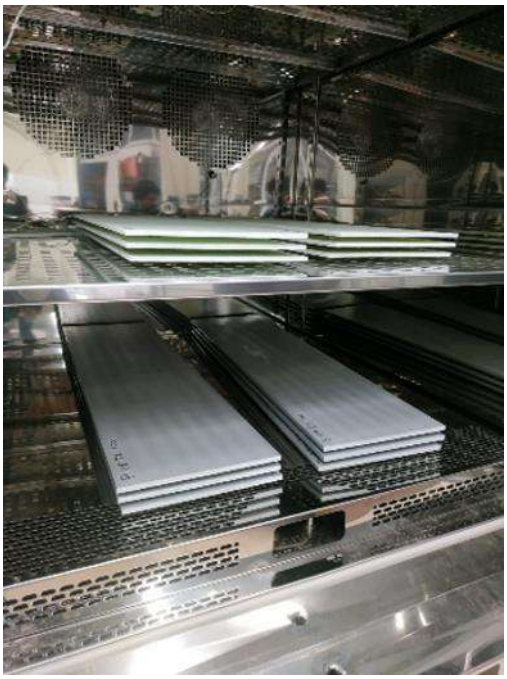
(a) Storage of pultruded GFRP laminates before specimen preparation



(b) Water immersion conditioning setup



(c) Environmental chamber used for hygrothermal aging



(d) Specimens during conditioning exposure

Figure 3.1: Materials and conditioning facilities used in the experimental programme.

3.2. Materials

The materials investigated in this dissertation consisted of two relatively thick pultruded glass fibre-reinforced polymer (GFRP) laminates supplied by Exel Composites. The two material systems were manufactured using the same type of glass-fibre reinforcement but different polymer matrices: unsaturated polyester and vinyl ester. In this dissertation, the materials are designated as P-UP and P-VE, respectively.

The laminates were produced by pultrusion, a continuous manufacturing process in which glass fibres are impregnated with a polymer resin and pulled through a heated die, where the composite is shaped and cured. The pultrusion direction corresponds to the principal fibre direction of the laminates.

Each pultruded laminate had nominal dimensions of 900 mm in length, 250 mm in width, and 8 mm in thickness. The laminate architecture consisted of seven reinforcement layers. Four layers contained randomly distributed glass fibres in the form of chopped strand mats, while the remaining three layers consisted mainly of continuous fibres aligned with the pultrusion direction. This reinforcement arrangement provides high longitudinal stiffness and strength while also improving the transverse and shear response of the material. The glass-fibre content was approximately 59% by mass for the P-UP laminates and 63% by mass for the P-VE laminates.

Standardised specimens were extracted from the laminates for tensile, compression, flexural, in-plane shear, and interlaminar shear testing. Tensile specimens were prepared in both the longitudinal direction, corresponding to 0° relative to the pultrusion direction, and the transverse direction, corresponding to 90°. The specimen geometries and dimensions were selected according to the relevant test standards and are presented in the following sections. Figure 3.2 presents the adopted specimen extraction layout, while Table 3.1 summarises the corresponding specimen labels, test types, and nominal geometries.

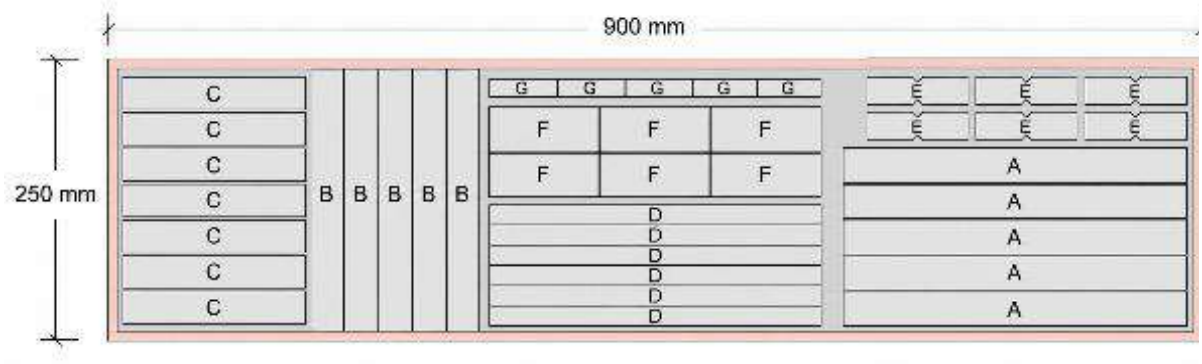


Figure 3.2: Specimen extraction layout for mechanical characterisation and DMA testing of the pultruded GFRP plate.

Table 3.1: Identification and geometry of the specimens used for mechanical and DMA testing.

Label	Test type	Thickness (mm)	Width (mm)	Length (mm)
A	Uniaxial tensile test at 0°	8	25	300
B	Uniaxial tensile test at 90°	8	25	250
C	Uniaxial compression test	8	25	125
D	Flexural test	8	15	240
E	In-plane shear test	8	20	76
F	Interlaminar shear test	8	40	80
G	Dynamic Mechanical Analysis (DMA)	8	10	60

3.3. Experimental Campaign

The mechanical characterisation of the pultruded GFRP laminates in this study was performed on two matrix systems: unsaturated polyester (P-UP) and vinyl ester (P-VE). All conditioned specimens were subjected to hygrothermal ageing through immersion in water at 60 °C for a duration of 24 months. Following the conditioning period, the specimens were divided into two groups. The first group, designated W60-24M-D, was removed from the water bath and allowed to dry under laboratory ambient conditions before testing. The second group, designated W60-24M-W, was tested immediately after removal from the conditioning bath while still in the wet condition, thereby preserving the effects of absorbed moisture during mechanical testing. Unconditioned specimens tested before exposure were designated as the reference (REF) series.

The experimental campaign comprised six mechanical tests: uniaxial tensile at 0° and 90° fibre orientations, compression, flexural, interlaminar shear (ILSS), and in-plane shear. Strain measurements were obtained where applicable; however, for some tests (i.e., flexural and ILSS), only the force, stress, and displacement at maximum load were recorded because of equipment limitations or invalid failure modes.

Reference values for the unaged specimens were obtained from the same batch of laminates before conditioning and were used as the baseline for assessing the effect of hygrothermal ageing on the mechanical performance of the GFRP laminates. Consequently, the experimental dataset provides a

consistent basis for evaluating the degradation behaviour of both P-UP and P-VE laminates and forms the foundation for the subsequent durability assessment and predictive modelling presented in this dissertation.

To ensure statistical reliability, multiple specimens were tested for each mechanical test, resin system, and conditioning state. The experimental programme therefore consisted of three specimen series, namely the reference (REF), dry-conditioned (W60-24M-D), and wet-conditioned (W60-24M-W) conditions. In total, 240 specimens were prepared for the experimental programme, comprising 120 P-UP and 120 P-VE specimens; however, DMA results were outside the scope of this dissertation and are therefore not discussed further. The complete experimental test matrix is summarised in Table 3.2.

Table 3.2: Test matrix and number of specimens for each mechanical test.

Mechanical Test	Fibre Orientation	Specimens per Series (per Resin System)	Conditioning Series	Total Specimens per Resin System	Total Specimens (P-UP + P-VE)
Uniaxial Tensile	0°	6	REF, W60-24M-D, W60-24M-W	18	36
Uniaxial Tensile	90°	5	REF, W60-24M-D, W60-24M-W	15	30
Uniaxial Compression	–	7	REF, W60-24M-D, W60-24M-W	21	42
Flexural	–	6	REF, W60-24M-D, W60-24M-W	18	36
In-plane Shear	–	6	REF, W60-24M-D, W60-24M-W	18	36
Interlaminar Shear (ILSS)	–	6	REF, W60-24M-D, W60-24M-W	18	36
Dynamic Mechanical Analysis (DMA)	–	4	REF, W60-24M-D, W60-24M-W	12	24
Total				**120**	**240**

3.4. Mechanical Characterization Tests

3.4.1. Testing equipment

Specimens were prepared using a CNC BETA MINI 6010 machine to cut the pultruded GFRP plates in accordance with the experimental layout shown in Figure 2. Cutting paths were designed with VCarve and executed under the control of UCCNC, ensuring uniform specimen dimensions and preserving material integrity for the mechanical tests, as shown in Figure 3.3.

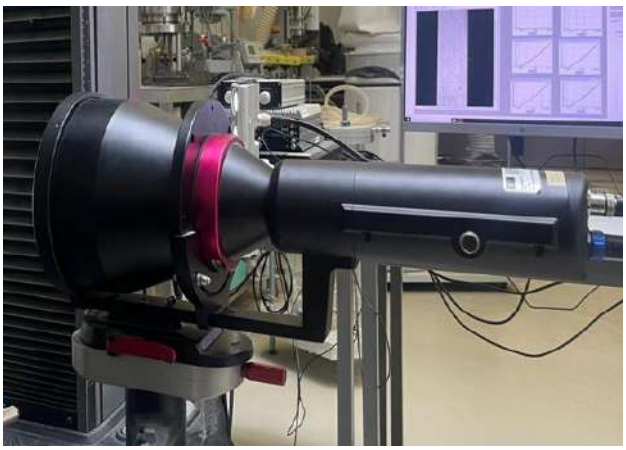


Figure 3.3: CNC BETA MINI 6010 cutting machine and use of UCCNC software.

The MTS Exceed E45.105 universal testing machine was the primary instrument employed for all mechanical tests in this experimental campaign. Designed for versatile mechanical testing, this system accommodates tension, compression, shear, and bending tests, ensuring consistent and reliable data collection. The machine is equipped with a load cell for accurate force measurement, a displacement sensor, a remote control, and modular components to support various test configurations. High-precision strain measurements were achieved using an MTS Advantage (AVX) video extensometer, while test control and data acquisition were handled via the MTS Test Suite TWE Elite and AVX software, respectively. Figure 3.4(a) and Figure 3.4(b) illustrate the machine and its video extensometer setup. For compression tests exceeding the 100 kN capacity of the MTS Exceed E45.105, a separate compression frame rated at 300 kN, as shown in Figure 3.4(c), was used. This system was controlled with the DynaTest software.



(a) MTS Exceed E45.105 universal testing machine



(b) MTS Advantage (AVX) video extensometer



(c) Compression frame for high-force tests

Figure 3.4: Test equipment used in the experimental programme.

3.4.2. Tensile test at 0° and 90°

The mechanical behaviour of the pultruded GFRP laminates was evaluated through uniaxial tensile tests conducted in accordance with ISO 527. Two orientations were considered: fibres aligned at 0° and 90° relative to the loading direction. For the 0° tests, specimens classified as Type A were used, while Type B specimens were employed for the 90° tests Figure 3.2. Dimensions and test conditions were defined according to ISO 527-1, Part 1: General Principles, and ISO 527-4, Part 4: Test Conditions for Isotropic Fibre-Reinforced Composites ('EN ISO 527-4', 1997), as shown in Figure 3.5.

The tests were performed under strain control at a constant crosshead speed of 2 mm/min. Considering the specimen thickness (8 mm), type classification (Type 2), and material system (glass-fibre reinforced), a jaw separation of 150 mm was used, with a gauge length of 50 mm for strain measurement using a video extensometer.

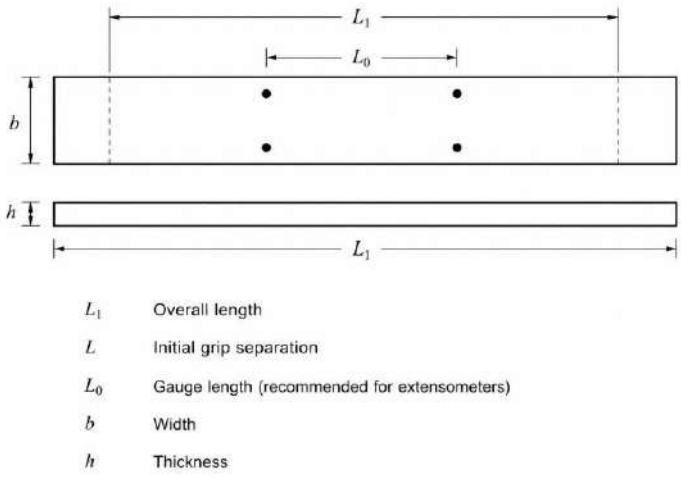


Figure 3.5: Type 2 geometry of the specimen used for uniaxial tensile tests with fibres oriented at 0° and 90° (adapted from 'EN ISO 527-4', 1997).

This procedure was successful for all specimens except those subjected to wet conditioning, where premature failures were observed at the grip region during the initial tests. To mitigate this issue, the tensile specimen geometry for the wet specimens (including both fibre orientations and resin types) was modified based on the Type 1B configuration specified in ISO 527. The specimen width was reduced from 25 mm to 20 mm, and the gauge section was shortened to promote failure within the central region rather than at the grips. The modified geometry was selected to improve the validity of tensile testing for the wet-conditioned specimens and to reduce the occurrence of premature grip failures. However, since the geometry modification was applied only to the wet-conditioned specimens, comparisons with the reference and dry-conditioned specimens should be interpreted with consideration of the potential

influence of specimen geometry. Figure 3.6 illustrates the Type 1B specimen geometry adopted for these wet-condition tests.

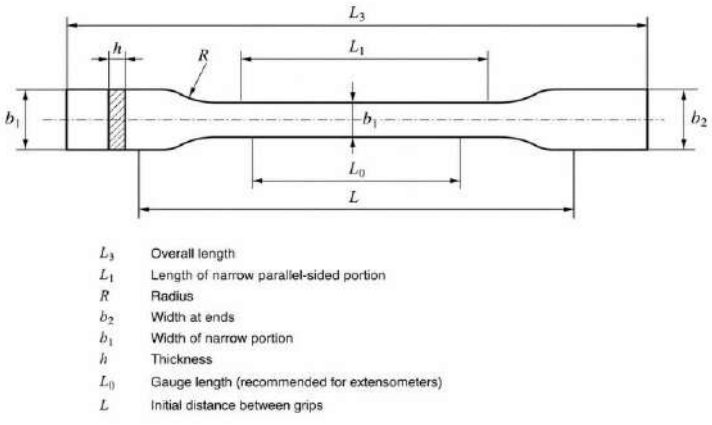


Figure 3.6: Type 1b geometry of the specimen used for uniaxial tensile tests (adapted from 'EN ISO 527-4', 1997).

Before testing, a standardised specimen preparation protocol was followed. For tensile testing, six 0° specimens and five 90° specimens were prepared per conditioning series for each resin system, namely unsaturated polyester (P-UP) and vinyl ester (P-VE). The central region of each specimen was lightly sanded to minimize light reflection during video extensometer measurements. Reference lines were marked for the gauge section for precise strain tracking and initial measurements, as shown in Figure 3.7. Width and thickness measurements were taken at both ends and at the centre of each specimen Figure 3.8(a), followed by specimen mass determination as shown in Figure 3.8(b). This preparation procedure was applied consistently to all specimens.

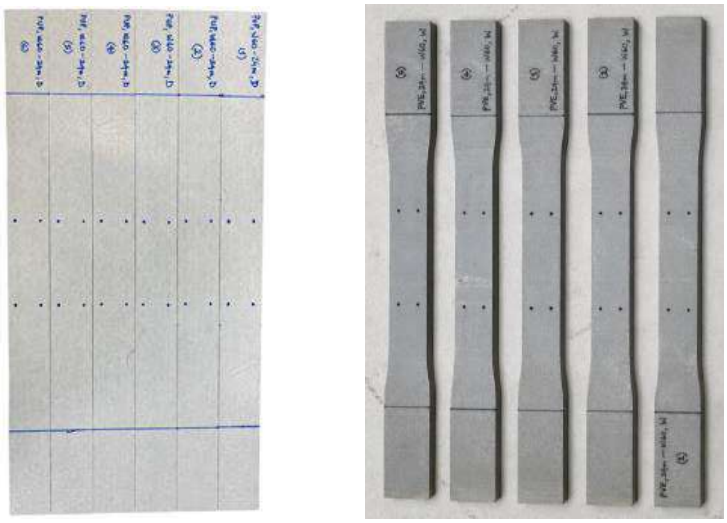


Figure 3.7: Reference lines marked on specimens for precise strain measurement in the gauge section.

All tests were carried out on the universal testing machine, MTS Exceed E45.105, equipped with a displacement sensor, an internal load cell, and a video extensometer to enable accurate strain measurement Figure 3.8(c). The setup allowed simultaneous recording of load, displacement, and strain throughout the test duration.

The tensile test results were subsequently used to evaluate the effects of 24 months of hygrothermal water immersion at 60 °C on the mechanical performance of P-UP and P-VE laminates. The methodology ensured that failures occurred within the gauge section and that measured strains accurately reflected the material response. This setup, combined with careful specimen preparation and proper instrumentation, provided reliable data for the analysis of tensile strength, elastic modulus, ultimate strain, and failure modes for both fibre orientations.



(a) Specimen dimension measurement using a digital calliper

(b) Specimen mass measurement using a digital balance

(c) Specimen mounted in the MTS testing machine with grips and video extensometer setup

Figure 3.8: Specimen preparation and tensile test setup.

3.4.3. In-plane shear test

The in-plane shear tests were conducted in accordance with ASTM D5379 to evaluate the shear response of the pultruded GFRP laminates. Type E specimens were used for this test as shown in Figure 3.2. According to ASTM D5379, the test is performed under strain control at a crosshead speed of 2 mm/min. Considering the specimen thickness (8 mm) and material type (glass-fibre systems), a central width of 12 mm was adopted, as recommended by the standard. Figure 3.9 and Figure 3.10 illustrate the specimen geometry and test configuration, respectively.

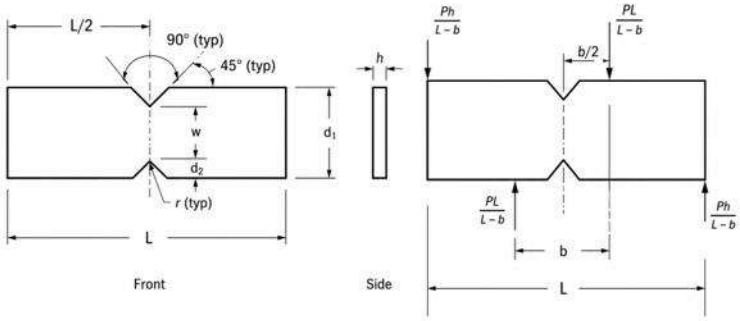


Figure 3.9: Geometry of the specimen used for in-plane shear tests (adapted from 'ASTM D5379', 2005).

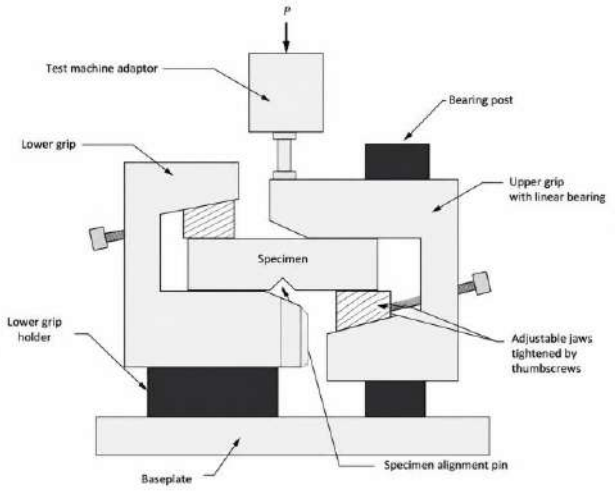
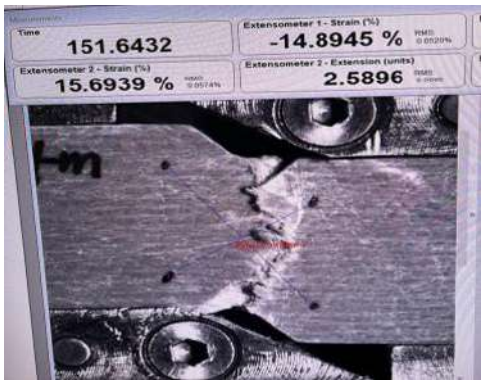


Figure 3.10: In-plane shear test setup (adapted from 'ASTM D5379', 2005).

Before testing, a preparation protocol was implemented to ensure accurate measurements. The specimens were lightly sanded in the gauge region where strain would be measured to prevent light reflection from interfering with the video extensometer. Four reference points were then marked along the gauge section, spaced 6 mm apart, to allow the video extensometer to track strain accurately, as shown in Figure 3.11(a) and Figure 3.11(b). Width and thickness measurements were recorded at both ends and at the centre of each specimen, and the specimens were weighed. This preparation procedure was repeated for all specimens.



(a) Marking of points for strain measurement on the in-plane shear specimen



(b) Strain measurements using video extensometer during the in-plane shear test

Figure 3.11: In-plane shear strain measurement.

All in-plane shear tests were performed using the MTS Exceed E45.105 universal testing machine, equipped with an internal load cell, a displacement sensor, and an MTS Advantage (AVX) video extensometer to capture precise strain measurements as shown in Figure 3.12. The MTS TestSuite TWE Elite and AVX software controlled the test parameters and recorded the data.

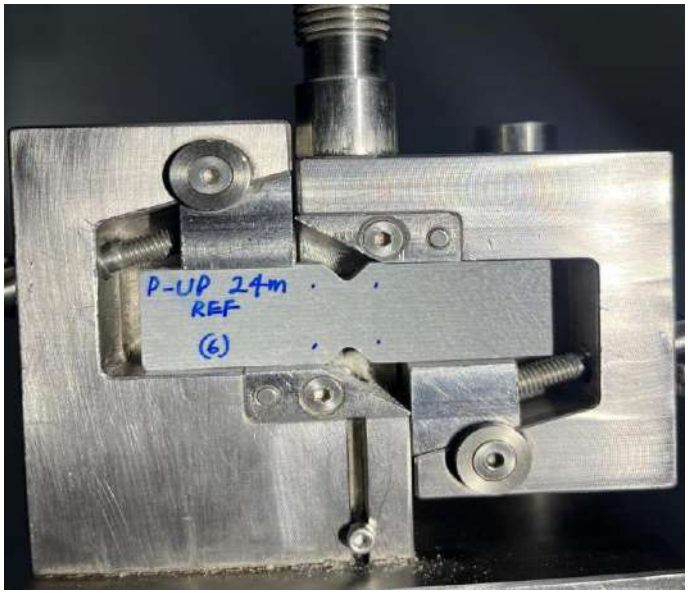
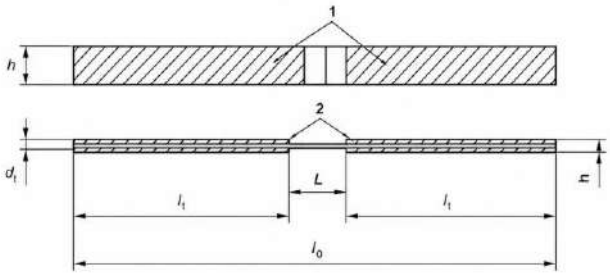


Figure 3.12: In-plane shear test.

3.4.4. Uniaxial compression test

Uniaxial compression tests were conducted in accordance with ISO 14126:1999, Fibre Reinforced Plastic Composites – Determination of Compressive Properties in the In-Plane Direction ('EN ISO 14126', 1999), using type "C" specimens (Figure 3.2). Strain-controlled testing was applied at a constant crosshead speed of 1 mm/min ± 0.5 mm/min. Considering the specimen thickness (8 mm), test type ("B2"), test method (method 2), and material classification ("glass-fibre systems"), a jaw separation of 25 mm and longitudinal reference points spaced 20 mm apart were adopted for strain measurement using a video extensometer. Figure 3.13 Illustrates the key geometric features of the specimens used for the uniaxial compression tests.

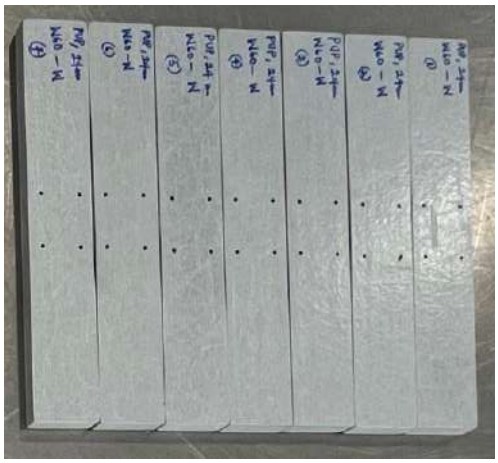


Dimension	Symbol
Overall length (minimum)	l_0
Thickness	h
Width	b
Distance between grips/fixtures	L
Length of grip/fixture (minimum)	l_t
Thickness of grip/fixture	d_t

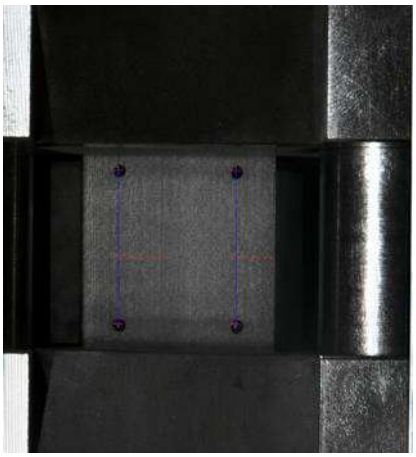
Figure 3.13: Specimen geometry used for compression tests (adapted from 'EN ISO 14126', 1999).

Before testing, all specimens were labelled for identification, and the central region was lightly sanded to ensure accurate strain measurement, as shown in Figure 3.14(a). Width, thickness (at both ends and the centre), and mass were recorded for each specimen.

The P-UP-DRY, P-UP-WET, and P-VE-WET specimens were tested using the MTS Exceed E45.105 universal testing machine, while the P-UP-REF, P-VE-REF, and P-VE-DRY specimens required the higher-capacity 300 kN testing frame to reach failure. For specimens tested on the MTS Exceed E45.105, compression was applied up to 30 kN while the video extensometer recorded strain to determine the elastic modulus as shown in Figure 3.14(b).



(a) central points marked on the specimens for extension measurement



(b) extension measurement using video extensometer during compression test

Figure 3.14: Compression strain measurement procedure.

Figure 3.15(a) illustrates the test setup for the MTS machine, while Figure 3.15(b) shows the high-capacity testing frame. This methodology allowed accurate measurement of maximum compressive load, stress, and displacement at failure for all specimens while maintaining specimen integrity and providing reproducible, high-quality data for analysis.



(a)Uniaxial compression test on the MTS Exceed E45.105



(b) High-capacity uniaxial compression test on the testing frame

Figure 3.15: Compression test setups.

3.4.5. Flexural test

Flexural tests were conducted using the MTS Exceed E45.105 universal testing machine, following the guidelines of ISO 14125:1998 (Fibre Reinforced Plastic Composites – Determination of Flexural Properties, 'EN ISO 14125', 1998). Type D specimens were used (Figure 3.2). Tests were performed under a constant crosshead speed of 5 mm/min. Considering the specimen thickness (8 mm), material classification (Class 3), and the adopted test method (three-point bending, Method A), a support span of 160 mm with cylindrical supports of 5 mm radius was applied, in accordance with the standard. The main specimen geometry is shown in Figure 3.16.

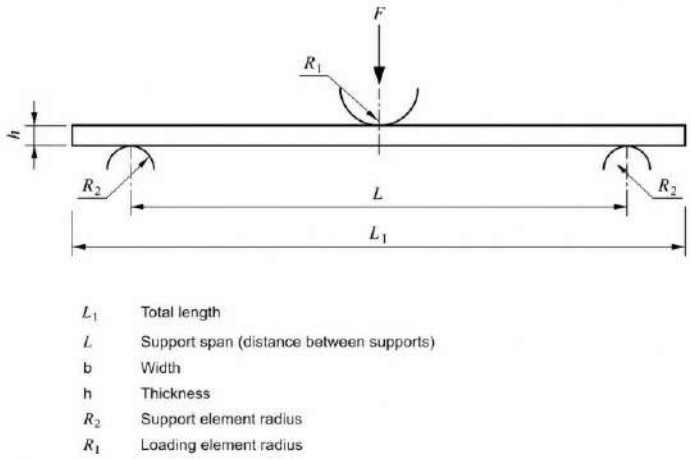


Figure 3.16: Setup used in the flexural tests and geometry of the corresponding specimen (adapted from 'EN ISO 14125', 1998).

Specimen preparation followed a standardized protocol like that used in previous tests. Each specimen was labelled, and its geometry and mass were recorded. No surface preparation was required, as strain measurements were not performed. Reference lines were marked at midspan (the load application point) and at the supports. Figure 3.17(a) illustrates the marked specimens for the flexural tests.

The tests were performed on the MTS Exceed E45.105, using the machine's standard load cell and displacement sensors. Figure 3.17(b) shows a photograph of the test setup, demonstrating the placement of the specimen and the load application.



(a) Marking of specimens for flexural tests (b) Flexural test setup

Figure 3.17: Flexural test preparation and setup.

3.4.6. Interlaminar shear test

Interlaminar shear testing was conducted using the MTS Exceed E45.105 universal testing machine, following ISO 14130:1997 (Fibre-reinforced plastic composites – Determination of apparent interlaminar shear strength by short-beam method, 'EN ISO 14130', 1997). Type "F" specimens were used (Figure 3.2), and tests were performed under strain control at a constant crosshead speed of 1 mm/min ± 0.2 mm/min. The standard specifies a support span of 40 mm, with cylindrical supports of 2 mm radius, and a loading element radius of 5 mm. The main specimen geometry is illustrated in Figure 3.18.

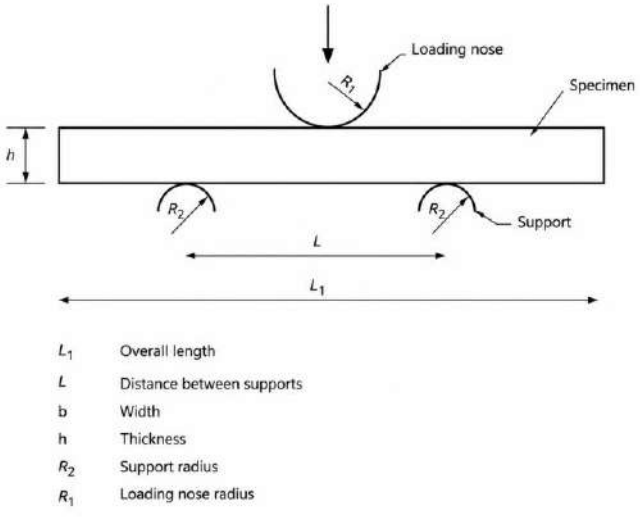
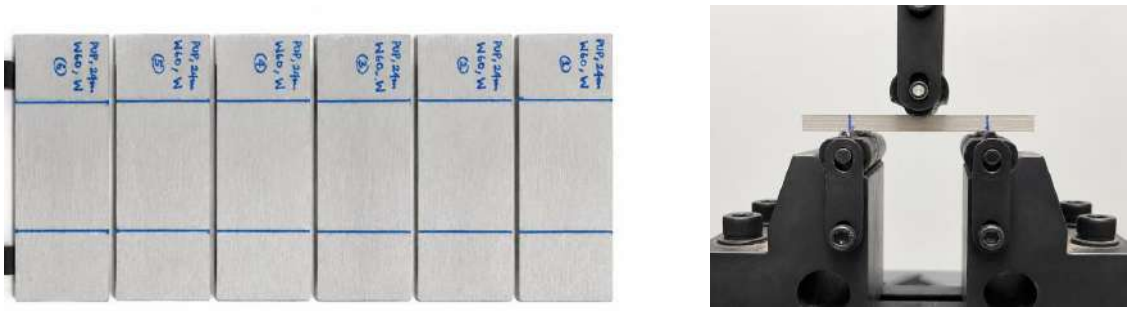


Figure 3.18: Configuration used for the interlaminar shear tests and geometry of the respective specimen (adapted from 'EN ISO 14130', 1997).

Specimen preparation was like the flexural test, differing only in the spacing between reference lines used for measurement. Figure 3.19(b) shows the marking of the specimens for interlaminar shear testing.

The tests utilized the same attachments as the flexural tests. Figure 3.19(b) shows a photograph of the test setup, including the placement of the specimen, supports, and loading element, demonstrating the configuration used for accurate measurement of interlaminar shear behaviour.



(a) Marking of specimens for interlaminar shear tests (b) Interlaminar shear test setup

Figure 3.19: Interlaminar shear test preparation and setup.

3.5. Results and Analysis

This section presents and analyses the mechanical properties obtained from the experimental testing of relatively thick pultruded GFRP specimens manufactured with unsaturated polyester (P-UP) and vinyl ester (P-VE) resin systems. The experimental programme included tensile tests in the 0° and 90° fibre directions, compression tests, flexural tests, in-plane shear tests, and interlaminar shear tests. The results of the conditioned specimens are compared with those of the corresponding unconditioned reference specimens to evaluate the effects of prolonged hygrothermal ageing on the mechanical behaviour of both material systems.

For each mechanical test, the results are presented for the P-UP and P-VE reference series, followed by the corresponding conditioned series. The reference specimens, designated REF, were tested in the unaged condition. The conditioned specimens were immersed in water at 60 °C for 24 months and were subsequently tested either after drying under laboratory conditions or in the wet condition. These series are designated W60-24M-D and W60-24M-W, respectively.

The specimen series are therefore identified using designations such as P-UP-REF, P-UP-W60-24M-D, and P-UP-W60-24M-W, where P represents the pultruded GFRP material, UP or VE identifies the resin system as unsaturated polyester or vinyl ester, respectively, and REF, W60-24M-D, or W60-24M-W indicates the conditioning state. Here, W60-24M-D denotes specimens immersed in water at 60 °C for 24 months and dried before testing, while W60-24M-W denotes specimens subjected to the same exposure and tested in the wet condition. This designation system facilitates the identification and comparison of the different resin systems and conditioning states throughout the results and analysis.

To obtain representative stress–strain and stress–displacement response curves for each conditioning state, a programmed Microsoft Excel workbook was used to generate average curves from the individual specimen results. The individual datasets were first interpolated onto a common independent-variable interval corresponding to strain for the tensile tests in the 0° and 90° fibre directions and the in-plane shear tests, and to displacement for the compression, flexural, and interlaminar shear tests. The corresponding stress values were then averaged at each interval using only the specimens containing valid data at that point.

3.5.1. Uniaxial tension with fibres oriented at 0°

The results obtained from the uniaxial tensile tests with fibres oriented at $0°$, including the elastic modulus (E), ultimate tensile strength (f_{tu}), ultimate tensile strain (ε_{tu}), and failure modes, were used to evaluate the influence of long-term hygrothermal ageing on the longitudinal tensile behaviour of the pultruded GFRP composites. The tensile modulus was determined in accordance with EN ISO 527-4:1997, using the stress–strain response between the strain limits of $\varepsilon_1 = 0.05\%$ and $\varepsilon_2 = 0.25\%$. Complete experimental results, including photographs of the tested specimens, are provided in the Appendix.

The mean tensile properties obtained for both resin systems under the different conditioning states are summarised in Table 3.3

Table 3.3: Mean results of the 0° uniaxial tensile tests for P-UP and P-VE specimens under different conditioning conditions

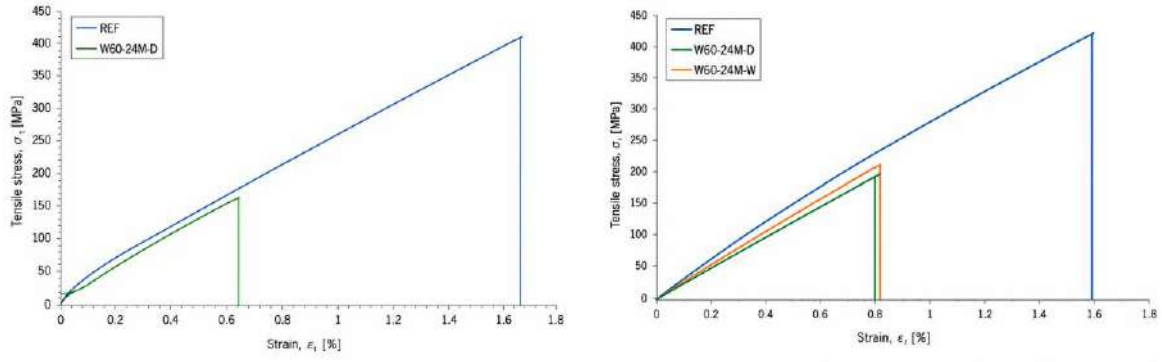
Resin System	Series	E [GPa] [1]	f_{tu} [MPa] [1]	ε_{tu} [%] [1]	Mode of Failure [2]
Unsaturated Polyester	REF	28.25 (3.5%)	407.18 (2.2%)	1.67 (2.5%)	XGM (6)
	W60-24M-D	27.53 (9.4%)	163.91 (3.6%)	0.63 (5.0%)	LAT (6)
	W60-24M-W	n. a	n. a	n. a	n. a
Vinyl Ester	REF	30.66 (5.6%)	417.88 (7.1%)	1.48 (6.3%)	XGM (6)
	W60-24M-D	29.80 (3.3%)	220.27 (5.5%)	0.81 (4.1%)	AGM (2), DGM (2), LAT (2)
	W60-24M-W	37.19 (3.5%)	225.51 (3.3%)	0.84 (6.9%)	LGM (4), SGM (1), AGM (1)

Notes: [1] Values expressed in parentheses represent the corresponding coefficient of variation (CoV).
[2] The values in parentheses indicate the number of specimens in which the respective failure mode occurred; n.a – not available.

As shown in Table 3.3hygrothermal conditioning had a pronounced effect on the tensile strength and ultimate tensile strain of both resin systems, whereas the elastic modulus remained comparatively stable. For the P-UP specimens, the tensile strength decreased from 407.18 MPa in the reference condition to 163.91 MPa following 24 months of conditioning at $60°C$ and dried at laboratory temperature, corresponding to approximately 40% strength retention. In contrast, the elastic modulus decreased only slightly from 28.25 GPa to 27.53 GPa, representing approximately 97% retention, while the ultimate tensile strain reduced from 1.67% to 0.63%.

The P-VE specimens exhibited superior tensile durability after conditioning. The tensile strength decreased from 417.88 MPa for the reference specimens to 220.27 MPa and 225.51 MPa for the dry and wet conditioned specimens, corresponding to approximately 53% and 54% retention, respectively. The elastic modulus was comparatively less affected than tensile strength, with the dry-conditioned specimens retaining approximately 97% of the reference modulus, while the wet-conditioned specimens showed an apparent increase that should be interpreted with caution.

The average stress–strain responses for both resin systems are presented in Figure 3.20.



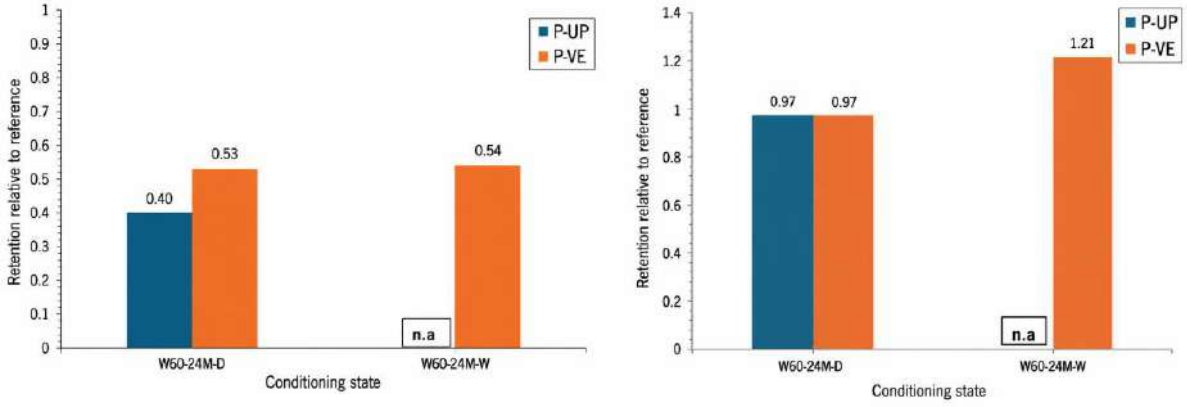
(a) P-UP specimens (b) P-VE specimens

Figure 3.20: Average tensile stress–strain curves of pultruded GFRP specimens in the 0° direction under different conditioning states.

The stress–strain curves in Figure 3.20 demonstrate that hygrothermal conditioning primarily affected the tensile strength and deformation capacity of the pultruded GFRP laminates. The initial linear elastic response, however, remained broadly comparable to that of the reference specimens. Although the P-VE wet specimens exhibited an apparent increase in elastic modulus, this result should be interpreted with caution. Overall, the longitudinal elastic response was less affected by ageing than the tensile strength and failure strain. Despite the relatively stable initial elastic response, failure occurred at significantly lower stresses and strains after conditioning, indicating reduced load-carrying capacity and ductility.

The degradation was more pronounced in the P-UP specimens than in the P-VE specimens. The P-UP dry specimens exhibited a substantial reduction in both ultimate tensile strength and failure strain, whereas

the P-VE specimens retained a greater proportion of their tensile performance. This behaviour indicates that the vinyl ester resin provided better resistance to moisture-induced degradation than the unsaturated polyester resin. The observed reduction in tensile performance is attributed primarily to moisture-induced plasticisation of the polymer matrix, hydrolytic degradation, and weakening of the fibre–matrix interface, which reduce the efficiency of stress transfer without significantly affecting the stiffness of the longitudinal glass fibres. To facilitate comparison between the two resin systems, the normalised retention of the tensile properties is presented in Figure 3.21.



(a) tensile strength (b) elastic modulus

Figure 3.21: Normalised retention of the 0° tensile properties of P-UP and P-VE specimens under different conditioning states. n.a = not available

During the experimental programme, the P-UP wet specimens failed prematurely in the gripping region rather than in the gauge section. These failures were classified as invalid according to EN ISO 527-4:1997 and were therefore excluded from the mechanical property evaluation. To minimise grip-induced stress concentrations, the specimen width was reduced from approximately 25 mm to 20 mm for the subsequent P-VE wet specimens. This modification successfully promoted valid gauge-section failures, suggesting improved load transfer and reduced grip-related effects during testing. Although elastic modulus is theoretically independent of specimen width, the modified geometry may have influenced the gripping conditions, specimen alignment and strain measurement. Therefore, the apparent increase in elastic modulus observed for the P-VE wet specimens should be interpreted with caution and should not necessarily be considered a true increase in material stiffness.

However, excluding the P-UP wet longitudinal tensile results represents an experimental limitation of this study, as it prevented a complete comparison between the P-UP and P-VE systems under wet-conditioned tensile loading. Consequently, the interpretation of resin-system effects on the wet longitudinal tensile response should be considered with caution.

Representative failure modes observed during the tensile tests are presented in Figure 3.22.

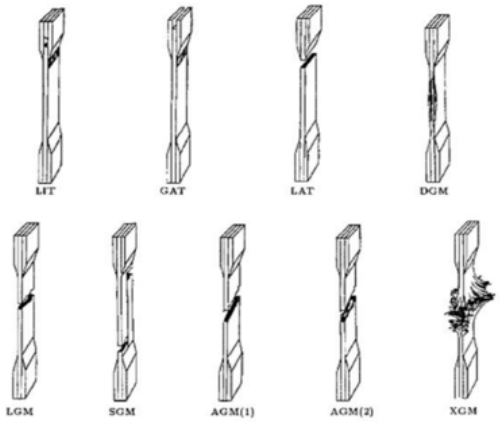


Figure 3.22: Failure modes observed during tensile tests (adapted from ASTM D3039/D3039M:2002).

As shown in Figure 3.22, the reference specimens predominantly exhibited XGM gauge-section failures, indicating valid tensile fractures within the gauge length. After conditioning, the P-UP dry specimens mainly exhibited LAT failures, whereas the P-VE dry and wet specimens displayed combinations of AGM, DGM, LGM, SGM, and gauge-section failures. Representative photographs of the observed failure modes are also presented in the Appendix. The occurrence of valid gauge-section failures in the modified P-VE wet specimens indicates that reducing the specimen width helped to mitigate premature grip-related failures.

Overall, the $0°$ tensile results demonstrate that long-term hygrothermal conditioning primarily reduced the tensile strength and deformation capacity of the pultruded GFRP laminates, while the longitudinal elastic modulus remained comparatively stable. Among the two resin systems investigated, the P-VE specimens exhibited superior retention of tensile properties after conditioning, indicating greater resistance to moisture-induced degradation than the P-UP specimens.

3.5.2. Uniaxial tension with fibres oriented at 90°

The results obtained from the uniaxial tensile tests with fibres oriented at $90°$, including the elastic modulus (E), ultimate tensile strength (f_{tu}), ultimate tensile strain (ε_{tu}), and observed failure modes, were used to evaluate the influence of long-term hygrothermal ageing on the transverse tensile behaviour of the pultruded GFRP composites. Unlike the $0°$ tensile configuration, where the applied load is primarily carried by the continuous glass fibres, the $90°$ tensile response is mainly governed by the polymer matrix and the fibre–matrix interface. Consequently, this loading direction is more sensitive to moisture-induced degradation mechanisms. The tensile modulus was determined in accordance with EN ISO 527-4:1997,

using the chord modulus calculated between strain limits of $\varepsilon_1 = 0.05\%$ and $\varepsilon_2 = 0.25\%$. Complete individual test results and specimen photographs are provided in the Appendix.

Table 3.4: Mean results of the 90° uniaxial tensile tests for P-UP and P-VE specimens under reference and conditioned states.

Resin System	Series	E [GPa] [1]	f_{tu} [MPa] [1]	ε_{tu} [%] [1]	Mode of Failure [2]
Unsaturated Polyester	REF	5.55 (4.0%)	53.69 (12.2%)	1.54 (2.6%)	AGM1(3), AGM2 (1), LAT (1)
	W60-24M-D	4.48 (6.8%)	23.33 (4.7%)	0.70 (5.7%)	AGM1(2), LGM (2), LAT (1),
	W60-24M-W	n. a	n. a	n. a	n. a
Vinyl Ester	REF	11.30 (11.6%)	59.15 (2.3%)	1.19 (9.0%)	LGM (3), AGM2(1), AGM1(1)
	W60-24M-D	8.99 (9.4%)	37.48 (6.0%)	0.70 (17.1%)	LGM (3), AGM1 (1), LAT (1)
	W60-24M-W	11.18 (10.0%)	46.85 6.2%)	0.71 (17.2%)	LGM (4) AGM (1)

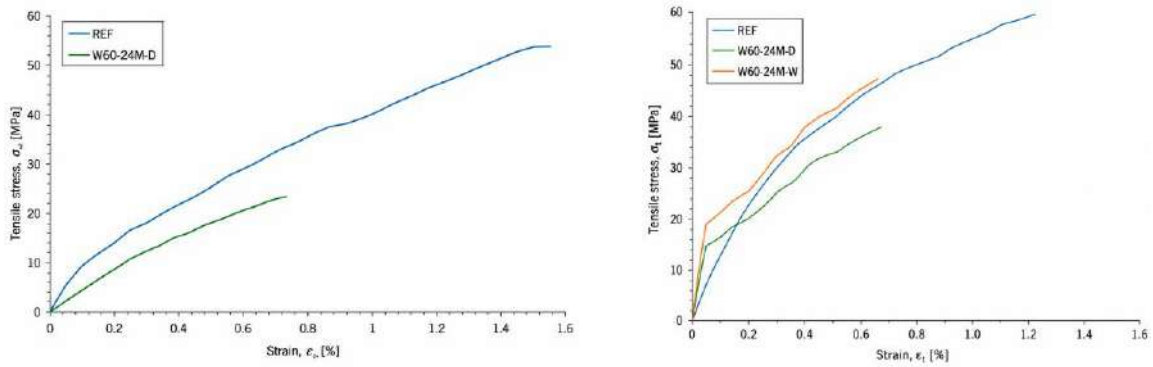
Notes: [1] Values expressed in parentheses represent the corresponding coefficient of variation (CoV).
[2] The values in parentheses indicate the number of specimens in which the respective failure mode occurred; n.a – not available.

The results presented in Table 3.4 indicate that the transverse tensile properties were considerably lower than those obtained for the 0° specimens, reflecting the fact that loading in the transverse direction is controlled primarily by the resin matrix and the fibre–matrix interface rather than the continuous reinforcing fibres. Consequently, the influence of hygrothermal ageing was more pronounced than in the longitudinal tensile configuration.

For the P-UP specimens, conditioning resulted in reductions in all measured tensile properties. The elastic modulus decreased from 5.55 GPa for the reference specimens to 4.48 GPa after conditioning, corresponding to approximately 81% modulus retention. The ultimate tensile strength decreased from 53.69 MPa to 23.33 MPa, representing approximately 43% strength retention, while the ultimate tensile strain reduced from 1.54% to 0.70%, corresponding to approximately 45% strain retention. These reductions indicate substantial deterioration of the matrix-dominated transverse tensile response following long-term hygrothermal exposure.

The P-VE specimens exhibited superior transverse tensile performance after conditioning. The tensile strength decreased from 59.15 MPa for the reference specimens to 37.48 MPa after drying, corresponding to approximately 63% strength retention, while the wet-conditioned specimens maintained a higher tensile strength of 46.85 MPa, equivalent to approximately 79% retention. Similarly, the elastic modulus remained close to the reference value after wet conditioning, with approximately 99% modulus retention, whereas the dry specimens retained approximately 80% of their initial stiffness. The ultimate

tensile strain decreased from 1.19% to 0.70% and 0.71% for the dry and wet-conditioned specimens, respectively. The average stress–strain responses for both resin systems are presented in Figure 3.23.



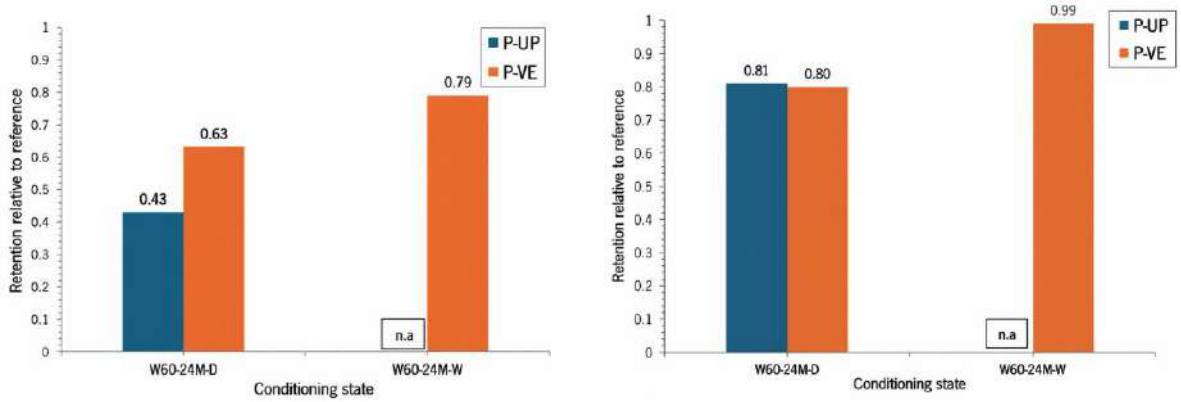
(a) P-UP specimens (b) P-VE specimens

Figure 3.23: Average tensile stress–strain curves of pultruded GFRP specimens in the 90° direction under different conditioning states.

The stress–strain curves shown in Figure 3.23 demonstrate that the transverse tensile response was more sensitive to environmental conditioning than the longitudinal elastic response. Compared with the 0° specimens, conditioning produced a more pronounced reduction in transverse elastic modulus, while reductions in tensile strength and ultimate tensile strain were also evident. The transverse response is governed more strongly by the polymer matrix and fibre–matrix interface, making it more susceptible to moisture-induced changes than the fibre-dominated longitudinal response. The P-UP specimens exhibited a substantial reduction in both ultimate tensile strength and strain, indicating significant degradation of the matrix-dominated load-transfer mechanism. In contrast, the P-VE specimens maintained higher tensile strengths after conditioning, particularly under wet conditions, confirming the superior resistance of the vinyl ester matrix to moisture-induced degradation.

Unlike the 0° specimens, where the longitudinal fibres dominate the mechanical response, the transverse tensile behaviour depends primarily on the integrity of the polymer matrix and the fibre–matrix interface. Moisture absorption therefore has a greater influence on crack initiation, interfacial debonding and matrix plasticisation, resulting in a more pronounced deterioration of the transverse tensile properties.

The normalised retention of the tensile properties is presented in Figure 3.24



(a) Ultimate tensile strength (b) Elastic modulus

Figure 3.24: Normalised retention of the 90° tensile properties of P-UP and P-VE specimens under different conditioning states. n.a = not available

The observed failure modes, classified according to EN ISO 527-4:1997 and presented in Figure 3.22, showed a transition from mainly gauge-section failures in the reference specimens to a combination of gauge and gripping-region failures after conditioning. The occurrence of LGM failures in the P-VE-WET specimens indicates that the modified specimen geometry effectively reduced premature grip-related failures.

3.5.3. In-plane shear tests

The in-plane shear test results were used to evaluate the influence of long-term hygrothermal ageing on the shear behaviour of the pultruded GFRP laminates. The evaluated parameters include the shear modulus (G), maximum in-plane shear stress ($\tau_{\max}$), shear strain at maximum shear stress ($\gamma_{\tau,\max}$), and the observed failure modes. The shear modulus was determined in accordance with ASTM D5379/D5379M:2012, using the shear stress–strain response between shear strain limits of $\gamma_1 = 0.25\%$ and $\gamma_2 = 0.65\%$. Complete individual test results and photographs of all tested specimens are presented in the Appendix.

The mean in-plane shear properties obtained for both resin systems under the different conditioning states are summarised in Table 3.5.

Table 3.5: Mean results of uniaxial in-plane shear tests for P-UP and P-VE specimens under reference and conditioned states.

Resin System	Series	G [GPa] [1]	τ_{max} [MPa] [1]	$\gamma_{\tau,max}$ [%] [1]	Mode of Failure [2]
Unsaturated Polyester	REF	2.89 (28.8%)	77.61 (2.7%)	3.13 (17.2%)	VGN (3), M(hv)GN (2)
	W60-24M-D	2.74 (14.7%)	42.09 (4.15%)	1.77 (7.1%)	VGN (2), M(hv)GN (4)
	W60-24M-W	2.42 (11.7%)	37.58 (4.0%)	1.76 (15.7%)	VGN (4), M(hv)GN (1)
Vinyl Ester	REF	2.90 (31.5%)	89.16 (3.1%)	4.07 (34.9%)	VGN (6)
	W60-24M-D	3.80 (15.3%)	71.18 (1.3%)	2.62 (11.9%)	VGN (6)
	W60-24M-W	3.95 (8.8%)	60.70 (4.0%)	2.15 (22.0%)	VGN (5), M(hv)GN (1)

Notes: [1] Values expressed in parentheses represent the corresponding coefficient of variation (CoV).
[2] Failure modes were classified according to ASTM D5379/D5379M-12. The values in parentheses indicate the number of specimens exhibiting each failure mode

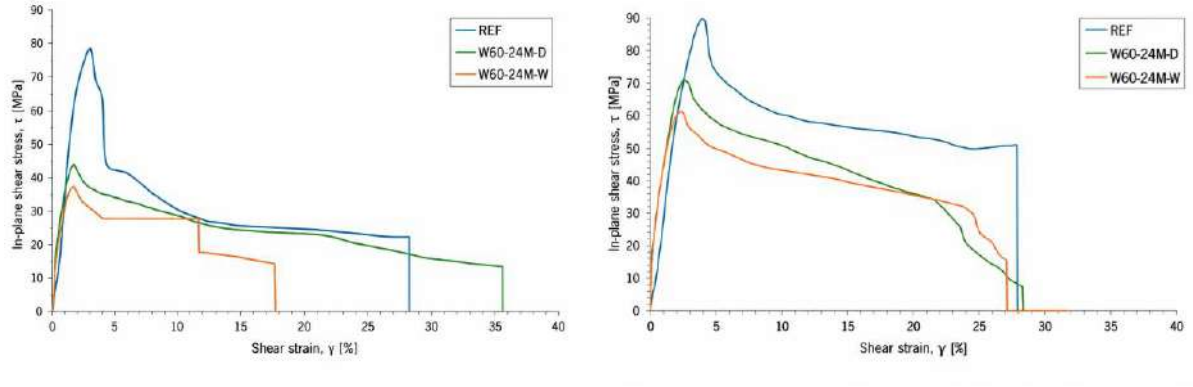
The results presented in Table 3.5 indicate that hygrothermal conditioning reduced the in-plane shear performance of both resin systems. Compared with the tensile properties in the longitudinal direction, the shear response exhibited greater sensitivity to environmental exposure, reflecting the increased dependence of shear loading on the integrity of the polymer matrix and the fibre–matrix interface.

For the P-UP specimens, the maximum shear stress decreased from 77.61 MPa for the reference specimens to 42.09 MPa and 37.58 MPa after dry and wet conditioning, corresponding to approximately 54% and 48% strength retention, respectively. The shear modulus decreased from 2.89 GPa to 2.74 GPa after drying and 2.42 GPa after wet conditioning. In contrast, the shear strain at maximum stress decreased from 3.13% to 1.77% and 1.76%, indicating a significant reduction in deformation capacity following long-term ageing.

The P-VE specimens initially exhibited higher in-plane shear properties than the P-UP specimens. The reference P-VE specimens achieved a maximum shear stress of 89.16 MPa, which decreased to 71.18 MPa after dry conditioning and 60.70 MPa when tested in wet conditions, corresponding to approximately 80% and 68% strength retention, respectively. Unlike the P-UP specimens, which exhibited a pronounced reduction in shear modulus after conditioning, the P-VE specimens showed an increase in shear modulus from 2.90 GPa in the reference condition to 3.80 GPa and 3.95 GPa after dry and wet conditioning, respectively. This behaviour may be associated with changes in matrix stiffness and moisture-induced effects within the polymer network. However, the shear strain at maximum stress

decreased from 4.07% for the reference specimens to 2.62% and 2.15% after dry and wet conditioning, respectively, indicating a reduction in deformation capacity following hygrothermal ageing.

The average in-plane shear stress–strain responses are presented in Figure 3.25.



(a) P-UP specimens (b) P-VE specimens

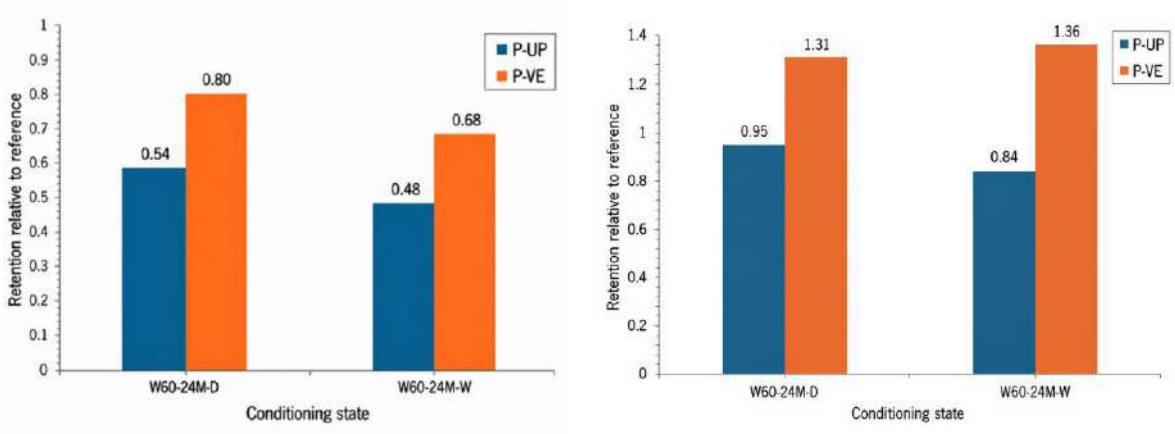
Figure 3.25: Average in-plane shear stress–strain curves of pultruded GFRP specimens under different conditioning states.

The stress–strain curves shown in Figure 3.25 demonstrate that hygrothermal conditioning significantly altered the in-plane shear behaviour of both resin systems. The reference specimens exhibited the highest peak shear stresses and the largest deformation capacities before failure, whereas both conditioned series showed lower peak stresses and earlier softening.

Unlike the tensile tests, where failure occurred almost immediately after reaching the ultimate load, the in-plane shear specimens exhibited progressive post-peak softening. This behaviour reflects the gradual development of matrix cracking, fibre–matrix debonding and local damage accumulation within the V-notched gauge section rather than catastrophic fracture. Consequently, the descending portions of the stress–strain curves represent progressive degradation of the load-carrying capacity during continued shear deformation.

The reduction in peak shear stress after conditioning indicates deterioration of the fibre–matrix interface resulting from moisture ingress. Water absorption promotes matrix plasticisation and hydrolytic degradation, weakening the interfacial bond responsible for transferring shear stresses between adjacent fibres and the surrounding resin. Consequently, the conditioned specimens exhibited lower shear strength and reduced shear strain capacity.

The normalised retention of the in-plane shear properties is presented in Figure 3.26.



(a) Shear strength (b) Shear modulus

Figure 3.26: Normalised retention of the in-plane shear properties of P-UP and P-VE specimens under different conditioning states.

The normalised retention results provide a direct comparison of the sensitivity of the two resin systems to the conditioning states. A clear difference was observed in shear-strength retention, with P-VE maintaining a substantially greater proportion of its reference strength than P-UP under both conditioning conditions. For both resin systems, the wet condition resulted in lower strength retention than the corresponding dried condition, indicating that residual moisture contributed to the reduction in shear performance. The results therefore demonstrate a stronger degradation response of P-UP in comparison with P-VE under the investigated hygrothermal exposure.

The normalised shear-modulus results showed a different response from shear strength. P-UP exhibited relatively high modulus retention despite the reduction in strength, whereas P-VE showed an apparent increase in modulus after conditioning. This contrast indicates that retention of stiffness does not necessarily imply retention of load-carrying capacity under ageing. The apparent increase in P-VE modulus should nevertheless be interpreted cautiously, considering the variability of the reference measurements and the absence of direct evidence confirming a post-curing mechanism.

Overall, the normalised results highlight that shear strength was considerably more sensitive to hygrothermal ageing than shear modulus, particularly for the P-UP system. They also demonstrate the importance of evaluating multiple mechanical properties when assessing the durability of GFRP composites, since changes in stiffness and strength may not follow the same trend.

Representative failure modes observed during the in-plane shear tests are presented in Figure 3.27

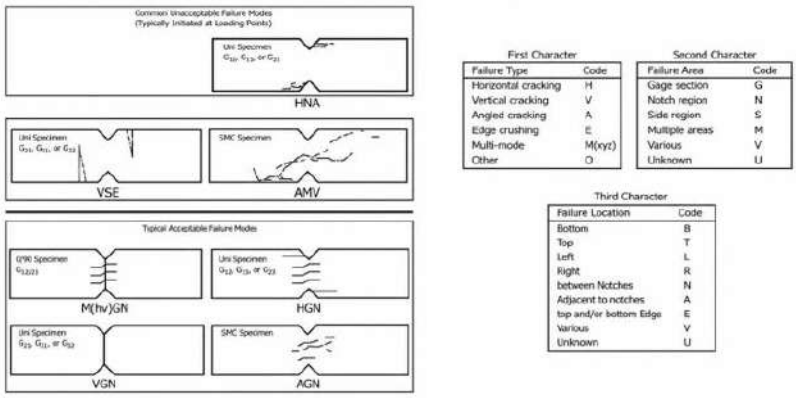


Figure 3.27: V-Notched Beam Shear Test Failure Codes and Typical Modes (adapted from ASTM D5379/D5379M-12).

The observed failure modes were predominantly classified as VGN (Vertical Gauge Notch) failures for both resin systems in the reference condition, indicating valid failures occurring within the gauge section in accordance with ASTM D5379/D5379M-12. Following conditioning, additional mixed failure modes, including M(hv)GN, became more frequent, particularly for the wet-conditioned specimens. These mixed failures indicate the development of both vertical and horizontal crack propagation within the gauge region as environmental degradation weakened the polymer matrix and fibre–matrix interface.

Despite the increased occurrence of mixed failure modes after conditioning, most failures remained concentrated within the V-notched gauge section, confirming that the adopted testing configuration provided reliable measurements of the in-plane shear behaviour.

3.5.4. Uniaxial compression

The results obtained from the uniaxial compression tests are presented and analysed in this section. The evaluated parameters include the maximum compressive load ($F_{\max}$), the corresponding maximum compressive stress ($\sigma_{\max}$), the displacement at maximum load ($\delta_{f,\max}$), and the observed failure modes. Owing to limitations associated with strain measurement during specimen loading, reliable strain data could not be obtained. Consequently, the analysis is based on the stress–displacement response and the maximum compressive stress recorded at failure. Complete individual test results and photographs of all tested specimens are presented in the Appendix.

The mean compressive properties of the reference and conditioned specimens are summarised in Table 3.6. Overall, prolonged hygrothermal ageing reduced the compressive performance of both resin systems. For the P-UP specimens, the maximum compressive stress decreased from 615.15 MPa in the reference

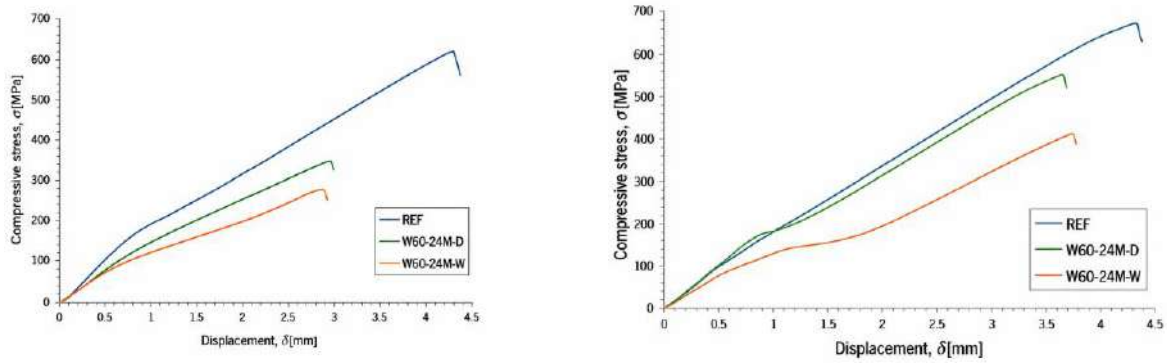
condition to 339.21 MPa and 270.09 MPa for the W60-24M-D and W60-24M-W conditions, respectively. Similarly, the P-VE specimens exhibited a reduction from 665.70 MPa to 554.01 MPa and 406.03 MPa after drying and wet conditioning, respectively. Although both resin systems experienced reductions in compressive strength after conditioning, the P-VE laminates maintained higher compressive strength than the corresponding P-UP specimens under all conditioning states.

Table 3.6: Mean results of the uniaxial compression tests for P-UP and P-VE specimens under different conditioning conditions.

Resin System	Series	F_{max} [kN] [1]	σ_{max} [MPa] [1]	$\delta_{f,max}$ [mm] [1]	Mode of Failure [2]
Unsaturated Polyester	REF	124.38 (9.4%)	615.15 (9.4%)	4.25 (7.5%)	Complex fracture (7)
	W60-24M-D	67.09 (4.9%)	339.21 (4.6%)	2.98 (8.3%)	Complex fracture (7)
	W60-24M-W	57.30 (12.2%)	270.09 (10.9%)	2.90 (13.5%)	Complex fracture (7)
Vinyl Ester	REF	134.57 (9.8%)	665.70 (10.0%)	4.27 (6.6%)	Complex fracture (7)
	W60-24M-D	109.56 (6.7%)	554.01 (6.8%)	3.54 (5.7%)	Complex fracture (7)
	W60-24M-W	81.91 (6.5%)	406.03 (6.4%)	3.83 (4.8%)	Complex fracture (7)

Notes: [1] Values expressed in parentheses represent the corresponding coefficient of variation (CoV).
[2] The values in parentheses indicate the number of specimens in which the respective failure mode occurred; n.a – not available

The average compressive stress–displacement curves for the P-UP and P-VE specimens are presented in Figure 3.28 For both resin systems, the conditioned specimens exhibited lower compressive stresses than the corresponding reference specimens throughout the loading process, confirming the detrimental influence of prolonged hygrothermal exposure. The reference specimens also maintained higher load-carrying capacity over a greater displacement range before failure, whereas the conditioned specimens reached lower peak stresses and failed at smaller displacements. The reduction in compressive response was particularly pronounced for the P-UP laminates, while the P-VE specimens retained a comparatively greater proportion of their original compressive behaviour.



(a) P-UP specimens (b) P-VE specimens

Figure 3.28: Average compressive stress–displacement curves of the pultruded GFRP specimens under different conditioning states.

To facilitate comparison between the two resin systems, the normalised compressive strength retention relative to the corresponding reference specimens is presented in Figure 3.29. The P-UP specimens retained approximately 55% and 44% of their reference compressive strength after drying and wet conditioning, respectively. In comparison, the P-VE specimens retained approximately 83% and 61% of their reference compressive strength after drying and wet conditioning, respectively, demonstrating substantially better resistance to hygrothermal degradation under compressive loading. These results indicate that the vinyl ester matrix provided greater protection against moisture-induced deterioration than the unsaturated polyester system.

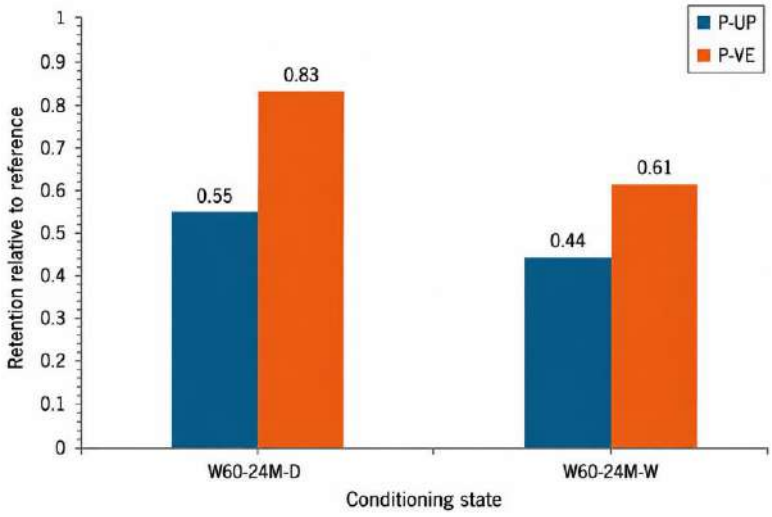


Figure 3.29: Normalised compressive strength retention of P-UP and P-VE specimens under dry and wet conditioning states relative to their respective reference series.

The observed failure modes following compression testing were classified according to the mechanisms illustrated in Figure 3.30, which include in-plane cut, complex fracture, continuous thickness shear,

splitting/dispersion, and delamination. All specimens predominantly exhibited complex fracture, irrespective of resin system or conditioning state. This failure mode is characterised by the simultaneous occurrence of several damage mechanisms during compressive loading, including fibre fracture, matrix cracking, local shear failure, and delamination. The consistency of this failure mode across all conditioning states indicates that hygrothermal ageing primarily reduced the laminates' compressive load-carrying capacity without significantly altering the dominant failure mechanism.

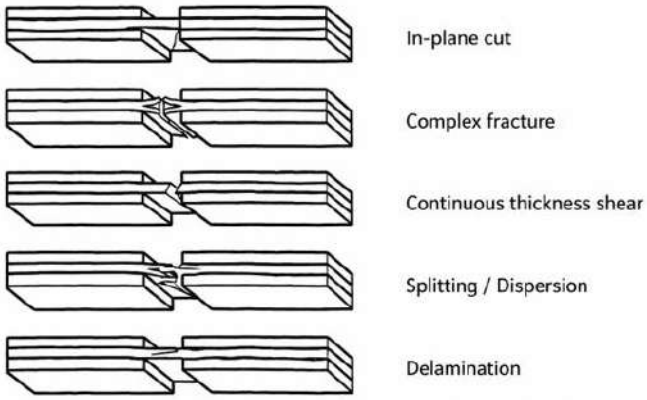


Figure 3.30: Failure modes observed during uniaxial compression tests (adapted from EN ISO 14126:2000).

3.5.5. Flexural tests

The results obtained from the three-point flexural tests are presented and analysed in this section. The evaluated parameters include the maximum applied load ($F_{\max}$), the corresponding maximum flexural stress ($\sigma_{\max}$), the displacement at maximum load ($\delta_{f,\max}$), and the observed failure modes.

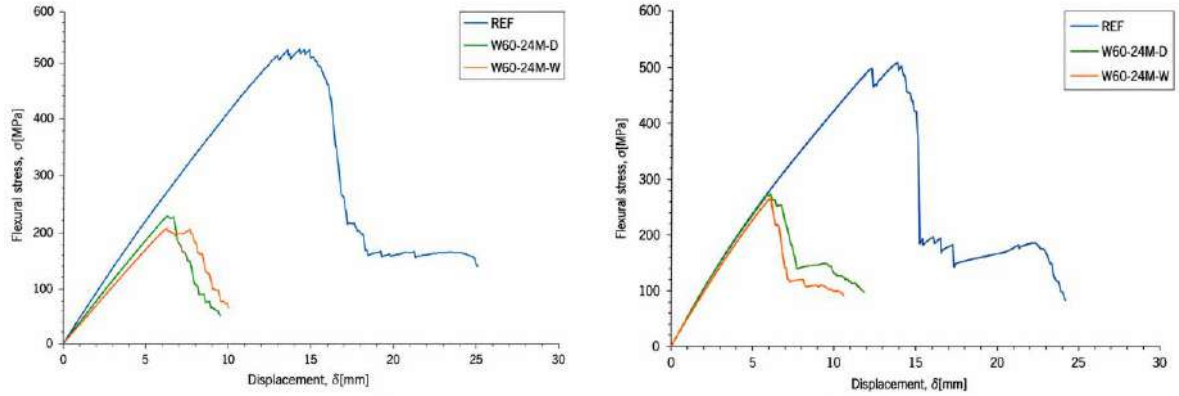
The analysis focuses on the stress–displacement response and the maximum flexural strength at failure. The mean flexural properties of the reference and conditioned specimens are summarised in Table 3.7, while complete individual test results and photographs of all tested specimens are presented in the Appendix. Overall, hygrothermal ageing resulted in a substantial reduction in the flexural strength of both resin systems. The P-UP specimens exhibited a reduction in maximum flexural stress from 520.35 MPa in the reference condition to 219.93 MPa and 207.69 MPa after drying and wet conditioning, respectively. Similarly, the P-VE specimens showed a reduction from 509.18 MPa to 274.79 MPa and 271.30 MPa for the dry and wet conditions, respectively.

Table 3.7: Mean results of the three-point flexural tests for P-UP and P-VE specimens under different conditioning conditions.

Resin System	Series	F_{max} [kN] [1]	σ_{max} [MPa] [1]	$\delta_{f,max}$ [mm] [1]	Mode of Failure [2]
Unsaturated Polyester	REF	2.08 (4.7%)	520.35 (8.4%)	13.86 (5.1%)	Tensile fracture of the fibre (6)
	W60-24M-D	0.86 (7.5%)	219.93 (8.7%)	6.11 (2.6%)	Tensile fracture at outermost layer (6)
	W60-24M-W	0.85 (7.2%)	207.69 (10.9%)	6.06 (4.4%)	Tensile fracture at outermost layer (6)
Vinyl Ester	REF	1.94 (16.6%)	509.18 (3.6%)	13.19 (6.2%)	Tensile fracture of the fibre (6)
	W60-24M-D	1.14 (8.5%)	274.79 (8.0%)	7.06 (2.7%)	Tensile fracture at outermost layer (6)
	W60-24M-W	1.14 (7.2%)	271.30 (6.4%)	7.20 (4.2%)	Tensile fracture at outermost layer (6)

Notes: [1] Values expressed in parentheses represent the corresponding coefficient of variation (CoV).
[2] The values in parentheses indicate the number of specimens in which the respective failure mode occurred; n.a – not available

The average flexural stress–displacement curves for the P-UP and P-VE specimens are presented in Figure 3.31. For both resin systems, the conditioned specimens exhibited lower peak flexural stresses than the corresponding reference specimens, confirming the detrimental effect of prolonged hygrothermal exposure. The reference specimens also maintained higher load-carrying capacity over a larger displacement range, whereas the conditioned specimens showed earlier softening and failure. The reduction in peak stress was more pronounced for the P-UP laminates, while the P-VE specimens retained a comparatively higher post-conditioning response.



(a) P-UP Specimens (b) P-VE Specimens

Figure 3.31: Average flexural stress–displacement curves of the pultruded GFRP specimens under different conditioning states

To facilitate comparison between the two resin systems, the flexural strength retention relative to the corresponding reference specimens is presented in Figure 3.32. The P-UP specimens retained approximately 42% and 40% of their reference flexural strength after drying and wet conditioning,

respectively. In comparison, the P-VE specimens retained approximately 54% and 53%, indicating superior retention after drying and comparable performance under wet conditions.

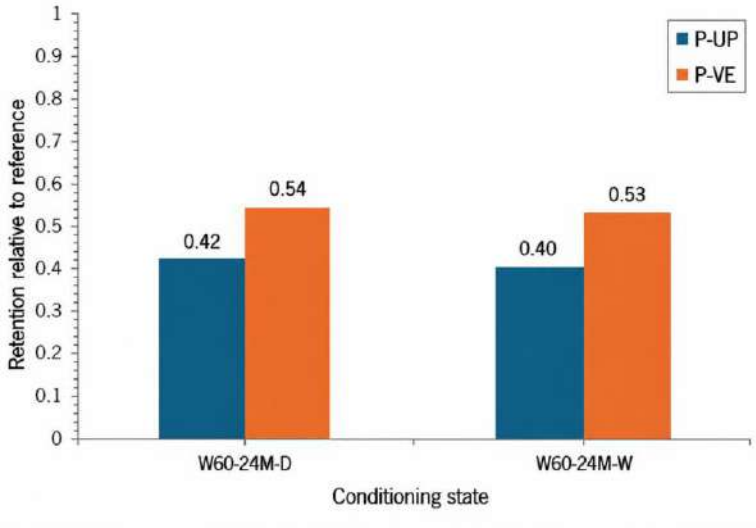


Figure 3.32: Normalised flexural strength retention of P-UP and P-VE specimens under dry and wet conditioning states relative to their respective reference series.

The failure modes observed during the flexural tests were classified according to the mechanisms presented in Figure 3.33. The reference specimens primarily exhibited tensile failure at the bottom surface, indicating that failure initiated in the region subjected to the highest tensile stress during bending. After conditioning, failure behaviour changed, with failures occurring mainly at the outermost layer and involving tensile and interlaminar mechanisms. These changes indicate that ageing affected the damage development process within the laminate, particularly in regions subjected to combined tensile and interlaminar stresses.

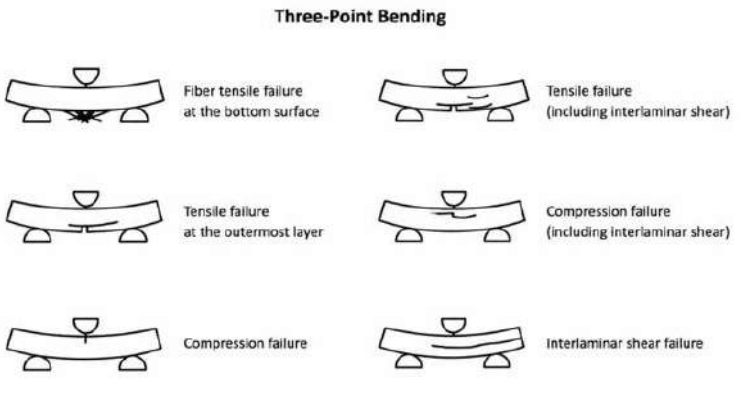


Figure 3.33: Failure modes observed during flexural tests (adapted from EN ISO 14125:1998).

Overall, the flexural results demonstrate that prolonged hygrothermal ageing significantly reduced the flexural performance of the pultruded GFRP laminates. Although both resin systems experienced

substantial degradation, the P-VE laminates generally exhibited better retention of flexural strength than the P-UP laminates, indicating greater resistance of the vinyl ester matrix to moisture-induced degradation under the investigated conditioning conditions.

3.5.6. Interlaminar shear test (short beam)

The results obtained from the interlaminar shear tests are presented and analysed in this section. The evaluated parameters include the maximum applied load ($F_{\max}$), the corresponding maximum interlaminar shear stress ($\tau_{\max}$), the displacement at failure ($\delta_{f,\max}$), and the observed failure modes. Owing to limitations associated with strain measurement during the tests, reliable strain data could not be obtained. Consequently, the analysis is based on the stress–displacement response and the maximum interlaminar shear stress recorded at failure. The mean interlaminar shear properties of the reference and conditioned specimens are summarised in Table 3.8.

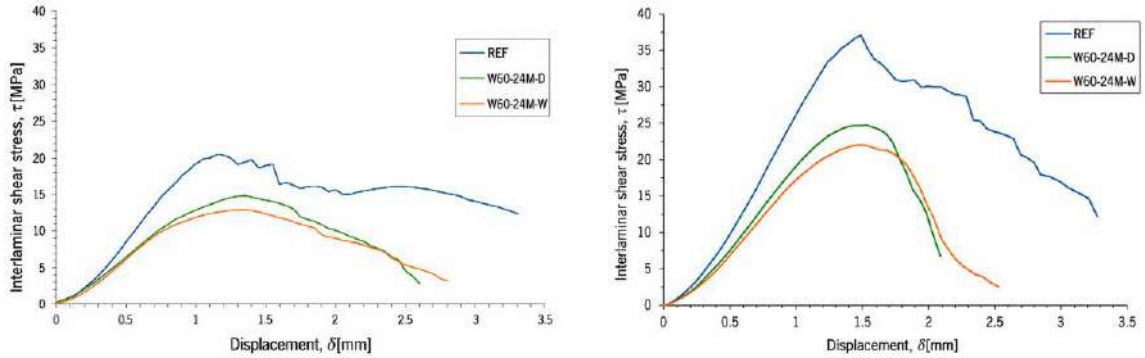
Table 3.8: Mean apparent interlaminar shear strength results from short-beam tests for P-UP and P-VE specimens under different conditioning conditions.

Resin System	Series	$F_{\max}$[kN] [1]	$\tau_{\max}$ [MPa] [1]	$\delta_{f,\max}$ [mm] [1]	Mode of Failure [2]
Unsaturated Polyester	REF	9.15 (9.0%)	21.32 (9.0%)	1.28 (15.56%)	Single Shear (3) Multiple Shear (2)
	W60-24M-D	6.27 (4.8%)	14.83 (4.71%)	1.42 (2.6%)	Single Shear (2) Multiple Shear (4)
	W60-24M-W	5.52 (9.45%)	12.92 (9.15%)	1.35 (5.78%)	Single Shear (3) Multiple Shear (3)
Vinyl Ester	REF	15.95 (2.74%)	37.18 (2.74%)	1.55 (4.8%)	Single Shear (2) Multiple Shear (4)
	W60-24M-D	10.67 (3.59%)	25.25 (3.3%)	1.59 (6.15%)	Tension (6)
	W60-24M-W	9.81 (2.65%)	22.59 (2.39%)	1.61 (6.21%)	Tension (6)

Notes: [1] Values expressed in parentheses represent the corresponding coefficient of variation (CoV).
[2] The values in parentheses indicate the number of specimens in which the respective failure mode occurred; n.a – not available.

Overall, hygrothermal ageing reduced the interlaminar shear performance of both resin systems. For the P-UP specimens, the maximum interlaminar shear stress decreased from 21.32 MPa in the reference condition to 14.83 MPa and 12.92 MPa for the W60-24M-D and W60-24M-W conditions, respectively. Similarly, the P-VE specimens exhibited a reduction from 37.18 MPa to 25.25 MPa and 22.59 MPa after drying and wet conditioning, respectively. Although both resin systems experienced a reduction in interlaminar shear strength following conditioning, the P-VE laminates maintained higher absolute interlaminar shear strength under all conditioning states.

The average interlaminar shear stress–displacement curves for the P-UP and P-VE specimens are presented in Figure 3.34. For both resin systems, the conditioned specimens exhibited lower peak interlaminar shear stresses than the corresponding reference specimens, confirming the detrimental influence of prolonged hygrothermal exposure. The reference specimens also maintained higher load-carrying capacity over a greater displacement range, whereas the conditioned specimens exhibited earlier softening and failure. The reduction in peak stress was evident for both resin systems, with the P-UP laminates showing a greater reduction after conditioning.



(a) P-UP specimens (b) P-VE specimens

Figure 3.34: Average interlaminar shear stress–displacement curves of the pultruded GFRP specimens under different conditioning states.

To facilitate comparison between the two resin systems, the normalised interlaminar shear strength retention relative to the corresponding reference specimens is presented in Figure 3.35. The P-UP specimens retained approximately 70% and 61% of their reference interlaminar shear strength after drying and wet conditioning, respectively. The P-VE specimens retained approximately 68% and 61%, indicating that both resin systems experienced comparable relative reductions after prolonged hygrothermal ageing.

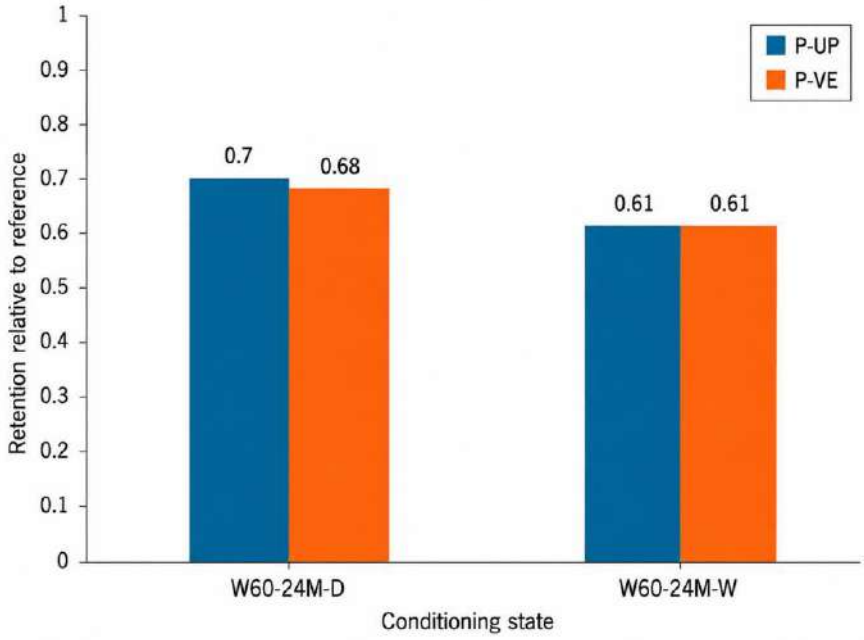


Figure 3.35: Normalised interlaminar shear strength retention of P-UP and P-VE specimens under dry and wet conditioning states relative to their respective reference series.

The observed failure modes were classified according to the criteria illustrated in Figure 3.36, where single shear and multiple shear failures are considered acceptable interlaminar shear failure modes. The reference P-UP specimens predominantly exhibited combinations of single and multiple shear failures, indicating that failure occurred primarily through interlaminar shear. Following conditioning, the P-UP specimens continued to exhibit acceptable shear failure modes, although an increased occurrence of multiple shear failures was observed.

In contrast, the conditioned P-VE specimens predominantly exhibited tensile failure rather than interlaminar shear failure. This indicates that hygrothermal exposure may have altered the failure behaviour of the laminate; however, the absence of a consistent interlaminar shear failure mode suggests that the calculated values should be interpreted with caution. The premature tensile failures may have limited the ability of the specimens to develop a characteristic interlaminar shear failure, and therefore the measured values may not fully represent the intrinsic interlaminar shear strength of the conditioned P-VE laminates.

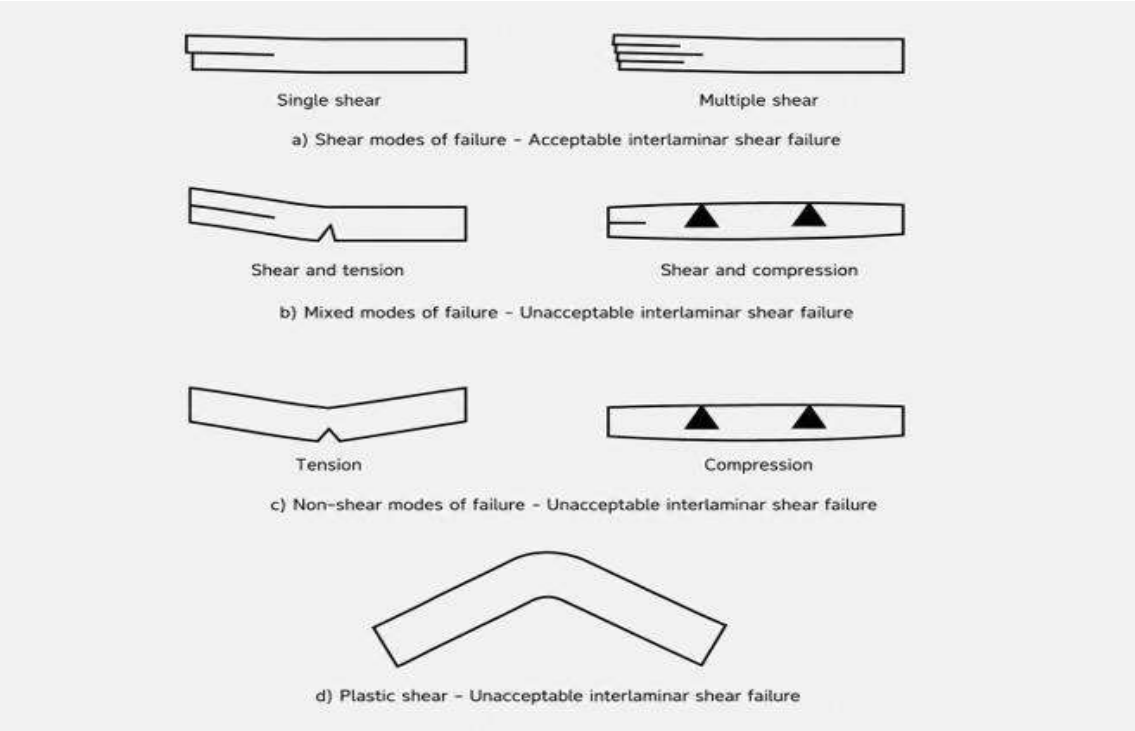


Figure 3.36: Classification of failure modes observed during interlaminar shear testing (adapted from ASTM D2344/D2344M).

Overall, the interlaminar shear results demonstrate that prolonged hygrothermal ageing reduced the interlaminar shear performance of both pultruded GFRP laminates. Although both resin systems exhibited similar relative reductions in interlaminar shear strength, the P-VE laminates maintained higher absolute strength throughout the conditioning programme. The observed changes in failure mode further indicate that hygrothermal ageing influenced the damage mechanisms within the laminate, particularly by contributing to premature tensile failure in some conditioned P-VE specimens, which limited the occurrence of the intended interlaminar shear failure mode.

THIS PAGE WAS INTENTIONALLY LEFT BLANK

4. Physics-Informed Neural Network Study

4.1. Introduction and Modelling Rationale

This chapter develops and evaluates a Bayesian physics-informed neural network (BPINN) for predicting the tensile-strength retention of pultruded glass fibre-reinforced polymer (GFRP) composites subjected to environmental ageing. Two resin systems are considered: unsaturated polyester (P-UP) and vinyl ester (P-VE), with longitudinal (0°) and transverse (90°) fibre orientations, under dry and wet conditioning conditions at three exposure temperatures and four exposure durations.

The engineering question addressed in this analysis is fundamentally a service-life question: how much of its original tensile capacity will the material retain after extended periods of service under temperature and exposure conditions that have not been directly tested? Addressing this question requires extrapolation, and extrapolation represents a critical limitation of purely empirical models. Therefore, the modelling strategy adopted in this study combines three key components:

1. A flexible statistical learner. A neural network is employed to capture systematic variations associated with resin systems, fibre orientations, and conditioning states that cannot be fully represented by a single closed-form equation.
2. An embedded degradation law. An Arrhenius–Weibull governing relationship is incorporated as a soft physical constraint across the temperature–time domain, including regions where experimental measurements are unavailable. This constraint provides physical consistency during extrapolation beyond the measured experimental domain.
3. A Bayesian treatment. The network weights and physical parameters are represented as probability distributions rather than single deterministic values, allowing predictions to be accompanied by credible intervals and enabling the apparent activation energy to be estimated together with its associated uncertainty.

The Bayesian formulation provides additional practical value by quantifying the confidence associated with model predictions. A deterministic model may provide a degradation curve; however, it does not indicate the extent to which that prediction is supported by the available experimental evidence. For long-term service-life projections extending beyond the available experimental duration, the ability to quantify prediction uncertainty is essential. Section 4.11 demonstrates that establishing a trustworthy estimate of

prediction confidence requires careful evaluation beyond simply obtaining a model prediction and presents the procedures adopted to assess uncertainty calibration.

To enable a meaningful assessment of the contribution of the Bayesian formulation, a deterministic Arrhenius–Weibull model with identical physical assumptions is developed using the same dataset and evaluated under the same validation protocol. This reference model is presented in Section 4.3.8, while the comparison between the Bayesian and deterministic approaches is discussed in Section 4.12.

The chapter is organised as follows. Section 4.2 describes the dataset and the definition of tensile-strength retention. Section 4.3 presents the modelling methodology, including the neural network architecture, Bayesian formulation, governing physical model, imposed constraints, training objective, and deterministic reference model. Sections 4.4 to 4.9 describe the model fitting strategy, training behaviour, identification of physical parameters, assessment of physics-based constraints, in-sample performance evaluation, and fitted degradation curves. Section 4.10 presents the leakage-safe validation procedure used to evaluate model predictive performance. Section 4.11 examines uncertainty calibration and reproducibility, while Section 4.12 compares the performance of the Bayesian and deterministic models. Section 4.13 presents the long-term durability projection. Finally, Section 4.14 discusses the limitations of the modelling approach, and Section 4.15 summarises the principal findings of the chapter.

4.2. Dataset

4.2.1. Composition and response variable

The dataset was compiled from experimental investigations on the durability of pultruded GFRP composites previously conducted at the University of Minho[51],[52] together with the experimental results obtained in the present study. The tensile dataset comprises 312 specimen-level observations: 37 unaged reference coupons and 275 aged coupons. Only the raw measured tensile strength (column 'Tensile Strength') was used as the modelling response. Any retention values already present in the source file were deliberately excluded from the modelling pipeline; retention is computed internally from raw strengths so that the normalisation is transparent and reproducible.

For an aged coupon, tensile-strength retention is defined relative to the mean strength of the corresponding unaged reference population of the same resin and fibre orientation:

$$R = \frac{\sigma_{aged}}{\overline{\sigma}_{ref}} \tag{4.1}$$

where $\overline{\sigma}_{ref}$ is the mean tensile strength of the matching reference group. Reference populations are defined by resin and orientation only; conditioning state and exposure temperature do not apply to unaged material.

Table 4.1: Composition of the tensile modelling dataset.

Dataset component	Count
Total tensile observations	312
Unaged reference coupons	37
Aged coupons	275
Independent aged exposure settings	54
Material-condition cells	8
Resin systems	2
Fibre orientations	2
Conditioning states	2
Exposure temperatures	3
Exposure durations	4

4.2.2. Reference populations

The four reference populations and their descriptive statistics are given in Table 4.2. The large difference between longitudinal and transverse strength reflects the dominant role of fibre orientation in the tensile response. The low coefficients of variation for the 0° groups indicate good repeatability, although the PVE 0° reference population contains only five coupons and therefore carries greater uncertainty in its mean. That uncertainty is not ignored: the reference mean is treated as a Student-t distributed quantity when raw strengths are reconstructed from predicted retention.

Table 4.2: Reference tensile-strength statistics by resin and fibre orientation.

Reference group	n	Mean [MPa]	SD [MPa]	SE [MPa]	CoV [%]
PUP — 0°	12	415.097	10.910	3.149	2.63
PUP — 90°	10	53.989	4.847	1.533	8.98
PVE — 0°	5	456.414	10.175	4.550	2.23
PVE — 90°	10	60.947	2.919	0.923	4.79

4.2.3. Exposure settings and replicate balancing

A critical distinction is made between the number of coupons and the amount of independent environmental information. Although 275 aged coupons are available, they represent only 54 distinct exposure settings, where a setting is the unique combination of resin, orientation, conditioning state, temperature and duration. The remaining coupons are replicates. Replicates quantify within-group experimental scatter but do not add new ageing conditions; the number of independent conditions governs how well a temperature–time degradation trend can be identified. The distribution of independent exposure settings across the investigated temperatures and the corresponding baseline prediction errors are summarised in Table 4.3.

Because the number of replicates differs between settings, unweighted coupon-level fitting would allow heavily replicated settings to dominate calibration. Each coupon likelihood is therefore weighted by the reciprocal of its group size, so that every exposure setting contributes equally to the objective regardless of how many coupons it contains.

Table 4.3: Exposure design by temperature, with the error of a constant-mean predictor for reference.

Exposure temperature	Number of exposure settings [n]	Constant-mean baseline RMSE [pp]
293.15 K (20 °C)	16	16.88
313.15 K (40 °C)	16	9.77
333.15 K (60 °C)	22	25.88

The four exposure durations are 91.3125, 182.625, 365.25, 730.5 days, corresponding to approximately three months, six months, one year and two years. The longest exposure measured is therefore two years, which should be kept in view when reading the 50-year projection in Section 4.13.

4.3. Methodology

4.3.1. Overview

The BPINN learns the logarithm of retention as a function of the material-condition indicators and the exposure variables:

$$u_\theta(x) = \log R(x), x = [c, 1/T, \log(1+t)] \tag{4.2}$$

where c is the one-hot encoding of resin, orientation, and conditioning state. The two continuous inputs are entered as t, inverse temperature $1/T$ and the transformed duration $log(1+t)$, each standardised on the training set. The inverse temperature is used because it is the natural argument of the Arrhenius relation; the logarithmic time transform is used because degradation data span durations differing by an order of magnitude. The overall architecture of the proposed BPINN framework is illustrated in Figure 4.1. The framework consists of the neural network prediction pathway, the embedded Arrhenius–Weibull degradation relationship, the imposed physical constraints, and the combined optimisation objective used during model training.

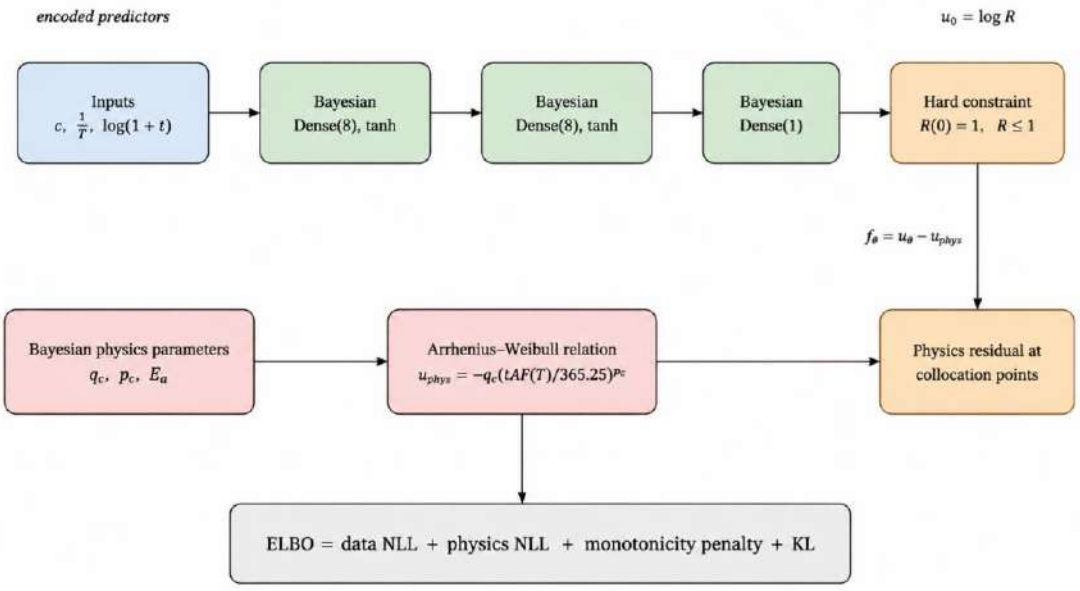


Figure 4.1: Schematic representation of the variational Bayesian physics-informed neural network (BPINN), showing the neural network prediction pathway, embedded Arrhenius–Weibull degradation relation, imposed physical constraints and combined training objective.

4.3.2. Bayesian neural network and variational inference

Unlike a conventional neural network, where the weights and biases are represented by fixed values, a Bayesian neural network (BNN) treats these parameters as probability distributions. This formulation allows the model to capture uncertainty in the learned relationships between the input variables and the predicted tensile-strength retention. Therefore, the BPINN provides not only a mean prediction but also an estimation of the confidence associated with that prediction.

The Bayesian treatment is particularly relevant for durability modelling because experimental ageing datasets are often limited in terms of exposure duration and environmental conditions. When predictions are extended beyond the measured experimental range, uncertainty associated with model parameters and limited observations becomes increasingly important. Representing the network parameters probabilistically enables this uncertainty to be propagated into the final predictions.

Since the exact posterior distribution of the network parameters is computationally difficult to obtain for neural networks, variational inference is adopted to approximate the posterior distribution. In this approach, a parameterised probability distribution is optimised to represent the uncertainty in the network weights by balancing agreement with the experimental data and consistency with the assumed prior distribution.

In this study, the variational Bayesian framework provides a probabilistic representation of tensile-strength retention degradation and enables uncertainty quantification during long-term extrapolation. This allows the predicted degradation behaviour to be interpreted together with the associated confidence level rather than as a single deterministic prediction.

4.3.3. Governing degradation relation

Temperature enters through an Arrhenius acceleration factor, which expresses the central assumption of accelerated ageing: that raising the temperature is equivalent to extending the exposure time.

$$AF(T) = \exp\left[\frac{E_a}{R_g}\left(\frac{1}{T_{ref}} - \frac{1}{T}\right)\right] \tag{4.5}$$

Here R_g is the universal gas constant (8.3145 J mol^{-1} K^{-1}) and T_{ref} is the reference temperature of 298.15 K.

The acceleration factor is applied to the exposure duration, and the resulting effective time drives a Weibull-type degradation law:

$$u_{phys}(t, T, c) = -q_c \left(\frac{tAF(T)}{365.25} \right)^{p_c} \tag{4.6}$$

The degradation rate q_c and the shape exponent p_c are indexed by the material-condition cell c, allowing the eight resin–orientation–condition combinations to degrade at different rates and with different curve shapes. The activation energy is shared across all material-condition cells, representing the assumption that a common apparent activation energy can approximate the temperature sensitivity of the degradation process within the investigated composite system. This structure is deliberately the same as that of the deterministic hierarchical model reported earlier, so that the two analyses differ in inference method rather than in physical content.

4.3.4. Hard constraints

Two physical requirements are enforced exactly by construction rather than by penalty. Retention must equal unity at zero exposure, and it must never exceed unity. Both follow from the output parameterisation:

$$u_\theta(t) = -\frac{\log(1+t)}{s} \text{softplus}(g_\theta(x)), u_\theta(0) = 0, u_\theta \leq 0 \tag{4.7}$$

where s is a fixed scale set by the longest training duration and g_θ is the raw network output. The softplus guarantees non-positive log-retention, and the leading factor vanishes at $t = 0$. Because these are structural, they hold for every posterior sample without any tuning, and they are verified numerically in Section 4.7.

A third requirement — that strength must not recover with time — is imposed as a penalty rather than structurally, because it constrains a derivative:

$$\mathcal{P}_{mono} = \frac{1}{N_c} \sum_{j=1}^{N_c} \left[\max\left(0, \frac{\partial u_\theta}{\partial \log(1+t)}\right) \right]^2 \tag{4.8}$$

The derivative is obtained by automatic differentiation at the collocation points, and only positive values are penalised. This constraint reflects the irreversible nature of environmental degradation, where tensile-

strength retention is expected to decrease or remain constant with increasing exposure duration rather than exhibit artificial recovery during prediction.

4.3.5. Training objective

The complete objective combines four terms:

$$\mathcal{L} = \mathcal{L}_{data} + \lambda_{phys}\mathcal{L}_{phys} + \lambda_{mono}\mathcal{P}_{mono} + \frac{\beta}{N_g} D_{KL} \tag{4.9}$$

in which λ_{phys} and λ_{mono} weight the physics and monotonicity terms, D_{KL} is the Kullback–Leibler divergence of the posterior from the prior, N_g is the number of independent exposure settings, and β is the warm-up coefficient. The data term represents the agreement between model predictions and experimental observations while accounting for variability within the dataset.

$$\mathcal{L}_{data} = \frac{1}{\sum_i \omega_i} \sum_i \omega_i \left[\frac{\left(y_i - u_{\theta,i}\right)^2}{2\sigma_{obs}^2} + \log\sigma_{obs} + \frac{1}{2}\log 2\pi \right] \tag{4.10}$$

and the physics term measures disagreement with the governing relation:

$$\mathcal{L}_{phys} = \frac{1}{2\sigma_{phys}^2} \cdot \frac{1}{N_c} \sum_{j=1}^{N_c} \left(u_{\theta,j} - u_{phys,j}\right)^2 \tag{4.11}$$

where ω_i are the replicate-balancing weights of Section 4.2.3 and σ_{obs} is the learned coupon-level scatter on the log-retention scale. The physics term provides the main mechanism for introducing degradation behaviour consistent with the governing physical relationship: at each iteration, a fresh batch of 128 collocation points is drawn at random across the entire temperature–time domain — not only where measurements exist — and the network output is compared with the governing relation at those points. This is what propagates physical structure into regions of the design space that contain no data, and it provides the basis on which extrapolation beyond the measured domain rests.

The KL term is divided by the number of independent exposure settings so that the objective is correctly scaled as a per-setting evidence lower bound rather than a per-coupon one.

4.3.6. Predictive quantities

Three distinct predictive distributions are reported. They differ in the sources of uncertainty they incorporate, and the distinction is material to the interpretation of the accuracy figures presented later in this chapter. Each is obtained by sampling the posterior:

$$u_\theta, u_\theta + \frac{\sigma_{obs}}{\sqrt{n_{rep}}}\varepsilon, u_\theta + \sigma_{obs}\varepsilon, \varepsilon \sim \mathcal{N}(0,1) \tag{4.12}$$

where ε is a standard normal variate and n_{rep} is the number of replicate coupons averaged to form the measured group mean. The three predictive quantities considered for uncertainty evaluation are summarised in Table 4.4.

Table 4.4: The three predictive intervals reported by the model.

Predictive quantity	Sources of uncertainty included	Appropriate use
Mean curve	Posterior parameter uncertainty only	The latent degradation trend
Group mean	Parameter uncertainty + $\sigma_{obs}/\sqrt{n_{rep}}$	Comparison with a measured group mean of n_{rep} coupons — the correct calibration test
Single coupon	Parameter uncertainty + σ	Prediction of one new individual coupon

This distinction matters directly. Every measured point plotted in this chapter is itself the mean of several replicate coupons, and its own sampling error is $\sigma_{obs}/\sqrt{n_{rep}}$. Comparing such a point against the mean-curve interval, which contains no measurement error at all, systematically understates coverage; comparing it against the single-coupon interval, which contains the full coupon scatter, systematically overstates it. The group-mean interval is the matched comparison, and it is the one used for all calibration statements in Section 4.11.

Predicted retention is converted back to raw tensile strength by multiplying by the reference mean, which is itself sampled from its Student-t posterior so that reference-population uncertainty propagates into the predicted strength:

$$\hat{\sigma}_{tensile} = R \cdot \overline{\sigma}_{ref} \tag{4.13}$$

This conversion allows the model-predicted retention values to be expressed in terms of tensile strength, enabling direct comparison with experimental measurements.

4.3.7. Model configuration

The two settings with the greatest influence on model performance, namely the training duration and initial posterior spread, were selected based on leave-one-temperature-out validation rather than training loss alone, as discussed in Section 4.11.

Table 4.5 lists the configuration used for all reported results. The two settings with the greatest influence on model performance, namely the training duration and initial posterior spread, were selected based on leave-one-temperature-out validation rather than training loss alone, as discussed in Section 4.11.

Table 4.5: Model configuration used for all reported results

Setting	Value	Role
Hidden layers × width	2 × 8 (tanh)	Deliberately small; physics carries much of the structure
Prior standard deviation	1.0	Weight prior
Initial posterior spread ρ_0	-3.0	Starting width of each variational posterior
Training epochs	400	Selected by held-out validation
Learning rate	3e-03	Adam optimiser
Collocation points per epoch	128	Where physics is enforced
Physics scale σ_{phys}	0.012	Tolerance on governing-equation agreement
Monotonicity weight	5	Penalty on strength recovery
KL warm-up epochs	120	Delays regularisation
Ensemble members	10	Independence fits pooled for all reported results

Table 4.6: Parameter counts of the Bayesian model

Quantity	Count
Bayesian neural weights and biases	153
Bayesian physical parameters	17
Total random parameters	170
Trainable variational values	341

The parameter composition of the Bayesian model is summarised in Table 4.6. The model contains 170 random parameters represented by 341 trainable variational values, consisting of a mean and a spread for each parameter. Although the number of parameters is relatively large compared with the number of independent exposure settings, the Bayesian formulation, physical constraints, and group balancing strategy help to regularise the estimation process.

4.3.8. Deterministic reference model

To establish what the Bayesian treatment contributes, a deterministic model with identical physical content is fitted to the same data. It uses the same acceleration factor, the same Weibull degradation form, and the same per-cell parameterisation with a single shared activation energy, so that the two models differ in how their parameters are estimated and in what they report, but not in the physics they assume.

The deterministic model is fitted by robust nonlinear least squares on the log-retention scale, using a soft-L1 loss to limit the influence of outlying exposure settings, with parameters bound to physically admissible ranges and twenty-four random initialisations retained by best objective value. It is fitted to the same group-balanced exposure settings and validated under the identical leave-one-temperature-out protocol described in Section 4.10.1. We estimate uncertainty in its activation energy by bootstrap resampling of the exposure settings, the standard approach for a deterministic fit.

4.4. Ensemble Fitting Strategy

All Bayesian results reported in this chapter are produced by pooling the posterior draws of 10 independently initialised fits rather than by a single training run. The justification is empirical and is set out in full in Section 4.11.2: A single variational fit can be sensitive to random initialisation, which may influence the estimated parameters and uncertainty intervals. Therefore, the reported Bayesian results are obtained by combining the posterior distributions from 10 independently initialised model runs. This ensemble approach improves reproducibility and provides more stable estimates of the predicted quantities. An interval narrower than the reproducibility of the procedure that generates cannot be quoted as a statement of uncertainty, so the reproducibility of the reported result is treated here as a property to be verified rather than assumed.

Pooling independently fit is the standard remedy. Mean-field variational inference is known to under-disperse — it finds one mode of the posterior and reports its local curvature — and an ensemble of independently initialised runs samples across modes. The ensemble does not make individual predictions more accurate in this application; the held-out error (9.58 pp) is statistically indistinguishable from the seed-averaged error of single fits (9.19 ± 0.90 pp). Its purpose is to show that the reported result is independent of the seed used, and that the reported intervals widen accordingly.

4.5. Training Behaviour

Figure 4.2 shows the evolution of the objective components for a representative member. The physics residual falls by roughly three orders of magnitude within the first few tens of epochs, as the network is pulled onto the Arrhenius–Weibull manifold, after which the data term continues to improve more slowly. The learned coupon scatter σ_{obs} settles at approximately 0.148 on the log-retention scale, corresponding to roughly 15.9% coupon-to-coupon variability, which is consistent with the measured within-group scatter of the experimental campaign.

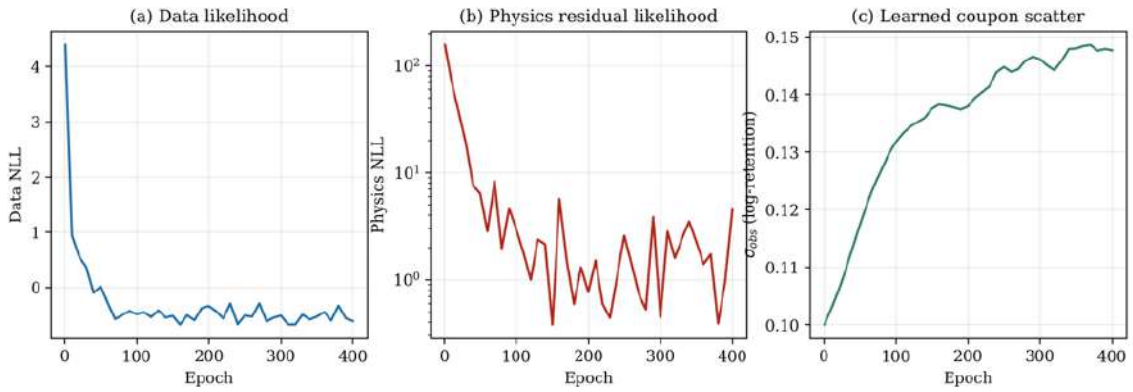


Figure 4.2: Evolution of the training objective: (a) data negative log-likelihood, (b) physics-residual negative log-likelihood on a logarithmic axis, and (c) the learned coupon scatter.

The visible noise in the traces is expected and not a sign of instability: each epoch draws a fresh Monte Carlo sample of the weights and a fresh batch of collocation points, so the objective is stochastic by construction.

4.6. Inferred Physical Parameters

The posterior estimates of the degradation parameters for each material-condition combination are summarised in Table 4.7. The degradation-rate parameters show relatively narrow variation across the eight cells, reflecting the limited number of independent exposure conditions available for each

combination. Since the same temperature and duration levels are shared across different resin systems, fibre orientations, and conditioning states, the available data do not provide sufficient evidence to conclude that one specific material configuration exhibits significantly different degradation kinetics from another at the 90% credible level.

Table 4.7: Posterior degradation-rate and shape parameters by material-condition cell (ensemble-pooled draws).

Material-condition cell	q [median]	q 90% interval	p [median]	p 90% interval
PUP | 0° | Dry	0.0773	[0.0669, 0.0878]	0.661	[0.604, 0.710]
PUP | 0° | Wet	0.0826	[0.0650, 0.0919]	0.651	[0.610, 0.718]
PUP | 90° | Dry	0.0719	[0.0622, 0.0861]	0.634	[0.599, 0.674]
PUP | 90° | Wet	0.0727	[0.0654, 0.0834]	0.649	[0.594, 0.696]
PVE | 0° | Dry	0.0736	[0.0658, 0.0816]	0.643	[0.609, 0.681]
PVE | 0° | Wet	0.0733	[0.0652, 0.0851]	0.642	[0.596, 0.702]
PVE | 90° | Dry	0.0712	[0.0630, 0.0798]	0.627	[0.581, 0.668]
PVE | 90° | Wet	0.0698	[0.0620, 0.0800]	0.629	[0.591, 0.673]

The influence of ensemble averaging on the estimated apparent activation energy is evaluated by comparing the ensemble-pooled posterior with a single variational model fit. The resulting estimates and associated uncertainty intervals are presented in Table 4.8. The ensemble approach produces a slightly wider uncertainty interval, reflecting the variability between independent model initialisations, while providing a more reproducible estimate of the degradation parameter.

Table 4.8: Apparent activation energy: ensemble-pooled posterior versus a single variational fit.

Estimate	Median [kJ/mol]	90% interval [kJ/mol]	Interval width
Ensemble-pooled (reported)	54.11	[51.14, 57.14]	6.00
Single variational fit (reference)	53.65	[51.07, 56.25]	5.18

The posterior distributions of the degradation-rate parameter, degradation-shape parameter, and apparent activation energy obtained from the ensemble of Bayesian models are presented in Figure 4.3. These parameters describe the inferred degradation behaviour of the different material-condition combinations and provide insight into the uncertainty associated with the adopted physics-informed formulation.

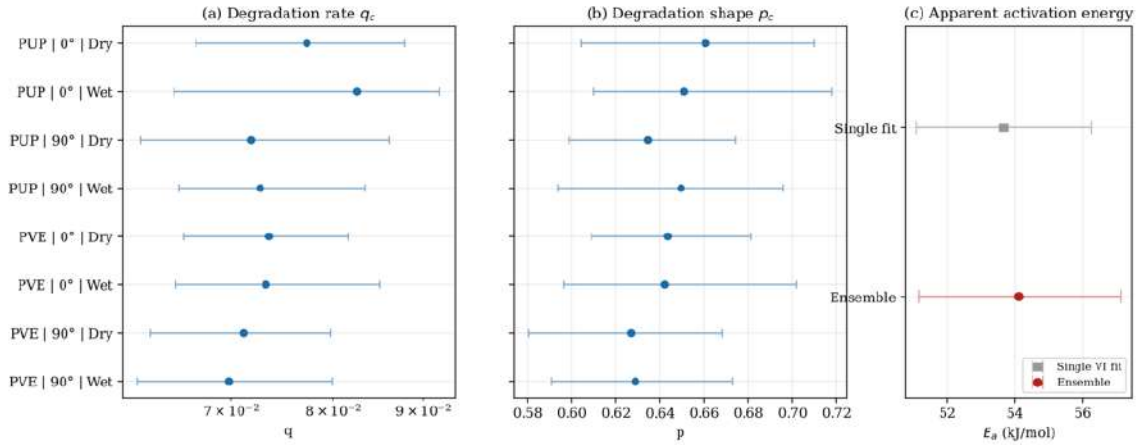


Figure 4.3: Posterior physical parameters with 90% credible intervals: (a) degradation rate q by cell, (b) shape exponent p by cell, and (c) the global apparent activation energy, comparing the ensemble-pooled posterior with a single variational fit.

The apparent activation energy obtained from the ensemble model was 54.1 kJ/mol, with a 90% credible interval between 51.1 and 57.1 kJ/mol. The wider interval compared with the single-fit estimate reflects the variability between independently trained Bayesian models. However, the estimated range remains relatively narrow, indicating good consistency of the temperature-acceleration behaviour captured by the ensemble approach. It should be noted that this apparent activation energy represents a temperature-dependent fitting parameter within the adopted Arrhenius formulation and should not be interpreted as direct evidence of a single physical degradation mechanism.

4.7. Physics-Constraint Audit

Before any predictive accuracy is reported, the physical constraints introduced in Section 4.3.4 were verified numerically on a dense grid spanning all material-condition cells and the complete temperature–time domain. The results of this constraint audit are summarised in **Error! Switch argument not specified.**.

Table 4.9: Numerical audit of the embedded physical constraints.

Constraint	Requirement	Measured value	Status
Initial condition $R(0)$ = 100%	Boundary error = 0	0.00e+00	Satisfied exactly
Monotonic degradation	No positive time-gradient	0.000 of grid points	Satisfied
Governing-equation agreement	RMSE $\lesssim \sigma_{phys}$ = 0.012	0.0150 (log-retention)	Consistent

The first two constraints hold to machine precision because they are structural rather than penalised. The third is a soft constraint, and the achieved residual is of the same order as the tolerance σ_{phys}, indicating that the network is genuinely tracking the governing relation rather than ignoring it.

4.8. In-Sample Posterior Diagnostics

The quantities reported in this section are computed using the same exposure settings used during model fitting and therefore represent diagnostic measures rather than independent estimates of predictive accuracy. The resulting in-sample performance indicators and uncertainty coverage metrics are summarised in Table 4.10. They are presented because they expose systematic structure in the residuals that held-out summaries would obscure. The predictive accuracy of the model is established in Section 4.10, using leakage-safe leave-one-temperature-out validation

Table 4.10: In-sample posterior diagnostics (not an unbiased estimate of predictive accuracy)

Diagnostic	Value
RMSE (percentage points)	8.45
MAE (percentage points)	6.45
R^2	0.667
90% mean-curve coverage	0.278
90% group-mean coverage	0.815
90% coupon-interval coverage	0.944
Median group-mean interval width (pp)	19.49

The agreement between the predicted and observed tensile-strength retention values is presented in Figure 4.4. The comparison is based on the 90% group-mean credible intervals, which include both posterior parameter uncertainty and measurement variability associated with replicate specimens.

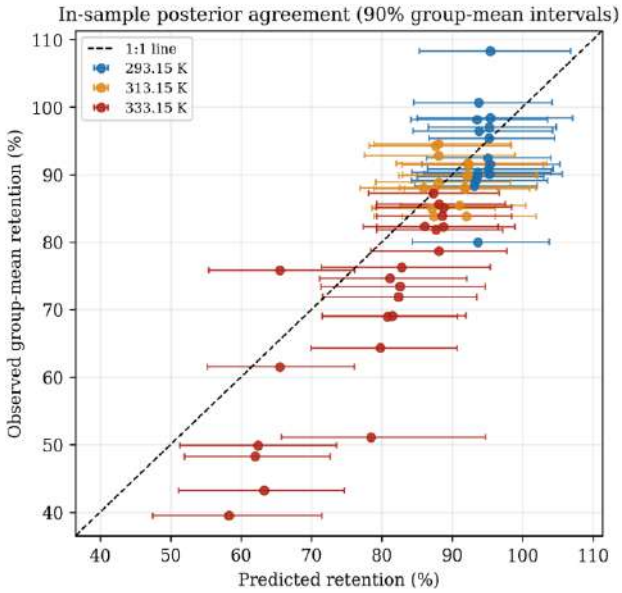


Figure 4.4: In-sample agreement between predicted and observed group-mean retention, with 90% group-mean credible intervals, coloured by exposure temperature.

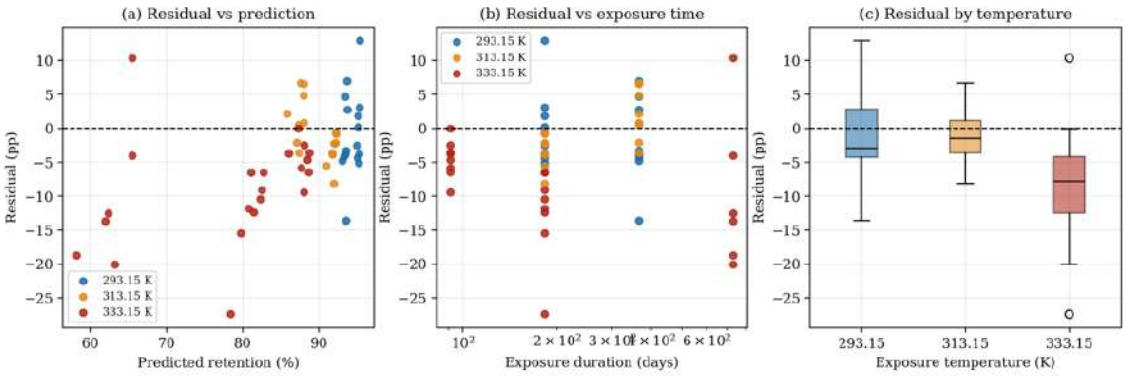


Figure 4.5: Residual diagnostics: (a) residual against predicted retention, (b) residual against exposure duration, and (c) residual distribution by exposure temperature. Positive residuals indicate that the model under-predicts retention.

The majority of observations follow the 1:1 reference line, indicating that the model captures the general degradation trend across the investigated temperature and exposure conditions. However, larger deviations are observed for some measurements, particularly at lower retention values, where the available experimental observations are more limited.

The residual statistics for each exposure temperature are summarised in Table 4.11. These values provide a quantitative assessment of whether prediction errors remain centred around zero across the investigated temperature range.

Table 4.11: In-sample residuals by exposure temperature (observed minus predicted retention).

Exposure temperature	Mean residual [pp]	SD [pp]	Minimum [pp]	Maximum [pp]
293.15 K	-0.84	6.13	-13.62	12.90
313.15 K	-0.73	4.17	-8.14	6.64
333.15 K	-8.87	7.80	-27.37	10.33

Panel (c) of Figure 4.5 and Table 4.11 identify the dominant systematic feature of the model: the residuals at 333.15 K are not centred on zero. The mean residual there is -8.87 percentage points, whereas the two lower temperatures are approximately unbiased. A residual of that sign means the model is systematically optimistic at the highest temperature — it predicts more surviving strength than was measured. This is not random scatter, and Section 4.10.3 returns to it as the central technical finding of the chapter.

A second observation concerns the upper limit of the model. Two of the 54 observed groups mean exceed 100% retention, the largest being approximately 108%. Because retention is capped at unity by construction (Section 4.3.4), these two settings cannot be reproduced by the model under any parameter values, and they impose a small irreducible floor on the achievable in-sample error. Values above 100% reflect normal experimental scatter about the reference mean rather than a strengthening mechanism.

4.9. Posterior Degradation Curves

The posterior tensile-strength retention curves obtained from the Bayesian physics-informed model are presented in Figure 4.6. The curves represent the predicted degradation behaviour for the eight material-condition combinations across the three exposure temperatures, together with the associated 90% credible intervals. The measured group means are included to assess how well the model captures the experimentally observed degradation trends.

In general, the model reproduces the expected degradation behaviour, with tensile-strength retention decreasing progressively with increasing exposure duration and temperature. The degradation rate is more pronounced at 333.15 K compared with the lower exposure temperatures, demonstrating the influence of accelerated ageing conditions. The widening of the credible intervals with increasing exposure duration reflects the increasing uncertainty associated with predictions beyond the available experimental observations.

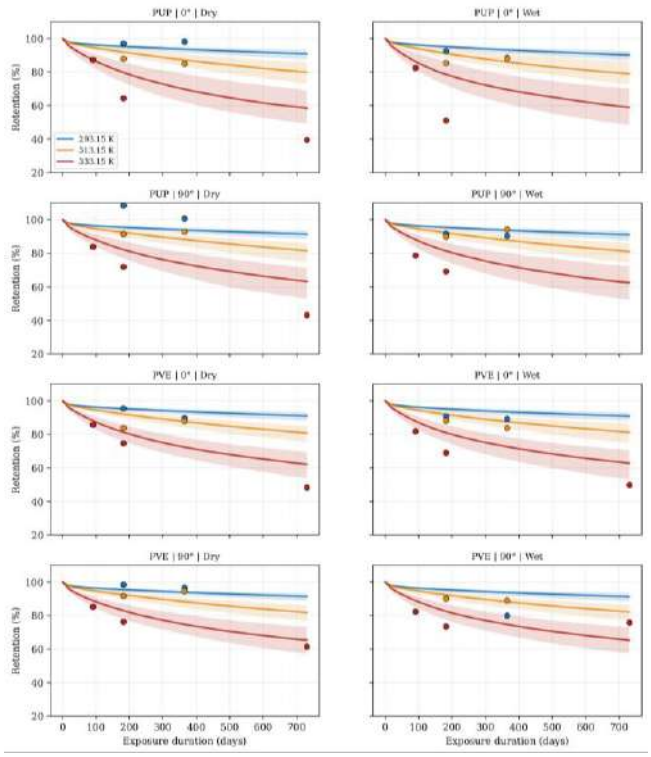


Figure 4.6: Posterior tensile-strength retention curves with 90% credible bands for all eight material-condition cells at the three exposure temperatures. Filled markers are measured group means.

4.10. Predictive Validation

4.10.1. Validation protocol and metrics

Predictive performance was evaluated using complete leave-one-temperature-out validation. In each validation fold, all observations associated with one exposure temperature were excluded from model calibration, and predictions were generated using only the remaining two temperatures. With three exposure temperatures available, this resulted in three independent validation cases.

This protocol is substantially more demanding than a random train–test split. A random split would place replicate coupons from the same exposure setting on both sides of the partition, allowing the model to recall a condition it has effectively already seen. Holding out a complete temperature forecloses that and forces genuine extrapolation in temperature. This validation strategy represents a demanding assessment of model generalisation because the model is required to predict behaviour at a temperature that was not included during training. Therefore, the procedure evaluates the ability of the physics-informed formulation to interpolate and extrapolate across the temperature domain.

The three reported metrics are defined as follows:

$$\mathrm{RMSE} = \sqrt{\frac{1}{n}\sum_{i=1}^{n}(y_i - \hat{y}_i)^2} \tag{4.14}$$

$$\mathrm{MAE} = \frac{1}{n}\sum_{i=1}^{n}|y_i - \hat{y}_i| \tag{4.15}$$

$$R^2 = 1 - \frac{\sum_i (y_i - \hat{y}_i)^2}{\sum_i (y_i - \overline{y})^2} \tag{4.16}$$

where y_i is the measured value, $\hat{y}_i$ the corresponding predicted value, y the mean of the measured values, and n the number of observations entering the metric.

RMSE penalises large errors more heavily and is used as the principal measure. MAE gives the typical error magnitude. The coefficient of determination requires careful interpretation in this setting and is discussed in Section 4.10.4.

4.10.2. Held-out results

The predictive performance of the Bayesian physics-informed neural network was evaluated using the complete leave-one-temperature-out validation procedure described in Section 4.10.1. The results for each withheld temperature are presented in Table 4.12.

Table 4.12: Leave-one-temperature-out validation results (ensemble). The baseline predicts the mean retention of the training folds.

Held-out temperature	Settings	RMSE [pp]	MAE [pp]	R^2	Baseline RMSE (pp)	90% coverage
293.15 K	16	6.41	4.69	-0.061	16.88	0.875
313.15 K	16	4.11	3.33	-0.549	9.77	1.000
333.15 K	22	18.22	15.39	-0.595	25.88	0.455
Mean of folds	54	9.58	7.80	—	17.51	0.777

Across the three validation folds, the model achieved an average RMSE of 9.58 percentage points and an average MAE of 7.80 percentage points. The Bayesian physics-informed model consistently outperformed the constant-mean baseline, demonstrating that the learned degradation relationship provides additional predictive capability beyond using only the average retention value of the training data. The reported mean-of-fold values represent an equal weighting of the three withheld temperature conditions. This approach was selected because each temperature represents an independent validation

scenario. A pooled calculation weighting each observation equally would give greater influence on the temperature condition containing more measurements and was therefore not adopted.

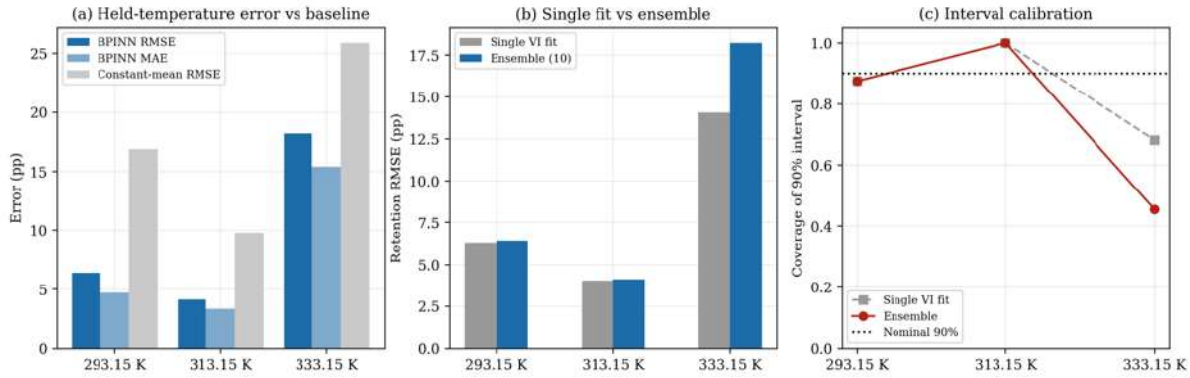


Figure 4.7: Leave-one-temperature-out validation: (a) held-temperature error against a constant-mean baseline, (b) single variational fit compared with the ensemble, and (c) empirical coverage of the nominal 90% intervals.

Performance is markedly uneven across folds. The 293.15 K and 313.15 K folds are predicted well, with RMSE of 6.41 and 4.11 percentage points, respectively. The 333.15 K fold is predicted substantially less well, at 18.22 percentage points — roughly four times the error of the 313.15 K fold.

4.10.3. 333.15 K fold

The behaviour observed at the highest exposure temperature represents an important finding because it highlights the limitation of applying a single degradation relationship across the full temperature range.

1. In-sample bias. Even when 333.15 K data are included in fitting, the residuals at that temperature retain a mean offset of -8.87 percentage points (Table 4.11), in a consistent direction, while the two lower temperatures are unbiased.
2. Held-out error. When 333.15 K is withheld entirely, the prediction error rises to 18.22 percentage points against 4.11 at 313.15 K.
3. Instability. Across repeated fits, essentially all of the run-to-run variability in the pooled result originates in this fold: its RMSE varies by ±2.60 percentage points across seeds, while the other two folds vary by roughly ±0.25 percentage points (Table 4.15).

Taken together, these indicate a model-form limitation rather than noise. A single global activation energy cannot simultaneously reconcile all three temperatures, and the fitted compromise sits closer to the two lower ones. The physically meaningful reading is that the degradation mechanism at 333.15 K may differ from that operating at 293.15 K and 313.15 K, in which case time–temperature superposition across the full range is not strictly valid.

It must also be acknowledged that the 333.15 K fold is confounded by the experimental design. The two lower temperatures were both tested at 182.6 and 365.25 days only, whereas the 333.15 K condition carries the shortest and the longest exposures in the dataset — 91.3 and 730.5 days — neither of which appears anywhere else. Withholding that temperature therefore demands simultaneous extrapolation in both temperature and duration. The elevated error therefore cannot be attributed to temperature alone. What the additional evidence above establishes is that the difficulty is not solely a design artefact: the in-sample bias persists even when the 333.15 K data are used in fitting, which a purely design-driven explanation would not predict.

This finding bears directly on the long-term projection of Section 4.13. That projection rests entirely on Arrhenius time–temperature equivalence, and the evidence above indicates that the equivalence is imperfect over precisely the temperature ranges from which the acceleration is inferred. The projection therefore represents the behaviour implied by the fitted model rather than a validated forecast.

4.10.4. Interpretation of negative R^2

The R^2 values in Table 4.12 are negative in all three folds. This arises from the definition of the statistic under the present validation scheme rather than from a deficiency in the model. Within a single fold, R^2 is computed against the mean of that fold's own observations, a quantity that is unavailable at prediction time because the fold has been withheld. The comparison is therefore made against a reference predictor with access to the mean retention of the withheld temperature. A negative value under such a comparison does not indicate an absence of predictive capability.

The deployable comparison is with a predictor that uses only information available before the withheld temperature is observed: the mean retention of the training folds. The model achieves a lower error than this baseline in every fold, by margins of 10.5 pp at 293.15 K, 5.7 pp at 313.15 K, and 7.7 pp at 333.15 K. Both statistics are reported here, together with the explanation above, so that the behaviour of the coefficient of determination under whole-temperature validation is transparent.

4.11. Uncertainty Calibration and Reproducibility

The value of a Bayesian formulation rests on whether its stated uncertainty is meaningful. Two properties are examined in this section: whether the stated intervals contain the measured values at the nominal rate, and whether the stated uncertainty is at least as large as the reproducibility of the procedure that produces it.

4.11.1. Interval calibration

Calibration was assessed by comparing the nominal uncertainty intervals produced by the model with the proportion of experimental observations contained within those intervals. A well-calibrated model should achieve empirical coverage close to the corresponding nominal confidence level. The calibration performance of the single variational fit and the ensemble approach is summarised in Table ***4.13***, while the corresponding calibration curves are presented in Figure 4.8.

The comparison shows the relationship between the expected interval coverage and the experimentally observed coverage across different confidence levels. Points below the diagonal line indicate that the predicted intervals are narrower than required, corresponding to over-confident uncertainty estimates.

Table 4.13: Interval calibration on in-sample group means.

Nominal level	Single fit — empirical coverage	Ensemble — empirical coverage
50%	0.370	0.370
60%	0.537	0.519
70%	0.704	0.593
80%	0.741	0.722
90%	0.796	0.778
95%	0.852	0.852

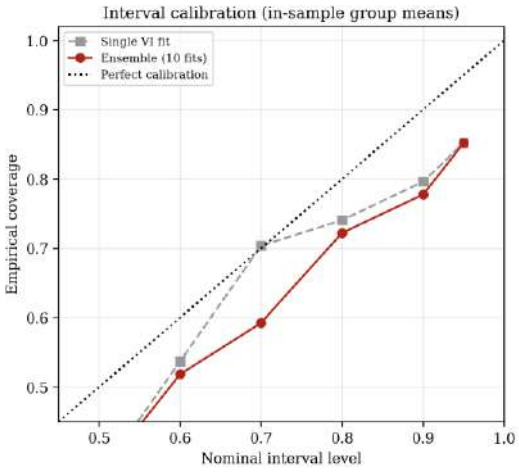


Figure 4.8: Calibration curve: empirical coverage against nominal interval level for a single variational fit and for the pooled ensemble. Points below the diagonal indicate over-confident intervals.

Under held-out validation, the nominal 90% group-mean interval achieves an empirical coverage of 0.777 (Table 4.12). It remains modestly optimistic: a stated 90% interval corresponds in practice to

approximately 78% coverage. This residual over-confidence is characteristic of mean-field variational inference, and the empirical coverage is therefore reported alongside the nominal level throughout this chapter.

The initial posterior spread ρ_0 and the training length were selected on held-out validation rather than on the training objective, because these two settings govern calibration as much as they govern accuracy: too small an initial spread, or too long a training run, leaves the variational posteriors close to their initialisation and produces intervals that are narrow for reasons unrelated to the information in the data. Table 4.14 reports the consequence of the alternative setting on identical folds and identical metrics.

Table 4.14: Effect of the initial posterior spread and training length on held-out accuracy and interval calibration (nominal level 0.90 throughout).

Configuration	RMSE [pp]	Mean-curve coverage	Group-mean coverage	Coupon coverage
ρ_0 = −4, 600 epochs	9.45	0.248	0.638	0.848
ρ_0 = −3, 400 epochs, single fit	8.13	0.375	0.852	0.939
ρ_0 = −3, 400 epochs, ensemble (adopted)	9.55	0.439	0.777	0.894

Group-mean coverage improves from 0.638 under the narrower initialisation to 0.777 under the adopted settings, at essentially unchanged held-out accuracy. The single fit shown in the middle row records a higher coverage still, but that figure belongs to one particular seed; the seed-averaged value across seven repetitions is 0.774 ± 0.071, which the ensemble reproduces almost exactly. This is the reason they report them to keep the distinction between the three quantities; the pattern seen on every metric in this chapter: the ensemble does not outperform a single fit; it reproduces the average of many single fits without depending on a favourable one.

For completeness, the coverage of the mean-curve and coupon intervals under held-out validation is 0.439 and 0.894, respectively. As explained in Section 4.3.6, neither is a valid calibration test against group means; they are reported so that the distinction between the three quantities remains auditable.

4.11.2. Reproducibility across random seeds

The reproducibility of the procedure was examined by repeating the complete validation under different random initialisations. Each row of Table 4.15 corresponds to one full repetition of the entire validation procedure, with the random seed as the only altered quantity. The results motivate the ensemble strategy adopted in Section 4.4.

Table 4.15: Sensitivity of the complete validation result to the random seed (single variational fits).

Seed	Mean fold RMSE (pp)	Mean fold MAE (pp)	90% coverage	RMSE 293 K	RMSE 313 K	RMSE 333 K
42	8.14	6.84	0.852	6.28	4.05	14.10
1	8.35	6.92	0.837	6.10	4.37	14.58
7	10.11	8.34	0.716	6.36	4.25	19.72
2024	9.84	8.22	0.695	6.51	4.16	18.84
99	9.95	8.34	0.716	6.15	4.47	19.22
123	8.23	6.87	0.852	5.86	4.63	14.19
777	9.69	8.08	0.746	6.46	3.92	18.69
Mean ± SD	9.19 ± 0.90	—	0.774 ± 0.071	—	—	17.05 ± 2.60

Mean fold RMSE varies between 8.14 and 10.11 percentage points depending only on the seed, with a standard deviation of 0.90 percentage points. Two observations follow. First, quoting the result of any single run — including a favourable one — would overstate the precision of the method; the ensemble result is reported instead precisely because it is reproducible. Second, the variability is not spread evenly: the 293.15 K and 313.15 K folds are stable to approximately ±0.25 percentage points, whereas the 333.15 K fold varies by ±2.60. The instability and the model-form limitation identified in Section 4.10.3 are the same phenomenon.

Applying the same test to the apparent activation energy gives a necessary condition that any reported interval must satisfy. A credible interval must be at least as wide as the spread obtained by re-running the procedure; otherwise, it describes the local behaviour of the optimiser rather than the uncertainty in the quantity itself.

Table 4.16: Reported uncertainty in the apparent activation energy compared with its reproducibility across random seeds.

Configuration	E_a spread across seeds [kJ/mol]	Reported 90% interval width [kJ/mol]	Interval wider than seed spread?
ρ_0 = −4, 600 epochs	2.78	2.53	No — interval not defensible
ρ_0 = −3, 400 epochs, single fit	2.38	5.22	Yes
ρ_0 = −3, 400 epochs, ensemble (adopted)	2.38	6.00	Yes

Under the narrower initialisation, the activation energy moves by 2.78 kJ/mol between seeds while each run reports a 90% interval only 2.53 kJ/mol wide: the stated uncertainty is narrower than the run-to-run noise, and successive runs produce intervals that do not overlap one another. Under the adopted settings, the reported interval (6.00 kJ/mol) exceeds the seed spread (2.38 kJ/mol), and the interval is therefore self-consistent. The test requires only a small number of additional fits and applies to any variational Bayesian model for which intervals are reported.

Two consequences follow. First, the ensemble result is the one reported throughout this chapter, since it is reproducible whereas a single fit is not. Second, intervals obtained from this model are reported together with their empirical coverage (0.78 against a nominal 0.90), because the nominal level alone overstates the confidence supported by the data.

4.12. Comparison with the Deterministic Reference Model

The Bayesian model and the deterministic reference model of Section 4.3.8 share the same physical content — the same acceleration factor, the same Weibull degradation form and the same per-cell parameterisation with a shared activation energy — were fitted to the same group-balanced exposure settings and were validated under the same leave-one-temperature-out protocol. They differ only in how their parameters are estimated and in what each report alongside its prediction.

Table 4.17: Comparison of the deterministic reference model and the Bayesian physics-informed neural network.

Criterion	Deterministic Arrhenius–Weibull	Bayesian PINN [ensemble]
Retention RMSE (pp)	9.40	9.58
Retention MAE (pp)	7.67	7.80
In-sample RMSE (pp)	4.46	8.45
Estimation	Robust nonlinear least squares	Variational inference, pooled ensemble
Uncertainty reported	Bootstrap interval on parameters only	Posterior predictive intervals on every prediction
Empirical interval coverage	Not available for predictions	0.777 at nominal 0.90
Initial condition $R(0)$=1	Imposed by functional form	Enforced exactly by construction
Monotonic degradation	Not explicitly enforced	Penalised via automatic differentiation
Physics enforced away from data	No — fitted at observations only	Yes — 128 collocation points per epoch across the whole domain
Apparent E_a (kJ/mol)	77.75 [59.5, 103.6]	54.11 [51.1, 57.1]

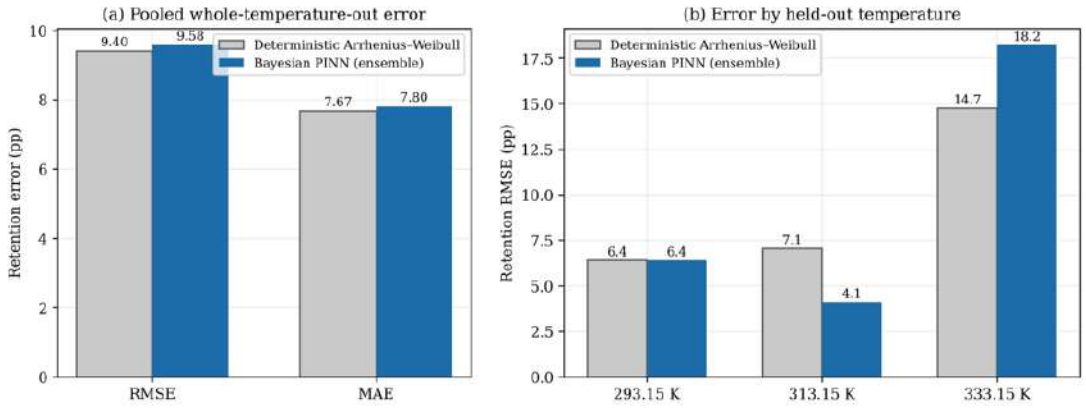


Figure 4.9: Whole-temperature-out predictive error of the deterministic reference model and the Bayesian physics-informed neural network: (a) pooled across folds and (b) by held-out temperature.

On predictive accuracy, the two approaches are equivalent: 9.40 against 9.58 percentage points RMSE, a difference far inside the seed-to-seed variability of ±0.90 percentage points established in Table 4.15. The Bayesian model is therefore not the more accurate of the two. Its contribution lies elsewhere: it delivers calibrated predictive intervals on every prediction rather than on the parameters alone, it enforces the boundary and monotonicity conditions exactly rather than by assumption, and it constrains the governing relation throughout the temperature–time domain rather than only where measurements happen to exist.

Panel (b) shows that the two models degrade under the same conditions. Both predict the 293.15 K fold well and both degrade sharply at 333.15 K (14.7 and 18.2 percentage points respectively). That the difficulty identified in Section 4.10.3 appears in a model of entirely different construction is further evidence that it originates in the data and the assumed physics rather than in the fitting method.

Two further differences are apparent. The deterministic model fits the calibration data more closely (4.46 against 8.45 percentage points in-sample) while predicting held-out temperatures no better, which is the signature of a closer fit to features that do not generalise; the Bayesian priors and the collocation constraint act as a regulariser against this. Separately, one of the eight deterministic shape parameters converged to the lower bound of its admissible range, indicating that the corresponding cell-level curve shape is not identified by the available data. The Bayesian posteriors remain interior, expressing the same weak identification as interval width rather than as a parameter pinned against a constraint.

The two estimates of apparent activation energy differ appreciably, although their intervals overlap and both are wide — the appropriate conclusion from three exposure temperatures. The disagreement between two defensible methods applied to identical data is informative: it indicates that E_a is weakly identified under the present experimental design and supports its treatment as an apparent predictive parameter rather than as a measured material property.

4.13. Long-Term Retention Projection

Following validation, the fitted ensemble was used to project long-term behaviour for a representative service condition: PUP resin, 0° fibre orientation, Wet conditioning, at 293.15 K (20 °C), which is the lowest exposure temperature tested and the closest of the three to an ambient service environment. Measured data for this condition extends to one year; the projection is extended to 50 years.

The two-year exposure present in the wider dataset occurs only at 333.15 K. At 293.15 K, the longest measurement available is one year, and the 50-year projection for this condition extends fifty times beyond the last supporting observation.

Table 4.18:Projected tensile-strength retention for PUP, 0°, Wet conditioning at 293.15 K (20 °C).

Exposure (years)	Median retention (%)	90% lower (%)	90% upper (%)	Interval width (pp)
1	93.0	90.8	94.6	3.8
2	90.0	86.6	92.5	5.9
5	83.7	77.1	89.2	12.1
10	76.7	65.3	85.8	20.5
20	68.0	50.6	81.5	30.9
30	62.1	41.8	78.4	36.5
40	57.6	35.3	75.9	40.6
50	54.2	30.8	73.9	43.1

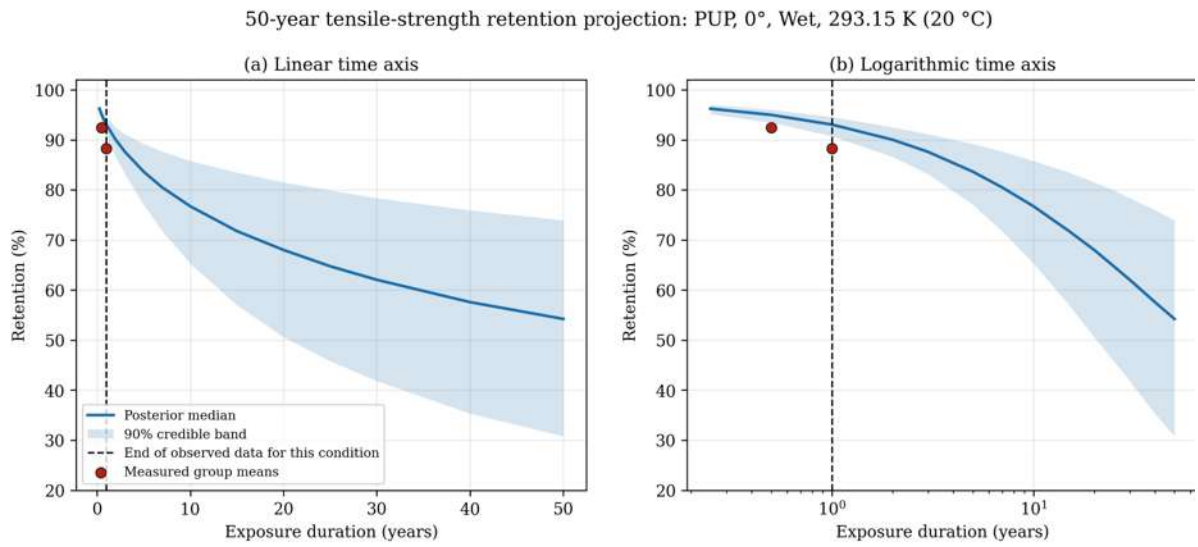


Figure 4.10: Fifty-year tensile-strength retention projection for PUP, 0°, Wet conditioning at 293.15 K (20 °C), on (a) linear and (b) logarithmic time axes. The dashed line marks the last measurement available for this condition.

The projection predicts a median retention of approximately 54% at 50 years, with a 90% credible band from 31% to 74%. Degradation is progressive throughout: the curve declines relatively rapidly over the first few years and then flattens, with no abrupt loss of capacity implied at any point in the horizon.

The most informative feature of the figure is not the median but the width of the band. The interval spans approximately 4 percentage points at one year, where measurements exist, and widens to approximately 43 percentage points at 50 years. That widening is the model correctly reporting that the available data constrain long-horizon behaviour only weakly. It is the principal practical advantage of the Bayesian treatment: a deterministic curve through the same points would present the 50-year value with no such warning.

Three qualifications attach to this projection:

1. It is an extrapolation of roughly 50× beyond the last measurement available for this condition. No measurement in this study validates the model at any horizon beyond two years, and none beyond one year at 293.15 K.
2. It inherits the limitation of Section 4.10.3. The projection depends entirely on Arrhenius time–temperature equivalence, and the evidence presented there indicates that this equivalence is imperfect across the tested temperature range.
3. The stated interval itself is mildly optimistic. Empirical coverage under held-out validation is 0.78 against a nominal 0.90 (Section 4.11.1), so the true band at 50 years is wider than plotted.

The projection accordingly represents the long-term behaviour implied by the fitted model under the stated assumptions and does not constitute a validated service-life prediction. Confirmation would require longer exposure durations and additional independent temperatures.

4.14. Limitations

The limitations below are stated in order of how much they constrain the conclusions that may be drawn.

1. Independent exposure conditions. Although 275 aged coupons were tested, they represent only 54 independent exposure settings across three temperatures and four durations. Replicates characterise experimental scatter but add no new ageing conditions. This is the binding constraint on the entire analysis, and no modelling method can remove it.
2. Departure from Arrhenius behaviour at 333.15 K. Documented in Section 4.10.3 through three independent lines of evidence. This is the most consequential technical limitation because time–temperature superposition is the assumption on which the long-term projection rests.
3. Residual over-confidence of the intervals. Mean-field variational inference under-disperses. Ensembling reduces but does not eliminate this: empirical coverage is 0.777 against a nominal 0.90, and the empirical figure is reported alongside every interval in this chapter.
4. Confounded temperature–duration coverage. Some durations occur only at particular temperatures, so temperature and duration effects cannot be fully separated across the experimental domain. The 333.15 K fold is affected most.
5. Weakly resolved cell-level parameters. The 90% intervals on q and p overlap substantially across the eight material-condition cells (Table 4.7), so differences in degradation kinetics between resin systems, orientations, and conditioning states are not resolved at the 90% level.
6. Extrapolation horizon. The 50-year projection extends approximately 50× beyond the last measurement available at the projected condition and is unvalidated at any horizon beyond two years anywhere in the dataset.
7. Scope. The analysis is restricted to tensile strength, which offered the most complete and internally consistent coverage of the design space. The flexural, compression, in-plane shear and interlaminar shear datasets were not modelled.
8. Two settings above 100% retention cannot be reproduced because retention is capped at unity by construction, imposing a small irreducible floor on in-sample error.

4.15. Summary

A variational Bayesian physics-informed neural network was developed for tensile-strength retention of pultruded GFRP composites, trained on 54 independent exposure settings derived from 275 aged coupons. The network embeds an Arrhenius–Weibull degradation relation enforced at collocation points across the whole temperature–time domain, imposes the initial condition and the retention ceiling exactly by construction, and penalises non-monotonic behaviour through automatic differentiation. All reported results poll 10 independently initialised fits.

Table 4.19: Summary of principal results.

Result	Value
Independent exposure settings	54
Leave-one-temperature-out RMSE (mean of folds)	9.58 percentage points
Leave-one-temperature-out RMSE (pooled over all settings)	12.34 percentage points
Leave-one-temperature-out MAE (mean of folds)	7.80 percentage points
Empirical coverage of nominal 90% intervals	0.777
Seed-to-seed reproducibility of mean fold RMSE	± 0.90 percentage points
Apparent activation energy	54.1 kJ/mol [51.1, 57.1]
Boundary condition $R(0)$ = 100%	Satisfied exactly
Monotonic degradation	Satisfied at all audited points
50-year median retention (PUP, 0°, Wet, 293.15 K)	54% [31, 74] extrapolation

Three conclusions follow. First, on predictive accuracy, the Bayesian model is equivalent to a deterministic model of identical physical content fitted to the same data; the Bayesian treatment is justified by the calibrated uncertainty and the enforced physical constraints it provides, not by an accuracy advantage it does not possess. Second, trustworthy uncertainty requires explicit verification: variational intervals can be narrower than the reproducibility of the procedure that generates them, a failure that is invisible in every accuracy metric and detectable only by the coverage and seed-sensitivity tests of Section 4.11. Third, the analysis identifies a physical finding independent of modelling method: degradation behaviour at 333.15 K is not adequately described by the same Arrhenius relation that fits the two lower temperatures, which both limits the long-term projection and indicates a specific direction for further experimental work.

The most valuable extension would be additional independent exposure conditions — further temperatures, and longer durations — since the number of independent settings, not the choice of modelling method, is what currently limits every conclusion in this chapter.

5. Conclusions and Future Development

5.1. Conclusions

This MSc Dissertation investigated the long-term durability of relatively thick pultruded glass fibre-reinforced polymer (GFRP) composites subjected to hygrothermal ageing, with particular emphasis on the influence of water exposure and elevated temperature on their mechanical performance. Two resin systems, unsaturated polyester (P-UP) and vinyl ester (P-VE), were investigated through a comprehensive experimental programme involving tensile, flexural, compression, in-plane shear, and interlaminar shear testing.

The experimental results demonstrated that prolonged water exposure at elevated temperature resulted in degradation of the mechanical performance of both composite systems. The extent of degradation depended on the resin system, conditioning state, exposure duration, and mechanical property considered. In general, P-VE composites exhibited better retention of mechanical properties than P-UP composites under prolonged ageing conditions; however, this improvement was not consistent for all loading modes, highlighting the influence of the governing damage mechanisms associated with each mechanical response.

For tensile behaviour, the results showed that elastic modulus was comparatively less affected by ageing than tensile strength. This indicates that stiffness measurements alone may not fully represent long-term durability, as strength-related properties are more sensitive to degradation of the polymer matrix and fibre–matrix interface. The transverse tensile response showed greater sensitivity to environmental exposure compared with the longitudinal direction due to its stronger dependence on matrix and interface properties.

Flexural, compression, in-plane shear, and interlaminar shear properties were also affected by hygrothermal ageing, confirming the sensitivity of matrix-dominated and interface-dominated responses to moisture and temperature exposure. Changes in observed failure modes further demonstrated that environmental ageing influenced the damage development mechanisms of the investigated composites.

The comparison between wet and dry aged specimens suggested that part of the observed degradation may be associated with reversible moisture-related effects, while the remaining reduction may result from irreversible changes within the composite structure. However, the experimental comparison alone cannot fully separate these contributions, and additional characterisation techniques, such as moisture uptake

measurements, diffusion analysis, and chemical characterisation, would be required to identify the underlying degradation mechanisms more precisely.

An important finding from the experimental programme was the difference between stiffness and strength retention. In several cases, the elastic modulus remained relatively stable while ultimate strength reduced considerably. Therefore, modulus retention alone cannot provide a complete assessment of the long-term durability of the investigated GFRP composites.

The predictive analysis extended the experimental investigation by developing a Bayesian physics-informed neural network (BPINN) framework for tensile-strength retention prediction under environmental ageing. Tensile data from the present study were combined with complementary datasets from previous MSc investigations to increase the available temperature–duration coverage. The developed model incorporated an Arrhenius–Weibull degradation constraint, Bayesian uncertainty estimation, and complete leave-one-temperature-out validation to evaluate its predictive capability beyond the calibration domain.

The modelling results demonstrated that the BPINN approach could capture the general degradation behaviour while providing uncertainty estimates associated with long-term predictions. The model achieved reliable performance within the range of available experimental conditions; however, increased prediction errors were observed when higher temperatures were completely excluded from model calibration. This highlights the difficulty of extrapolating degradation behaviour beyond the experimentally characterised temperature range and emphasises the importance of sufficiently diverse ageing datasets for reliable service-life prediction.

The limitations of the experimental and modelling approaches should also be acknowledged. The absence of valid tensile results for some PUP wet specimens and the limited number of available specimens for certain PVE wet conditions reduced the extent to which resin-dependent comparisons could be generalised. Furthermore, the predictive model was primarily developed and validated using tensile-strength data, while other mechanical properties require additional datasets before similar modelling approaches can be reliably applied.

Overall, this study provides an integrated experimental and data-driven framework for assessing and predicting the durability of relatively thick pultruded GFRP composites under hygrothermal ageing. The results demonstrate the importance of considering multiple mechanical responses and highlight the potential of physics-informed Bayesian approaches for improving confidence in long-term durability predictions.

5.2. Future Developments

Although this study provides valuable insight into the durability behaviour and predictive modelling of relatively thick pultruded GFRP composites, several areas require further investigation.

Future experimental work should include extended ageing programmes with additional temperature–duration combinations and larger specimen populations to improve the statistical reliability of degradation assessment. Increasing the number of independent exposure conditions would also improve the ability to distinguish the individual influence of temperature, exposure duration, resin type, and conditioning state on mechanical degradation.

Further investigation of degradation mechanisms is required through complementary characterisation techniques, including moisture absorption measurements, diffusion analysis, microscopy, spectroscopy, and chemical analysis. These approaches would provide a clearer understanding of the interaction between moisture, polymer degradation, fibre–matrix interface deterioration, and changes in failure mechanisms.

The predictive framework developed in this dissertation can be further improved by incorporating additional experimental datasets and extending the modelling approach beyond tensile strength. Future studies should investigate the prediction of flexural, compression, in-plane shear, and interlaminar shear degradation to provide a more comprehensive durability assessment covering different failure mechanisms.

The current modelling approach relies on an Arrhenius-based temperature acceleration assumption. Although this provides a physically informed basis for extrapolation, future research should evaluate alternative degradation formulations and investigate their applicability under wider environmental conditions, particularly where complex ageing mechanisms may occur at higher temperatures.

The uncertainty quantification capability of the Bayesian physics-informed neural network could also be further developed by incorporating additional sources of uncertainty, including experimental measurement uncertainty, specimen variability, and uncertainty associated with environmental exposure conditions.

Finally, long-term validation using field-exposed GFRP components or independent experimental datasets would be necessary to establish greater confidence in service-life prediction. Such validation would help bridge the gap between laboratory accelerated ageing results and the practical application of GFRP materials in long-term civil engineering structures.

REFERENCES

[1] S. Yang *et al.*, 'Effect of Different Environmental Conditions on Durabilities of Polyester- and Vinylester-Based Glass-Fiber-Reinforced Polymer Pultruded Profiles', *Front. Mater.*, vol. 9, Apr. 2022, doi: 10.3389/fmats.2022.862872.

[2] 'Lopez-Anido, R., Harik, I., Dutta, P., & Shahrooz, B. (2001). *Field Performance Evaluation of Multiple Fiber-Reinforced Polymer Bridge Deck Systems Over Existing Girders – Phase I: Final Report*. University of Maine; University of Kentucky; Cold Regions Research & Engineering Laboratory; University of Cincinnati.

[3] K. Liao, C. R. Schultheisz, and D. L. Hunston, 'Effects of environmental aging on the properties of pultruded GFRP'.

[4] A. Ruiz Emparanza, R. Kampmann, F. De Caso, C. Morales, and A. Nanni, 'Durability assessment of GFRP rebars in marine environments', *Constr. Build. Mater.*, vol. 329, Apr. 2022, doi: 10.1016/j.conbuildmat.2022.127028.

[5] S. Yang, W. Liu, Y. Fang, and R. Huo, 'Influence of hygrothermal aging on the durability and interfacial performance of pultruded glass fiber-reinforced polymer composites', *J. Mater. Sci.*, vol. 54, no. 3, pp. 2102–2121, Feb. 2019, doi: 10.1007/s10853-018-2944-6.

[6] J. M. Sousa, M. Garrido, J. R. Correia, and S. Cabral-Fonseca, 'Hygrothermal ageing of pultruded GFRP profiles: Comparative study of unsaturated polyester and vinyl ester resin matrices', *Compos. Part A Appl. Sci. Manuf.*, vol. 140, Jan. 2021, doi: 10.1016/j.compositesa.2020.106193.

[7] A. M. Visco, N. Campo, and P. Cianciafara, 'Comparison of seawater absorption properties of thermoset resins-based composites', *Compos. Part A Appl. Sci. Manuf.*, vol. 42, no. 2, pp. 123–130, Feb. 2011, doi: 10.1016/j.compositesa.2010.10.009.

[8] W. Cheng and Y. Cao, 'Strength degradation of GFRP cross-ply laminates in hydrothermal conditions', *APL Mater.*, vol. 12, no. 3, Mar. 2024, doi: 10.1063/5.0201999.

[9] B. Zafari, J. Toby Mottram, P. Purnell, S. Grammatikos, and M. Evernden, 'Hygrothermal Aging of Pultruded Fiber–Polymer Composite with Predictions for Design Service Lives', *Journal of Composites for Construction*, vol. 29, no. 1, Feb. 2025, doi: 10.1061/jccof2.cceng-4854.

[10] Q. Zhao, X.-L. Zhao, D. Zhang, J.-G. Dai, and X. Xue, 'Degradation of GFRP Bars with Epoxy and Vinyl Ester Matrices in a Marine Concrete Environment: An Experimental Study and Theoretical Modeling', *Journal of Composites for Construction*, vol. 28, no. 2, Apr. 2024, doi: 10.1061/jccof2.cceng-4474.

[11] S. M. Harle, 'Durability and long-term performance of fiber-reinforced polymer (FRP) composites: A review', Feb. 01, 2024, *Elsevier Ltd*. doi: 10.1016/j.istruc.2024.105881.

[12] J. R. Correia *et al.*, 'Effects of hygrothermal ageing on the mechanical properties of glass-fibre-reinforced polymer pultruded profiles', *Structural Engineering International: Journal of the International Association for Bridge and Structural Engineering (IABSE)*, vol. 20, no. 4, pp. 370–378, Nov. 2010, doi: 10.2749/101686610793557636.

[13] J. R. Correia, S. Cabral-Fonseca, F. A. Branco, J. G. Ferreira, M. I. Eusébio, and M. P. Rodrigues, 'DU RA BIL ITY OF PULTRUDED GLASS-FI BER-RE IN FORCED POLY ES TER PRO FILES FOR STRUC TURAL AP PLI CA TIONS', 2006.

[14] I. S. Abbood, S. A. Odaa, K. F. Hasan, and M. A. Jasim, 'Properties evaluation of fiber reinforced polymers and their constituent materials used in structures - A review', in *Materials Today: Proceedings*, Elsevier Ltd, 2021, pp. 1003–1008. doi: 10.1016/j.matpr.2020.07.636.

[15] A. Zaman, S. A. Gutub, and M. A. Wafa, 'A review on FRP composites applications and durability concerns in the construction sector', Dec. 2013. doi: 10.1177/0731684413492868.

[16] S. A. Grammatikos, M. Evernden, J. Mitchels, B. Zafari, J. T. Mottram, and G. C. Papanicolaou, 'On the response to hygrothermal aging of pultruded FRPs used in the civil engineering sector', *Mater. Des.*, vol. 96, pp. 283–295, Apr. 2016, doi: 10.1016/j.matdes.2016.02.026.

[17] S. I. Talabi, J. Tobin, B. Strom, I. Brownstein, V. Kunc, and A. A. Hassen, 'Recent and future developments in pultrusion technology with consideration for curved geometries: A review', *Compos. B Eng.*, vol. 283, p. 111678, Aug. 2024, doi: 10.1016/J.COMPOSITESB.2024.111678.

[18] J. R. Correia *et al.*, 'Mechanical properties of FRP materials at elevated temperature – Definition of a temperature conversion factor for design in service conditions', *Constr. Build. Mater.*, vol. 367, Feb. 2023, doi: 10.1016/j.conbuildmat.2023.130298.

[19] S. M. Harle, 'Durability and long-term performance of fiber-reinforced polymer (FRP) composites: A review', Feb. 01, 2024, *Elsevier Ltd*. doi: 10.1016/j.istruc.2024.105881.

[20] E. K. Ngoy, 'MODELLING AND PREDICTION OF THE ENVIRONMENTAL DEGRADATION OF FIBRE REINFORCED PLASTICS'.

[21] J. Qureshi, 'Fibre-Reinforced Polymer (FRP) in Civil Engineering', in *Next Generation Fiber-Reinforced Composites - New Insights*, IntechOpen, 2023. doi: 10.5772/intechopen.107926.

[22] T. Hasan *et al.*, 'Freeze-thaw durability of vacuum-infused glass fibre composites with unsaturated polyester and vinyl ester matrices', *Constr. Build. Mater.*, vol. 455, Dec. 2024, doi: 10.1016/j.conbuildmat.2024.139037.

[23] S. Budhe, M. D. Banea, S. de Barros, and L. F. M. da Silva, 'An updated review of adhesively bonded joints in composite materials', *Int. J. Adhes. Adhes.*, vol. 72, pp. 30–42, Jan. 2017, doi: 10.1016/j.ijadhadh.2016.10.010.

[24] M. F. Green, L. A. Bisby, A. Z. Fam, and V. K. R. Kodur, 'FRP confined concrete columns: Behaviour under extreme conditions', *Cem. Concr. Compos.*, vol. 28, no. 10, pp. 928–937, Nov. 2006, doi: 10.1016/j.cemconcomp.2006.07.008.

[25] Z. Senselova *et al.*, 'Hygrothermal Ageing of Glass and Carbon Fibre Composites Manufactured Using Different Resin Systems', *Polymers (Basel).*, vol. 18, no. 6, Mar. 2026, doi: 10.3390/polym18060696.

[26] B. Chandra Ray and D. Rathore, 'Environmental damage and degradation of FRP composites: A review report', *Polym. Compos.*, vol. 36, no. 3, pp. 410–423, Mar. 2015, doi: 10.1002/pc.22967.

[27] G. M. Park, J. M. Lee, J. Lee, and J. W. Wee, 'Hygrothermal degradation of short-glass-fiber reinforced polycarbonate: effect of fiber content and orientation, and modeling', *Npj Mater. Degrad.*, vol. 10, no. 1, Dec. 2026, doi: 10.1038/s41529-026-00774-z.

[28] Z. Senselova *et al.*, 'Hygrothermal Ageing of Glass and Carbon Fibre Composites Manufactured Using Different Resin Systems', *Polymers (Basel).*, vol. 18, no. 6, Mar. 2026, doi: 10.3390/polym18060696.

[29] B. Hassanpour and V. M. Karbhari, 'Characteristics and Models of Moisture Uptake in Fiber-Reinforced Composites: A Topical Review', Aug. 01, 2024, *Multidisciplinary Digital Publishing Institute (MDPI)*. doi: 10.3390/polym16162265.

[30] J. Zhu, Y. Deng, P. Chen, G. Wang, H. Min, and W. Fang, 'Prediction of Long-Term Tensile Properties of Glass Fiber Reinforced Composites under Acid-Base and Salt Environments', *Polymers (Basel).*, vol. 14, no. 15, Aug. 2022, doi: 10.3390/polym14153031.

[31] P. Cousin, M. Hassan, P. V. Vijay, M. Robert, and B. Benmokrane, 'Chemical resistance of carbon, basalt, and glass fibers used in FRP reinforcing bars', *J. Compos. Mater.*, vol. 53, no. 26–27, pp. 3651–3670, Nov. 2019, doi: 10.1177/0021998319844306.

[32] S. Yang *et al.*, 'Effect of Different Environmental Conditions on Durabilities of Polyester- and Vinylester-Based Glass-Fiber-Reinforced Polymer Pultruded Profiles', *Front. Mater.*, vol. 9, Apr. 2022, doi: 10.3389/fmats.2022.862872.

[33] M. Afroz, I. Patnaikuni, and S. Venkatesan, 'Chemical durability and performance of modified basalt fiber in concrete medium', *Constr. Build. Mater.*, vol. 154, pp. 191–203, Nov. 2017, doi: 10.1016/j.conbuildmat.2017.07.153.

[34] S. Yang *et al.*, 'Effect of Different Environmental Conditions on Durabilities of Polyester- and Vinylester-Based Glass-Fiber-Reinforced Polymer Pultruded Profiles', *Front. Mater.*, vol. 9, Apr. 2022, doi: 10.3389/fmats.2022.862872.

[35] H. Y. Kim, Y. H. Park, Y. J. You, and C. K. Moon, 'Short-term durability test for GFRP rods under various environmental conditions', *Compos. Struct.*, vol. 83, no. 1, pp. 37–47, Mar. 2008, doi: 10.1016/j.compstruct.2007.03.005.

[36] B. Benmokrane, A. H. Ali, H. M. Mohamed, A. ElSafty, and A. Manalo, 'Laboratory assessment and durability performance of vinyl-ester, polyester, and epoxy glass-FRP bars for concrete structures', *Compos. B Eng.*, vol. 114, pp. 163–174, Apr. 2017, doi: 10.1016/j.compositesb.2017.02.002.

[37] 'Textile glass-Yarns-Designation Verre textile-Fils-Designation', 2078.

[38] P. Cousin, M. Hassan, P. V. Vijay, M. Robert, and B. Benmokrane, 'Chemical resistance of carbon, basalt, and glass fibers used in FRP reinforcing bars', *J. Compos. Mater.*, vol. 53, no. 26–27, pp. 3651–3670, Nov. 2019, doi: 10.1177/0021998319844306.

[39] J. W. Chin, 'Durability of composites exposed to ultraviolet radiation', in *Durability of Composites for Civil Structural Applications*, Elsevier Ltd., 2007, pp. 80–97. doi: 10.1533/9781845693565.1.80.

[40] A. W. Signor, M. R. Vanlandingham, and J. W. Chin, 'Effects of ultraviolet radiation exposure on vinyl ester resins: characterization of chemical, physical and mechanical damage'. [Online]. Available: www.elsevier.com/locate/polydegstab

[41] A. Dinița, C. M. Rosca, M. Tănase, and A. Stancu, 'A Comprehensive Review on Bridging the Research Gap in AI-Driven Material Simulation for FRP Composites', 2025, *Tech Science Press*. doi: 10.32604/cmes.2025.066276.

[42] Z. H. Hao, P. Feng, S. Zhang, and Y. Zhai, 'Machine learning for predicting fiber-reinforced polymer durability: A critical review and future directions', Aug. 15, 2025, *Elsevier Ltd*. doi: 10.1016/j.compositesb.2025.112587.

[43] K. Zhang, K. Zhang, and R. Bao, 'Machine learning models to predict the residual tensile strength of glass fiber reinforced polymer bars in strong alkaline environments: A comparative study', *Journal of Building Engineering*, vol. 73, Aug. 2023, doi: 10.1016/j.jobe.2023.106817.

[44] F. Kibrete, T. Trzepieciński, H. S. Gebremedhen, and D. E. Woldemichael, 'Artificial Intelligence in Predicting Mechanical Properties of Composite Materials', Sep. 01, 2023, *Multidisciplinary Digital Publishing Institute (MDPI)*. doi: 10.3390/jcs7090364.

[45] L. Tao and X. Xue, 'AN IMPROVED RANDOM FOREST MODEL TO PREDICT BOND STRENGTH OF FRP-TO-CONCRETE', *Journal of Civil Engineering and Management*, vol. 30, no. 6, pp. 520–535, Jul. 2024, doi: 10.3846/jcem.2024.21636.

[46] P. Wang *et al.*, 'Predicting long-term tensile degradation of GFRP rebars embedded in concrete with a reconsidered environmental reduction factor CE', *Developments in the Built Environment*, vol. 20, Dec. 2024, doi: 10.1016/j.dibe.2024.100583.

[47] X. Liu, T. Q. Liu, and P. Feng, 'Long-term performance prediction framework based on XGBoost decision tree for pultruded FRP composites exposed to water, humidity and alkaline solution', *Compos. Struct.*, vol. 284, Mar. 2022, doi: 10.1016/j.compstruct.2022.115184.

[48] Z. H. Hao, S. Zhang, P. Feng, and Y. Zhai, 'Physics-guided machine learning with an early-age durability fingerprint for GFRP long-term evaluation', *Compos. B Eng.*, vol. 315, Apr. 2026, doi: 10.1016/j.compositesb.2026.113435.

[49] L. Ascione and L. Tromp, 'DESIGN OF FIBRE-POLYMER COMPOSITE STRUCTURES (CEN/TS 19101): BASIS OF DESIGN AND EFFECTS OF TEMPERATURE AND MOISTURE', p. 129, 2023, doi: 10.5281/zenodo.8066317.

[50] J. R. Correia *et al.*, 'Mechanical properties of FRP materials at elevated temperature – Definition of a temperature conversion factor for design in service conditions', *Constr. Build. Mater.*, vol. 367, Feb. 2023, doi: 10.1016/j.conbuildmat.2023.130298.

[51] N. A. A. Moura, 'Durabilidade de compósitos produzidos por pultrusão', Master's dissertation, Escola de Engenharia, Universidade do Minho, 2022.

[52] C. R. P. Leite, 'Durabilidade de compósitos FRP produzidos por pultrusão sob o efeito de envelhecimento natural e acelerado', Master's dissertation, Escola de Engenharia, Universidade do Minho, 2024.

Appendix A. Mechanical Test Results

Appendix A presents the detailed results obtained from the mechanical characterisation of pultruded GFRP laminates manufactured using unsaturated polyester (P-UP) and vinyl ester (P-VE) resin systems.

For each mechanical test, the results are presented in the following order: reference (REF) specimens, dry-conditioned specimens (W60-24M-D), and wet-conditioned specimens (W60-24M-W). Within each conditioning state, the P-UP series is presented first, followed by the corresponding P-VE series.

Each appendix includes information on the specimen designation, conditioning state, specimen dimensions, measured mechanical properties, representative stress–strain or stress–displacement curves, and photographs of the corresponding failure modes.

The measured specimen dimensions comprise the mass (M), total length (L), width (B), and thickness (H), which were measured at three locations along the specimen, wherever applicable.

Appendix A.1 – Flexural Test Results: P-UP-REF

1. Series Data

Designation	P-UP-REF
Resin type	Unsaturated polyester
Environment	Unconditioned reference specimens stored under laboratory conditions
Duration	N/A
Test type	Flexural test
Test standard	EN ISO 14125:1998
Test location	Structures Laboratory, University of Minho
Test date	09/04/2026
Observation	The GFRP specimens were tested in the unaged condition and served as the reference series

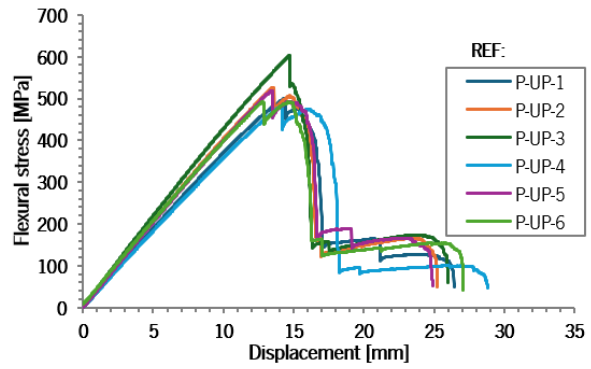
2. Specimen Dimensions

Specimen	H1	H2	H3	B1	B2	B3	L	M
1	7.9	8.0	7.9	15.6	15.5	15.5	240.5	53.5
2	7.9	7.9	7.9	15.4	15.6	15.5	240.5	54.0
3	7.9	7.9	7.9	15.5	15.7	15.5	240.5	53.8
4	7.9	8.0	7.9	15.4	15.6	15.6	240.0	52.7
5	7.9	7.9	8.0	15.6	15.6	15.5	240.0	54.2
6	7.9	8.0	7.9	15.7	15.5	15.5	240.0	53.8
Mean Value	**7.9**	**7.9**	**7.9**	**15.5**	**15.6**	**15.5**	**240.3**	**53.7**

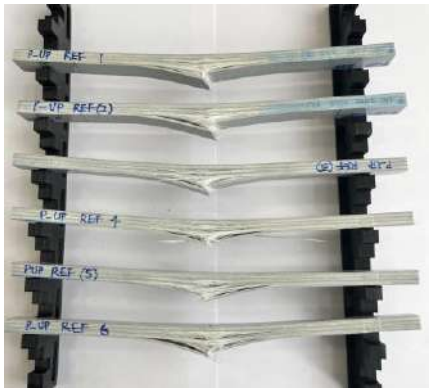
3. Main Results

Specimen	F_{max} [kN]	σ_{max} [MPa]	$\delta_{f,max}$ [mm]	Failure Mode
1	2.05	501.06	14.40	TFF
2	2.15	526.69	13.60	TFF
3	2.2	602.27	14.72	TFF
4	1.93	481.07	14.17	TFF
5	2.12	518.89	13.47	TFF
6	2.02	492.13	12.80	TFF
Mean Value(CoV)	**2.08(4.7%)**	**520.35(8.4%)**	**13.86(5.1%)**	

4. Graphs and Failure Modes



Stress–displacement relationships



Failure mode

Note: M.V. = Mean Value; CoV = Coefficient of Variation; n.a = Not available; H1–H3 = Specimen thickness (mm); B1–B3 = Specimen width (mm); L = Specimen length (mm); M = Specimen mass (g); TFF = Tensile Fracture in Fibre

Appendix A.2 – Flexural Test Results: P-VE-REF

1. Series Data

Designation	P-VE-REF
Resin type	Vinyl ester
Environment	Unconditioned reference specimens stored under laboratory conditions
Duration	N/A
Test type	Flexural test
Test standard	EN ISO 14125:1998
Test location	Structures Laboratory, University of Minho
Test date	09/04/2026
Observation	The GFRP specimens were tested in the unaged condition and served as the reference series

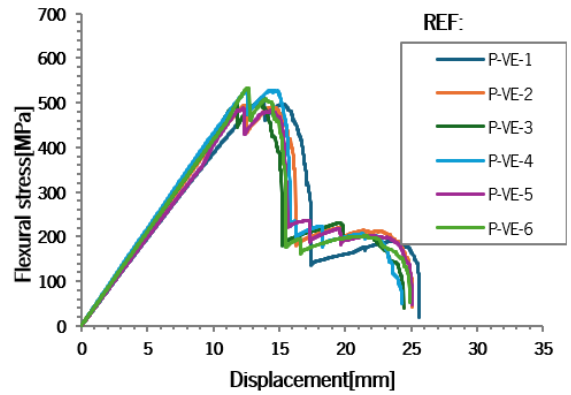
2. Specimen Dimensions

Specimen	H1	H2	H3	B1	B2	B3	L	M
1	7.9	7.9	7.9	15.4	15.3	15.3	240.0	52.8
2	7.9	8.0	8.0	15.3	15.4	36.0	240.0	54.3
3	8.0	8.0	8.0	15.4	15.4	36.0	240.0	54.7
4	8.0	7.9	7.9	15.4	15.4	39.0	240.0	54.5
5	8.0	8.0	8.0	15.4	15.4	35.0	240.0	53.8
6	8.0	8.0	8.0	15.4	15.3	43.0	240.0	54.9
Mean Value	**8.0**	**8.0**	**8.0**	**15.4**	**15.4**	**34.1**	**240.0**	**54.2**

3. Main Results

Specimen	F_{max} [kN]	σ_{max} [MPa]	$\delta_{f,max}$ [mm]	Failure Mode
1	1.30	510.54	13.68	TFF
2	2.00	494.90	12.52	TFF
3	2.05	499.97	13.67	TFF
4	2.13	528.20	14.33	TFF
5	2.01	488.13	12.30	TFF
6	2.17	533.31	12.63	TFF
Mean Value (CoV)	**1.94(16.72%)**	**520.35(3.60%)**	**13.86(6.19%)**	

4. Graphs and Failure Modes



Stress–displacement relationships



Failure mode

Note: M.V. = Mean Value; CoV = Coefficient of Variation; n.a = Not available; H1–H3 = Specimen thickness (mm); B1–B3 = Specimen width (mm); L = Specimen length (mm); M = Specimen mass (g); TFF = Tensile Fracture in Fibre.

Appendix A.3 – Flexural Test Results: P-UP-W60-24M-D

1. Series Data

Designation	P-UP-D
Resin type	Unsaturated polyester
Environment	Hygrothermal water immersion at 60°C, followed by drying under laboratory conditions
Duration	24 months
Test type	Flexural test
Test standard	EN ISO 14125:1998
Test location	Structures Laboratory, University of Minho
Test date	09/04/2026
Observation	The GFRP specimens were immersed in water at 60°C for 24 months, dried under laboratory conditions, and then tested

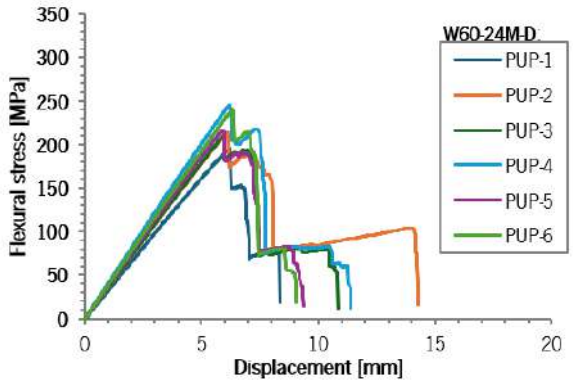
2. Specimen Dimensions

Specimen	H1	H2	H3	B1	B2	B3	L	M
1	8.1	8.0	8.1	15.4	15.2	15.2	240.0	54.72
2	7.9	8.0	8.0	15.5	15.2	15.3	240.0	53.7
3	8.0	8.0	8.0	15.4	15.3	15.4	240.0	54.0
4	8.0	8.1	8.1	15.6	15.4	15.6	240.0	54.3
5	8.1	8.0	8.0	15.4	15.4	15.5	240.0	53.7
6	7.9	7.9	7.9	15.5	15.5	15.5	240.0	51.7
Mean Value	**8.0**	**8.0**	**8.0**	**15.5**	**15.3**	**15.4**	**240.0**	**53.7**

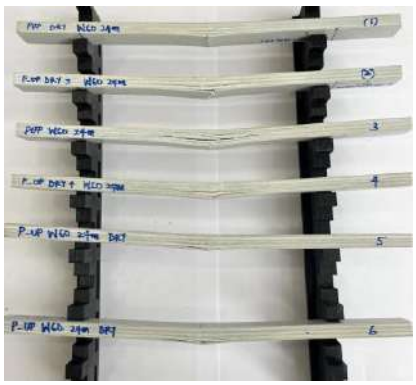
3. Main Results

Specimen	F_{max} [kN]	σ_{max} [MPa]	$\delta_{f,max}$ [mm]	Failure Mode
1	0.77	194.64	6.21	TFOL
2	0.86	214.21	6.12	TFOL
3	0.84	209.67	5.95	TFOL
4	0.88	244.74	6.18	TFOL
5	0.86	215.87	5.90	TFOL
6	0.97	240.46	6.32	TFOL
Mean Value (CoV)	**0.86(7.4%)**	**219.93(8.7%)**	**6.1(2.62%)**	

4. Graphs and Failure Modes



Stress–displacement relationships



Failure mode

Note: M.V. = Mean Value; CoV = Coefficient of Variation; n.a = Not available; B1–B3 = Specimen width (mm); H1–H3 = Specimen thickness (mm); L = Specimen length (mm); M = Specimen mass (g); TFOL = Tensile Fracture at the Outermost Layer.

Appendix A.4 – Flexural Test Results: P-VE-W60-24M-D

1. Series Data

Designation	P-VE-D
Resin type	Vinyl ester
Environment	Hygrothermal water immersion at 60°C, followed by drying under laboratory conditions
Duration	24 months
Test type	Flexural test
Test standard	EN ISO 14125:1998
Test location	Structures Laboratory, University of Minho
Test date	09/04/2026
Observation	The GFRP specimens were immersed in water at 60°C for 24 months, dried under laboratory conditions, and then tested

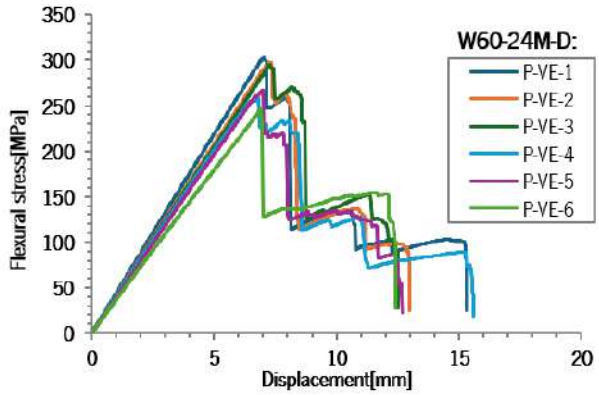
2. Specimen Dimensions

Specimen	H1	H2	H3	B1	B2	B3	L	M
1	7.9	7.8	7.9	15.6	15.3	15.5	240.0	54.72
2	7.9	7.9	7.9	15.6	15.3	15.5	240.0	53.7
3	7.9	7.9	7.9	15.6	15.3	15.5	240.0	54.0
4	7.5	7.4	7.5	15.5	15.5	15.5	240.0	54.3
5	7.9	7.9	7.9	15.3	15.3	15.4	240.0	53.7
6	7.9	7.9	7.9	15.3	15.5	15.6	240.0	51.7
Mean Value	**7.8**	**7.8**	**7.8**	**15.5**	**15.4**	**15.5**	**240.0**	**53.7**

3. Main Results

Specimen	F_{max} [kN]	σ_{max} [MPa]	$\delta_{f,max}$ [mm]	Failure Mode
1	1.25	303.4	7.05	TFOL
2	1.20	279.69	7.30	TFOL
3	1.20	294.67	7.27	TFOL
4	1.08	257.73	6.82	TFOL
5	1.11	267.00	7.00	TFOL
6	0.99	246.27	6.92	TFOL
Mean Value (CoV)	**1.14(8.3%)**	**277.76(8.6%)**	**7.1(2.72%)**	

4. Graphs and Failure Modes



Stress–displacement relationships



Failure mode

Note: M.V. = Mean Value; CoV = Coefficient of Variation; n.a = Not available; B1–B3 = Specimen width (mm); H1–H3 = Specimen thickness (mm); L = Specimen length (mm); M = Specimen mass (g); TFOL = Tensile Fracture at the Outermost Layer.

Appendix A.5 – Flexural Test Results: P-UP-W60-24M-W

1. Series Data

Designation	P-UP-W
Resin type	Unsaturated polyester
Environment	Hygrothermal water immersion at 60°C
Duration	24 months
Test type	Flexural test
Test standard	EN ISO 14125:1998
Test location	Structures Laboratory, University of Minho
Test date	09/04/2026
Observation	The GFRP specimens were subjected to hygrothermal water immersion at 60°C for 24 months and tested immediately after conditioning

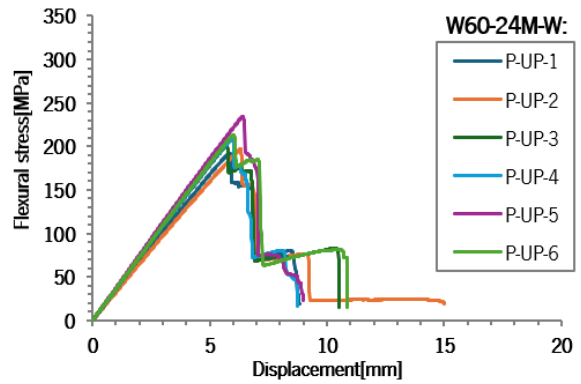
2. Specimen Dimensions

Specimen	H1	H2	H3	B1	B2	B3	L	M
1	7.9	7.8	7.9	15.6	15.3	15.5	240.0	50.55
2	7.9	7.9	7.9	15.6	15.3	15.5	239.5	51.9
3	7.9	7.9	7.9	15.6	15.3	15.5	240.0	51.8
4	7.5	7.4	7.5	15.5	15.5	15.5	240.0	51.5
5	7.9	7.9	7.9	15.3	15.3	15.4	240.0	51.8
6	7.9	7.9	7.9	15.3	15.5	15.6	239.5	52.3
Mean Value	**7.8**	**7.8**	**7.8**	**15.5**	**15.4**	**15.5**	**239.8**	**51.6**

3. Main Results

Specimen	F_{max} [kN]	σ_{max} [MPa]	$\delta_{f,max}$ [mm]	Failure Mode
1	0.79	191.60	5.87	TFOL
2	0.79	196.91	6.32	TFOL
3	0.82	201.67	5.73	TFOL
4	0.85	208.05	5.98	TFOL
5	0.95	234.67	6.43	TFOL
6	0.87	213.23	6.03	TFOL
Mean Value (CoV)	**0.84(7.5%)**	**207.69(7.37%)**	**6.1(4.40%)**	

4. Graphs and Failure Modes



Stress–displacement relationships



Failure mode

Note: M.V. = Mean Value; CoV = Coefficient of Variation; n.a = Not available; B1–B3 = Specimen width (mm); H1–H3 = Specimen thickness (mm); L = Specimen length (mm); M = Specimen mass (g); TFOL = Tensile Fracture at the Outermost Layer.

Appendix A.6 – Flexural Test Results: P-VE-W60-24M-W

1. Series Data

Designation	P-VE-W
Resin type	Vinyl ester
Environment	Hygrothermal water immersion at 60°C
Duration	24 months
Test type	Flexural test
Test standard	EN ISO 14125:1998
Test location	Structures Laboratory, University of Minho
Test date	09/04/2026
Observation	The GFRP specimens were subjected to hygrothermal water immersion at 60°C for 24 months and tested immediately after conditioning

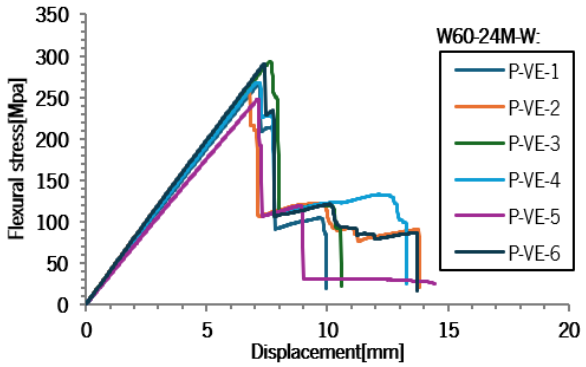
2. Specimen Dimensions

Specimen	H1	H2	H3	B1	B2	B3	L	M
1	8.2	8.1	8.1	15.2	15.2	15.5	240.0	54.92
2	8.2	8.1	8.2	15.5	15.2	15.2	240.0	55.3
3	8.1	8.1	8.0	15.2	15.5	15.4	240.0	54.7
4	8.1	8.1	8.1	15.3	15.3	15.3	240.0	55.3
5	8.0	8.0	8.1	15.3	15.2	15.2	240.0	52.5
6	8.2	8.1	8.1	15.5	15.2	15.2	240.0	55.1
Mean Value	**8.1**	**8.1**	**8.1**	**15.3**	**15.3**	**15.3**	**240.0**	**54.6**

3. Main Results

Specimen	F_{max} [kN]	σ_{max} [MPa]	$\delta_{f,max}$ [mm]	Failure Mode
1	1.12	267.16	7.18	TFOL
2	1.11	261.57	6.73	TFOL
3	1.23	293.19	7.65	TFOL
4	1.12	267.67	7.12	TFOL
5	1.01	247.99	7.13	TFOL
6	1.22	290.20	7.38	TFOL
Mean Value (CoV)	**1.14(7.0%)**	**271.31(6.4%)**	**7.2(4.2%)**	

4. Graphs and Failure Modes



Stress–displacement relationships



Failure mode

Note: M.V. = Mean Value; CoV = Coefficient of Variation; n.a = Not available; B1–B3 = Specimen width (mm); H1–H3 = Specimen thickness (mm); L = Specimen length (mm); M = Specimen mass (g); TFOL = Tensile Fracture at the Outermost Layer.

Appendix A.7 – Interlaminar shear Test Results: P-UP-REF

1. Series Data

Designation	P-UP-REF
Resin type	Unsaturated polyester
Environment	Unconditioned reference specimens stored under laboratory conditions
Duration	N/A
Test type	Interlaminar test
Test standard	ISO 14130:1997
Test location	Structures Laboratory, University of Minho
Test date	13/04/2026
Observation	The GFRP specimens were tested in the unaged condition and served as the reference series for comparison with the conditioned specimens.

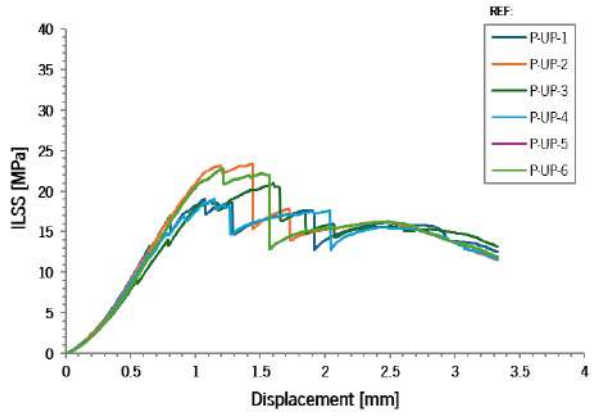
2. Specimen Dimensions

Specimen	H1	H2	H3	B1	B2	B3	L	M
1	8.2	8.1	8.1	40.6	40.6	40.7	80.1	47.39
2	8.2	8.1	8.2	40.5	40.5	40.6	80.0	47.8
3	8.1	8.1	8.0	40.7	40.5	40.6	80.0	47.2
4	8.1	8.1	8.1	40.5	40.6	40.7	80.0	47.3
5	8.0	8.0	8.1	40.5	40.5	40.7	80.0	47.8
6	8.2	8.1	8.1	40.5	40.7	40.5	80.1	47.3
Mean Value	**8.1**	**8.1**	**8.1**	**40.5**	**40.6**	**40.6**	**80.0**	**47.5**

3. Main Results

Specimen	F_{max}[kN]	τ_{max} [MPa]	$\delta_{f,max}$ [mm]	Failure Mode
1	8.19	19.04	1.07	Single shear
2	10.00	23.34	1.43	Multiple shear
3	8.98	20.98	1.61	Multiple shear
4	8.18	19.06	1.15	Single shear
5	9.76	22.73	1.21	Single shear
6	9.76	22.75	1.21	
Mean Value (CoV)	**9.15(9.0%)**	**21.32(9.0%)**	**1.28(15.56%)**	

4. Graphs and Failure Modes



Stress–displacement relationships



Failure mode

Note: M.V. = Mean Value; CoV = Coefficient of Variation; n.a = Not available; B1–B3 = Specimen width (mm); H1–H3 = Specimen thickness (mm); L = Specimen length (mm); M = Specimen mass (g).

Appendix A.8 – Interlaminar shear Test Results: P-VE-REF

1. Series Data

Designation	P-VE-REF
Resin type	Vinyl ester
Environment	Unconditioned reference specimens stored under laboratory conditions
Duration	N/A
Test type	Interlaminar shear test
Test standard	ISO 14130:1997
Test location	Structures Laboratory, University of Minho
Test date	14/04/2026
Observation	The GFRP specimens were tested in the unaged condition and served as the reference series for comparison with the conditioned specimens.

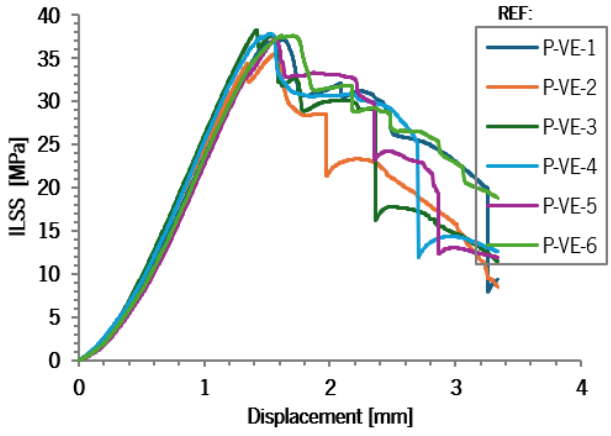
2. Specimen Dimensions

Specimen	H1	H2	H3	B1	B2	B3	L	M
1	8.0	7.9	8.0	40.5	40.3	40.5	80.0	48.3
2	7.9	7.9	7.9	40.4	40.4	40.5	80.0	48.2
3	8.0	8.0	7.9	40.4	40.4	40.6	80.0	47.8
4	8.0	8.0	8.0	40.3	40.5	40.3	80.0	48.6
5	7.9	8.0	7.9	40.6	40.4	40.5	80.0	48.0
6	8.0	8.0	8.0	40.6	40.4	40.6	80.1	48.3
Mean Value	**8.0**	**8.0**	**8.0**	**40.5**	**40.4**	**40.5**	**80.0**	**48.2**

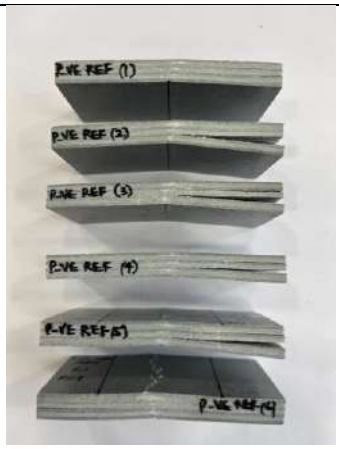
3. Main Results

Specimen	F_{max}[kN]	τ_{max} [MPa]	$\delta_{f,max}$ [mm]	Failure Mode
1	15.86	37.00	1.63	Multiple shear
2	15.14	35.42	1.57	Single shear
3	16.39	38.19	1.42	Multiple shear
4	16.19	37.72	1.53	Multiple shear
5	15.94	37.18	1.57	Multiple shear
6	16.17	37.52	1.61	Single shear
Mean Value (CoV)	**15.95(2.74%)**	**37.17(2.57%)**	**1.55(4.79%)**	

4. Graphs and Failure Modes



Stress–displacement relationships



Failure mode

Note: M.V. = Mean Value; CoV = Coefficient of Variation; n.a = Not available; B1–B3 = Specimen width (mm); H1–H3 = Specimen thickness (mm); L = Specimen length (mm); M = Specimen mass (g).

Appendix A.9 – Interlaminar shear Test Results: P-UP-W60-24M-D

1. Series Data

Designation	P-UP-D
Resin type	Unsaturated polyester
Environment	Hygrothermal water immersion at 60°C, followed by drying under laboratory conditions
Duration	24 months
Test type	Interlaminar shear test
Test standard	ISO 14130:1997
Test location	Structures Laboratory, University of Minho
Test date	13/04/2026
Observation	The GFRP specimens were immersed in water at 60°C for 24 months, dried under laboratory conditions, and then tested

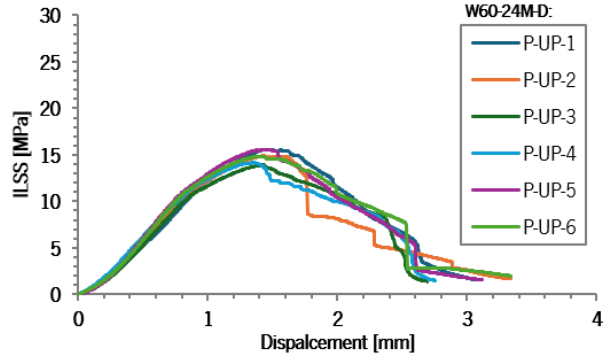
2. Specimen Dimensions

Specimen	H1	H2	H3	B1	B2	B3	L	M
1	7.9	7.9	7.8	40.2	40.2	40.2	80.1	45.9
2	7.9	7.8	7.9	40.3	40.5	40.6	80.0	46.0
3	7.8	7.8	7.8	40.4	40.4	40.2	80.0	45.8
4	7.9	7.8	7.9	40.4	40.6	40.3	80.0	46.0
5	7.9	7.9	7.9	40.3	40.2	40.3	80.0	46.1
6	7.9	7.9	7.9	40.3	40.2	40.3	80.1	46.1
Mean Value	**7.9**	**7.9**	**7.9**	**40.3**	**40.4**	**40.3**	**80.0**	**46.0**

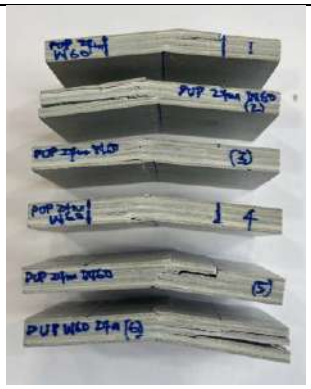
3. Main Results

Specimen	F_{max}[kN]	τ_{max} [MPa]	$\delta_{f,max}$ [mm]	Failure Mode
1	6.56	15.59	1.46	Single shear
2	6.32	14.89	1.43	Multiple shear
3	5.85	13.93	1.44	Multiple shear
4	5.99	14.15	1.36	Multiple shear
5	6.59	15.59	1.44	Single shear
6	6.30	14.86	1.41	Multiple shear
Mean Value (CoV)	**6.27(4.78%)**	**14.83(4.71%)**	**1.42(2.58%)**	

4. Graphs and Failure Modes



Stress–displacement relationships



Failure mode

Note: M.V. = Mean Value; CoV = Coefficient of Variation; n.a = Not available; B1–B3 = Specimen width (mm); H1–H3 = Specimen thickness (mm); L = Specimen length (mm); M = Specimen mass (g).

Appendix A.10 – Interlaminar shear Test Results: P-VE-W60-24M-D

1. Series Data

Designation	P-VE-D
Resin type	Vinyl ester
Environment	Hygrothermal water immersion at 60°C, followed by drying under laboratory conditions
Duration	24 months
Test type	Interlaminar shear test
Test standard	ISO 14130:1997
Test location	Structures Laboratory, University of Minho
Test date	13/04/2026
Observation	The GFRP specimens were immersed in water at 60°C for 24 months, dried under laboratory conditions, and then tested

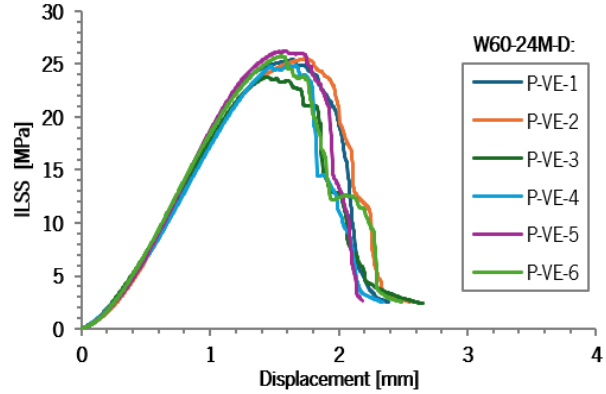
2. Specimen Dimensions

Specimen	H1	H2	H3	B1	B2	B3	L	M
1	8.0	8.0	8.0	40.6	40.3	40.4	80.0	47.7
2	8.1	8.0	8.0	40.3	40.3	40.2	80.1	47.9
3	8.0	8.0	8.0	40.3	40.3	40.2	80.0	47.6
4	8.1	8.0	8.0	40.5	40.3	40.2	80.0	47.7
5	8.0	8.0	8.0	40.3	40.3	40.3	80.0	47.7
6	8.0	8.0	8.0	40.2	40.3	40.4	80.1	47.7
Mean Value	**8.0**	**8.0**	**8.0**	**40.4**	**40.3**	**40.3**	**80.0**	**47.7**

3. Main Results

Specimen	F_{max}[kN]	τ_{max} [MPa]	$\delta_{f,max}$ [mm]	Failure Mode
1	10.68	25.38	1.63	Tension
2	10.82	25.49	1.74	Tension
3	9.99	23.80	1.44	Tension
4	10.53	24.88	1.61	Tension
5	11.09	26.24	1.59	Tension
6	10.91	25.73	1.55	Tension
Mean Value (CoV)	**10.67(3.59)**	**25.25(3.32%)**	**1.59(6.15%)**	

4. Graphs and Failure Modes



Stress–displacement relationships



Failure mode

Note: M.V. = Mean Value; CoV = Coefficient of Variation; n.a = Not available; B1–B3 = Specimen width (mm); H1–H3 = Specimen thickness (mm); L = Specimen length (mm); M = Specimen mass (g).

Appendix A.11 – Interlaminar shear Test Results: P-UP-W60-24M-W

1. Series Data

Designation	W60-24M-W
Resin type	Unsaturated Polyester
Environment	Exposed to accelerated hygrothermal ageing by water immersion at 60 °C
Duration	24 months
Test type	Interlaminar shear
Test standard	ISO 14130:1997
Test location	Structures Laboratory, University of Minho
Test date	13/04/2026
Observation	The GFRP specimens were subjected to hygrothermal water immersion at 60°C for 24 months and tested immediately after conditioning

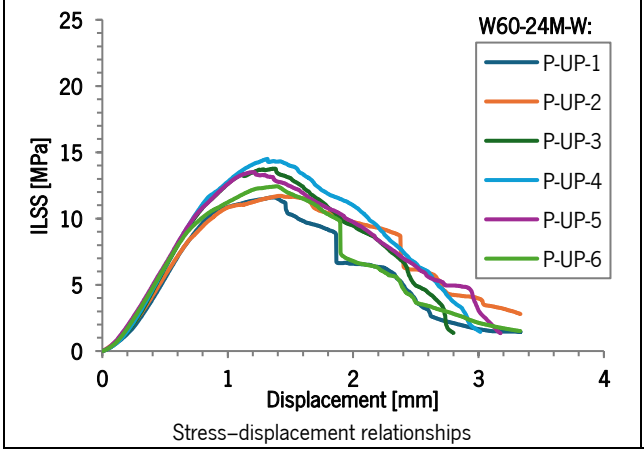
2. Specimen Dimensions

Specimen	H1	H2	H3	B1	B2	B3	L	M
1	7.9	7.9	7.9	40.4	40.2	40.2	80.1	47.3
2	7.9	7.9	7.9	40.3	40.3	40.5	80.1	47.4
3	8.0	8.0	8.0	40.3	40.5	40.3	80.1	48.1
4	8.0	8.0	8.0	40.2	40.2	40.4	80.0	48.0
5	8.0	8.0	8.0	40.4	40.4	40.4	80.0	48.2
6	7.9	7.9	7.9	40.5	40.3	40.3	80.0	47.1
Mean Value	**7.9**	**7.9**	**7.9**	**40.3**	**40.3**	**40.3**	**80.0**	**47.7**

3. Main Results

Specimen	F_{max}[kN]	τ_{max} [MPa]	$\delta_{f,max}$ [mm]	Failure Mode
1	4.92	11.60	1.36	Single shear
2	4.99	11.72	1.42	Single shear
3	5.9	13.77	1.38	Multiple shear
4	6.2	14.50	1.32	Multiple shear
5	5.79	13.51	1.20	Multiple shear
6	5.30	12.43	1.39	Single shear
Mean Value (CoV)	**5.52(9.45%)**	**12.92(9.15%)**	**1.35(5.78%)**	

4. Graphs and Failure Modes



Stress–displacement relationships



Failure mode

Note: M.V. = Mean Value; CoV = Coefficient of Variation; n.a = Not available; B1–B3 = Specimen width (mm); H1–H3 = Specimen thickness (mm); L = Specimen length (mm); M = Specimen mass (g)

Appendix A.12 – Interlaminar Shear Test Results: P-VE-W60-24M-W

1. Series Data

Designation	P-VE-W
Resin type	Vinyl ester
Environment	Exposed to accelerated hygrothermal ageing by water immersion at 60 °C
Duration	24 months
Test type	Interlaminar shear test
Test standard	ISO 14130:1997
Test location	Structures Laboratory, University of Minho
Test date	13/04/2026
Observation	The GFRP specimens were subjected to hygrothermal water immersion at 60°C for 24 months and tested immediately after conditioning

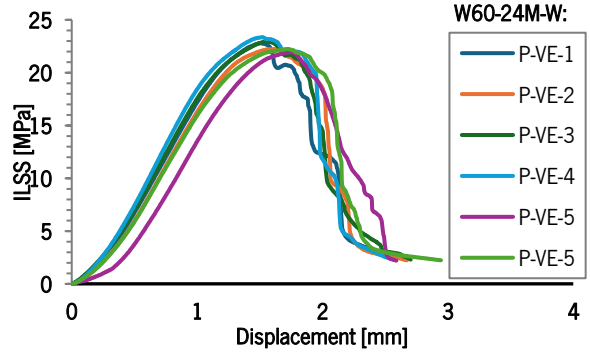
2. Specimen Dimensions

Specimen	H1	H2	H3	B1	B2	B3	L	M
1	8.1	8.1	8.1	40.1	40.2	40.4	80.1	49.2
2	8.0	8.0	8.0	40.2	40.3	40.3	80.1	48.6
3	8.1	8.0	8.2	40.1	40.2	40.1	80.1	49.3
4	8.1	8.1	8.2	40.2	40.2	40.2	80.0	49.2
5	8.1	8.0	8.0	40.2	40.2	40.2	80.0	49.1
6	8.1	8.0	8.6	40.2	40.2	40.1	80.0	48.7
Mean Value	**8.0**	**8.0**	**8.2**	**40.2**	**40.2**	**40.2**	**80.0**	**49.0**

3. Main Results

Specimen	F_{max}[kN]	τ_{max} [MPa]	$\delta_{f,max}$ [mm]	Failure Mode
1	9.89	22.81	1.51	Tension
2	9.58	22.23	1.62	Tension
3	9.98	22.98	1.56	Tension
4	10.16	23.36	1.52	Tension
5	9.45	21.95	1.74	Tension
6	9.80	22.24	1.72	Tension
Mean Value (CoV)	**9.81(2.65%)**	**22.59(2.39%)**	**1.61(6.21%)**	

4. Graphs and Failure Modes



Stress–displacement relationships



Failure mode

Note: M.V. = Mean Value; CoV = Coefficient of Variation; n.a = Not available; B1–B3 = Specimen width (mm); H1–H3 = Specimen thickness (mm); L = Specimen length (mm); M = Specimen mass (g).

Appendix A.13 - Tensile Test 0° Results: P-UP-REF

1. Series Data

Designation	P-UP-REF
Resin type	Unsaturated polyester
Environment	Unconditioned reference specimens stored under laboratory conditions
Duration	N/A
Test type	Tensile test 0°
Test standard	EN ISO 527-4:1997
Test location	Structures Laboratory, University of Minho
Test date	05/05/2026
Observation	The GFRP specimens were tested in the unaged condition and served as the reference series for comparison with the conditioned specimens.

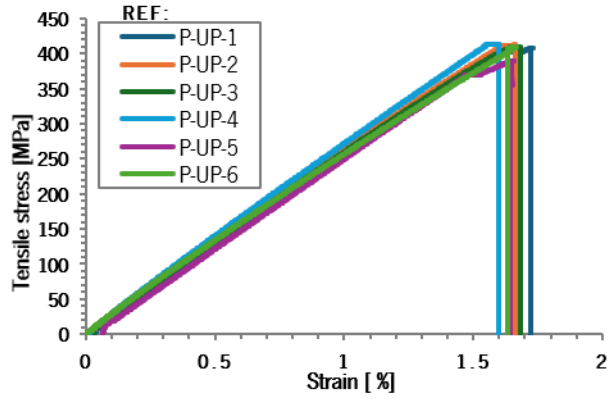
2. Specimen Dimensions

Specimen	H1	H2	H3	B1	B2	B3	L	M
1	7.9	7.9	8.0	25.5	25.5	25.6	300.0	111.9
2	7.9	7.9	7.9	25.6	25.7	25.7	300.0	109.5
3	8.0	8.0	8.0	25.5	25.4	25.5	300.0	111.3
4	7.9	7.9	7.9	25.6	25.6	25.6	300.0	111.9
5	8.1	7.9	7.9	25.5	25.6	25.6	300.0	111.1
6	8.0	7.9	8.0	25.4	25.6	25.5	300.0	111.2
Mean Value	**7.9**	**7.9**	**8.0**	**25.5**	**25.6**	**25.6**	**300.0**	**111.1**

3. Main Results

Specimen	E [GPa]	f_{tu} [MPa]	ε_{tu} [%]	Failure Mode
1	27.51	407.93	1.73	XGM
2	28.67	412.71	1.66	XGM
3	27.28	410.04	1.68	XGM
4	28.64	413.23	1.60	XGM
5	29.85	389.30	1.66	XGM
6	27.53	409.89	1.67	XGM
Mean Value (CoV)	**28.25(3.5%)**	**407.18(2.20%)**	**1.67(2.51%)**	

4. Graphs and Failure Modes



Stress–strain relationships



Failure mode

Note: M.V. = Mean Value; CoV = Coefficient of Variation; n.a. = Not available; B1–B3 = Specimen width (mm); H1–H3 = Specimen thickness (mm); L = Specimen length (mm); M = Specimen mass (g)

Appendix A.14 - Tensile Test 0° Results: P-VE-REF

1. Series Data

Designation	P-VE-REF
Resin type	Vinyl ester
Environment	Unconditioned reference specimens stored under laboratory conditions
Duration	N/A
Test type	Tensile test 0°
Test standard	EN ISO 527-4:1997
Test location	Structures Laboratory, University of Minho
Test date	20/04/2026
Observation	The GFRP specimens were tested in the unaged condition and served as the reference series for comparison with the conditioned specimens.

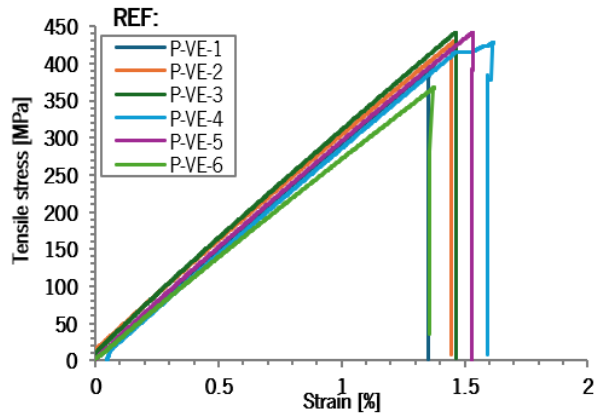
2. Specimen Dimensions

Specimen	H1	H2	H3	B1	B2	B3	L	M
1	7.9	7.9	8.0	25.5	25.5	25.6	300.0	112.3
2	7.9	7.9	7.9	25.6	25.7	25.7	300.0	112.3
3	8.0	8.0	8.0	25.5	25.4	25.5	300.0	113.7
4	7.9	7.9	7.9	25.6	25.6	25.6	300.0	113.4
5	8.1	7.9	7.9	25.5	25.6	25.6	300.0	109.1
6	8.0	7.9	8.0	25.4	25.6	25.5	300.0	112.9
Mean Value	**7.9**	**7.9**	**8.0**	**25.5**	**25.6**	**25.6**	**300.0**	**112.3**

3. Main Results

Specimen	E [GPa]	f_{tu} [MPa]	ε_{tu} [%]	Failure Mode
1	30.29	397.34	1.38	XGM
2	29.94	429.87	1.46	XGM
3	31.61	442.15	1.47	XGM
4	33.17	428.24	1.62	XGM
5	30.84	441.83	1.54	XGM
6	28.08	367.80	1.38	XGM
Mean Value (CoV)	**30.66(5.6%)**	**417.88(7.1%)**	**1.48(6.3%)**	

4. Graphs and Failure Modes



Stress–strain relationships



Failure mode

Note: M.V. = Mean Value; CoV = Coefficient of Variation; n.a. = Not available; B1–B3 = Specimen width (mm); H1–H3 = Specimen thickness (mm); L = Specimen length (mm); M = Specimen mass (g).

Appendix A.15 - Tensile Test 0° Results: P-UP-W60-24M-D

1. Series Data

Designation	P-UP-D
Resin type	Unsaturated polyester
Environment	Hygrothermal water immersion at 60°C, followed by drying under laboratory conditions
Duration	24 months
Test type	Tensile test 0°
Test standard	EN ISO 527-4:1997
Test location	Structures Laboratory, University of Minho
Test date	23/04/2026
Observation	The GFRP specimens were immersed in water at 60°C for 24 months, dried under laboratory conditions, and then tested

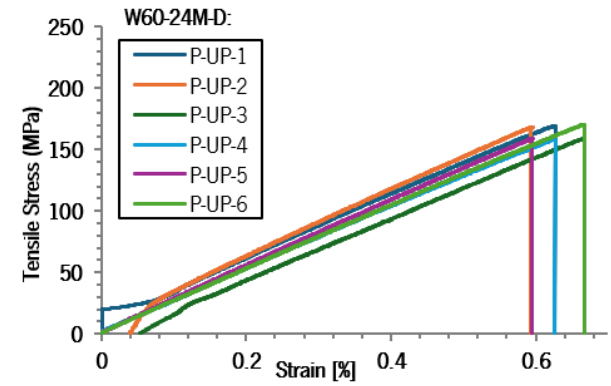
2. Specimen Dimensions

Specimen	H1	H2	H3	B1	B2	B3	L	M
1	7.8	7.8	7.8	25.3	25.2	25.4	300.0	106.7
2	7.9	7.9	7.8	25.3	25.1	25.2	300.0	108.0
3	7.8	7.8	7.9	25.3	25.2	25.4	300.0	107.2
4	7.9	7.9	7.9	25.2	25.3	25.3	300.0	106.9
5	7.9	7.9	7.8	25.2	25.2	25.3	300.0	107.7
6	7.9	7.9	7.9	25.3	25.2	25.4	300.0	107.6
Mean Value	**7.9**	**7.9**	**7.9**	**25.3**	**25.2**	**25.3**	**300.0**	**107.4**

3. Main Results

Specimen	E [GPa]	f_{tu} [MPa]	ε_{tu} [%]	Failure Mode
1	25.46	169.13	0.63	LAT
2	32.35	168.04	0.60	LAT
3	28.31	158.89	0.67	LAT
4	25.82	158.16	0.63	LAT
5	27.22	158.74	0.60	LAT
6	25.99	170.51	0.67	LAT
Mean Value (CoV)	**27.53(9.4%)**	**163.91(3.6%)**	**0.63(5.0%)**	

4. Graphs and Failure Modes



Stress–strain relationships



Failure mode

Note: M.V. = Mean Value; CoV = Coefficient of Variation; n.a. = Not available; B1–B3 = Specimen width (mm); H1–H3 = Specimen thickness (mm); L = Specimen length (mm); M = Specimen mass (g).

Appendix A.16 - Tensile Test 0° Results: P-VE-W60-24M-D

1. Series Data

Designation	P-VE-D
Resin type	Vinyl ester
Environment	Hygrothermal water immersion at 60°C, followed by drying under laboratory conditions
Duration	24 months
Test type	Tensile test 0°
Test standard	EN ISO 527-4:1997
Test location	Structures Laboratory, University of Minho
Test date	24/04/2026
Observation	The GFRP specimens were immersed in water at 60°C for 24 months, dried under laboratory conditions, and then tested

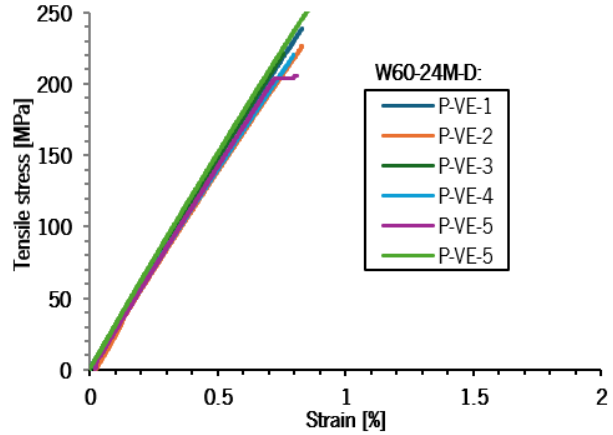
2. Specimen Dimensions

Specimen	H1	H2	H3	B1	B2	B3	L	M
1	8.1	8.0	8.0	25.4	25.2	25.3	300.0	111.9
2	8.3	8.5	8.1	25.5	25.2	25.3	300.0	112.2
3	8.1	8.1	8.0	25.3	25.3	25.2	300.0	112.6
4	8.0	8.0	8.0	25.4	25.2	25.3	300.0	109.6
5	8.3	8.3	8.2	25.2	25.2	25.3	300.0	113.5
6	8.2	8.1	8.1	25.2	25.2	25.1	300.0	113.1
Mean Value	**8.2**	**8.2**	**8.0**	**25.3**	**25.2**	**25.3**	**300.0**	**112.1**

3. Main Results

Specimen	E [GPa]	f_{tu} [MPa]	ε_{tu} [%]	Failure Mode
1	29.76	239.1	0.83	AGM 2
2	30.87	226.54	0.85	DGM
3	2995	221.50	0.76	LAT
4	28.31	220.18	0.80	LAT
5	29.22	208.46	0.83	DGM
6	30.8	205.83	0.86	LAT
Mean Value (CoV)	**29.80(3.3%)**	**220.27(5.54%)**	**0.81(4.09%)**	

4. Graphs and Failure Modes



Stress–strain relationships



Failure mode

Note: M.V. = Mean Value; CoV = Coefficient of Variation; n.a = Not available; B1–B3 = Specimen width (mm); H1–H3 = Specimen thickness (mm); L = Specimen length (mm); M = Specimen mass (g).

Appendix A.17 - Tensile Test 0° Results: P-VE-W60-24M-W

1. Series Data

Designation	P-VE-W
Resin type	Vinyl ester
Environment	Hygrothermal water immersion at 60°C
Duration	24 months
Test type	Tensile test 0°
Test standard	EN ISO 527-4:1997
Test location	Structures Laboratory, University of Minho
Test date	26/06/2026
Observation	The GFRP specimens were subjected to hygrothermal water immersion at 60°C for 24 months and tested immediately after conditioning

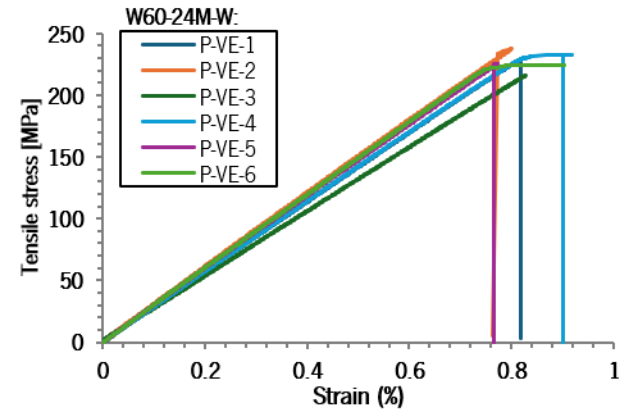
2. Specimen Dimensions

Specimen	H1	H2	H3	B1	B2	B3	L	M
1	8.1	8.0	8.1	20.4	20.2	20.2	300.0	113.3
2	8.1	8.1	8.1	20.3	20.2	20.3	300.0	114.0
3	8.0	8.0	8.0	20.4	20.2	20.2	300.0	110.5
4	8.1	8.1	8.1	20.4	20.2	20.3	300.0	114.0
5	8.1	8.1	8.1	20.1	20.1	20.3	300.0	114.5
6	8.1	8.1	8.1	20.4	20.2	20.2	300.0	114.7
Mean Value	**8.1**	**8.1**	**8.1**	**20.3**	**20.2**	**20.3**	**300.0**	**113.5**

3. Main Results

Specimen	E [GPa]	f_{tu} [MPa]	ε_{tu} [%]	Failure Mode
1	37.39	228.91	0.82	LGM
2	38.91	237.6	0.80	LGM
3	35.04	215.71	0.83	SGM
4	38.04	232.31	0.92	LGM
5	36.81	225.59	0.77	LGM
6	36.92	224.94	0.90	AGM 1
Mean Value (CoV)	**37.19(3.52%)**	**22.51(3.27%)**	**0.84(6.94%)**	

4. Graphs and Failure Modes



Stress–strain relationships



Failure mode

Note: M.V. = Mean Value; CoV = Coefficient of Variation; n.a = Not available; B1–B3 = Specimen width (mm); H1–H3 = Specimen thickness (mm); L = Specimen length (mm); M = Specimen mass (g).

Appendix A.18 - Tensile Test 90° Results: P-UP-REF

1. Series Data

Designation	P-UP-REF
Resin type	Unsaturated polyester
Environment	Unconditioned reference specimens stored under laboratory conditions
Duration	N/A
Test type	Tensile test 90°
Test standard	EN ISO 527-4:1997
Test location	Structures Laboratory, University of Minho
Test date	17/04/2026
Observation	The GFRP specimens were tested in the unaged condition and served as the reference series for comparison with the conditioned specimens.

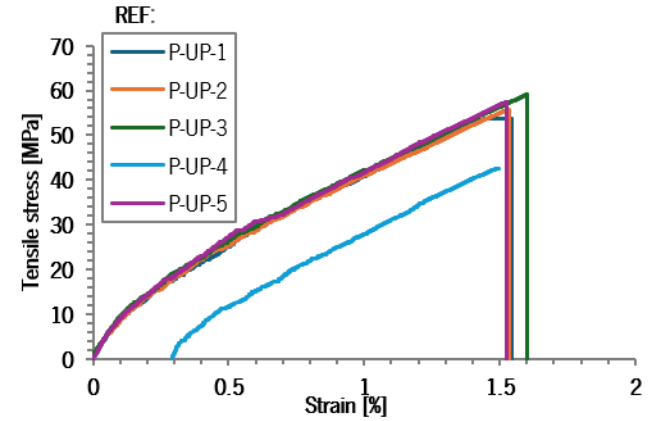
2. Specimen Dimensions

Specimen	H1	H2	H3	B1	B2	B3	L	M
1	8.0	7.9	8.0	25.6	25.7	25.7	249.0	91.9
2	7.9	7.9	8.0	25.6	25.6	25.6	249.5	91.7
3	8.0	8.0	7.9	25.5	25.5	25.5	249.5	92.0
4	8.0	8.0	7.9	25.7	25.6	25.6	249.0	92.0
5	8.0	7.9	8.0	25.6	25.5	25.5	249.5	92.0
Mean Value	**7.9**	**7.9**	**8.0**	**25.6**	**25.6**	**25.6**	**249.3**	**91.9**

3. Main Results

Specimen	E [GPa]	f_{tu} [MPa]	ε_{tu} [%]	Failure Mode
1	5.62	53.66	1.55	AGM (1)
2	5.18	55.81	1.54	LAT
3	5.71	59.08	1.60	AGM (2)
4	5.55	42.52	1.49	AGM (1)
5	5.71	57.39	1.53	AGM (1)
Mean Value (CoV)	**5.55(4.0%)**	**53.69(12.2%)**	**1.54(2.59%)**	

4. Graphs and Failure Modes



Stress–strain relationships



Failure mode

Note: M.V. = Mean Value; CoV = Coefficient of Variation; n.a = Not available; B1–B3 = Specimen width (mm); H1–H3 = Specimen thickness (mm); L = Specimen length (mm); M = Specimen mass (g).

Appendix A.19 - Tensile Test 90° Results P-VE-REF

1. Series Data

Designation	P-VE-REF
Resin type	Vinyl ester
Environment	Unconditioned reference specimens stored under laboratory conditions
Duration	N/A
Test type	Tensile test 90°
Test standard	EN ISO 527-4:1997
Test location	Structures Laboratory, University of Minho
Test date	17/04/2026
Observation	The GFRP specimens were tested in the unaged condition and served as the reference series for comparison with the conditioned specimens.

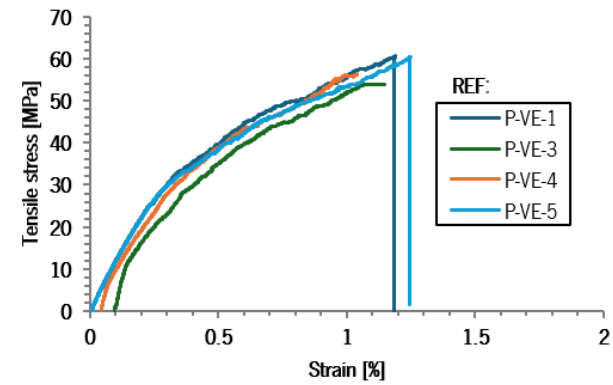
2. Specimen Dimensions

Specimen	H1	H2	H3	B1	B2	B3	L	M
1	8.0	7.9	8.0	25.6	25.7	25.7	249.0	92.2
2	7.9	7.9	8.0	25.6	25.6	25.6	249.5	92.8
3	8.0	8.0	7.9	25.5	25.5	25.5	249.5	92.5
4	8.0	8.0	7.9	25.7	25.6	25.6	249.0	92.2
5	8.0	7.9	8.0	25.6	25.5	25.5	249.5	92.4
Mean Value	**7.9**	**7.9**	**8.0**	**25.6**	**25.6**	**25.6**	**249.3**	**92.4**

3. Main Results

Specimen	E [GPa]	f_{tu} [MPa]	ε_{tu} [%]	Failure Mode
1	10.06	60.52	1.19	LGM
2	12.35	59.16	1.01	LGM
3	12.99	57.32	1.31	AGM (2)
4	10.86	58.44	1.20	AGM (1)
5	10.22	60.32	1.25	LGM
Mean Value (CoV)	**11.30(11.6%)**	**59.15(2.3%)**	**1.19(9.0%)**	

4. Graphs and Failure Modes



Stress–strain relationships



Failure mode

Note: M.V. = Mean Value; CoV = Coefficient of Variation; n.a = Not available; B1–B3 = Specimen width (mm); H1–H3 = Specimen thickness (mm); L = Specimen length (mm); M = Specimen mass (g).

Appendix A.20 - Tensile Test 90° Results P-UP-W60-24M-D

1. Series Data

Designation	P-UP-D
Resin type	Unsaturated polyester
Environment	Hygrothermal water immersion at 60°C, followed by drying under laboratory conditions
Duration	24 months
Test type	Tensile test 90°
Test standard	EN ISO 527-4:1997
Test location	Structures Laboratory, University of Minho
Test date	28/04/2026
Observation	The GFRP specimens were immersed in water at 60°C for 24 months, dried under laboratory conditions, and then tested

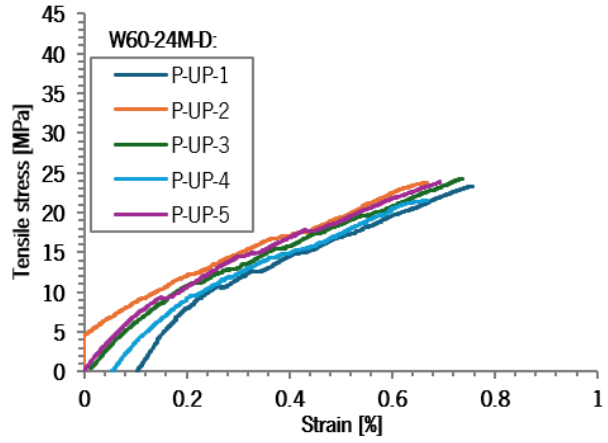
2. Specimen Dimensions

Specimen	H1	H2	H3	B1	B2	B3	L	M
1	7.9	7.9	7.9	25.3	25.4	25.6	248.0	88.3
2	7.9	7.9	7.9	25.4	25.3	25.3	248.0	88.3
3	7.9	7.9	7.9	25.5	25.4	25.4	248.0	88.3
4	7.9	7.9	7.9	25.4	25.3	25.4	248.0	88.3
5	8.0	7.9	7.9	25.4	25.5	25.5	248.0	88.3
6								
Mean Value	**7.9**	**7.9**	**7.9**	**25.4**	**25.4**	**25.4**	**248.0**	**88.3**

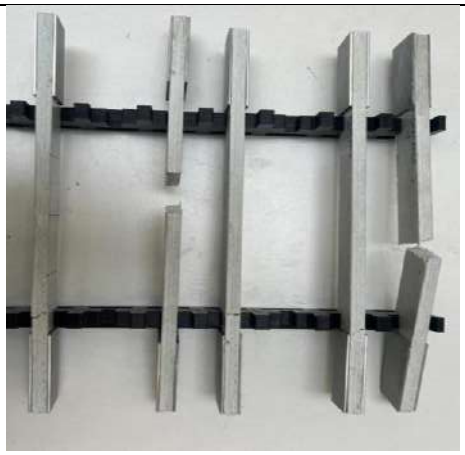
3. Main Results

Specimen	E [GPa]	f_{tu} [MPa]	ε_{tu} [%]	Failure Mode
1	5	23.34	0.76	AGM (1)
2	4.20	23.69	0.67	LAT
3	4.42	24.29	0.74	LGM
4	4.46	21.46	0.67	AGM (1)
5	4.34	23.84	0.69	LGM
Mean Value (CoV)	**4.48(6.8%)**	**23.33(4.7%)**	**0.70(5.72%)**	

4. Graphs and Failure Modes



Stress–strain relationships



Failure mode

Note: M.V. = Mean Value; CoV = Coefficient of Variation; n.a. = Not available; B1–B3 = Specimen width (mm); H1–H3 = Specimen thickness (mm); L = Specimen length (mm); M = Specimen mass (g).

Appendix A.21 - Tensile Test 90° Results P-VE-W60-24M-D

1. Series Data

Designation	P-VE-D
Resin type	Vinyl ester
Environment	Hygrothermal water immersion at 60°C, followed by drying under laboratory conditions
Duration	24 months
Test type	Tensile test 90°
Test standard	EN ISO 527-4:1997
Test location	Structures Laboratory, University of Minho
Test date	30/06/2026
Observation	The GFRP specimens were immersed in water at 60°C for 24 months, dried under laboratory conditions, and then tested

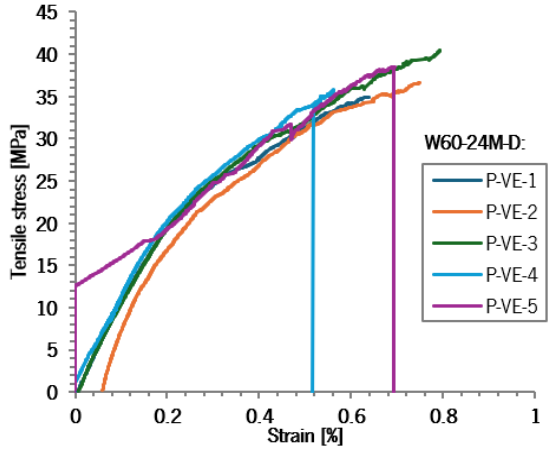
2. Specimen Dimensions

Specimen	H1	H2	H3	B1	B2	B3	L	M
1	8.1	8.1	8.0	25.1	25.2	25.1	249.0	91.8
2	8.1	8.1	8.0	24.2	25.3	25.1	249.0	91.7
3	8.1	8.1	8.1	25.1	25.2	25.2	249.0	91.7
4	8.3	8.1	8.5	25.1	25.1	25.1	249.0	91.9
5	8.0	8.1	8.1	25.1	25.1	25.1	249.0	92.3
6								
Mean Value	**8.1**	**8.1**	**8.2**	**24.9**	**25.1**	**25.1**	**249.0**	**91.9**

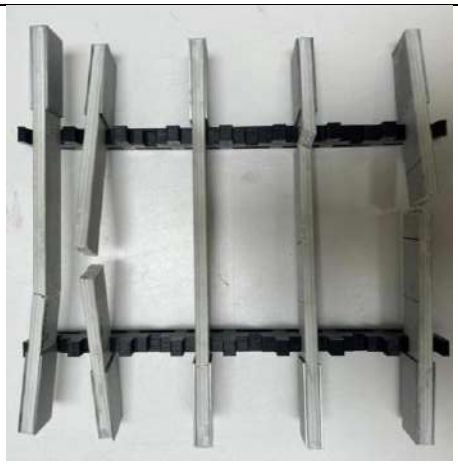
3. Main Results

Specimen	E [GPa]	f_{tu} [MPa]	ε_{tu} [%]	Failure Mode
1	8.49	34.91	0.64	LGM
2	10.47	37.26	0.87	LGM
3	8.68	40.41	0.79	LAT
4	8.46	35.81	0.56	LGM
5	8.84	39.03	0.69	AGM (1)
Mean Value (CoV)	**8.99(9.4%)**	**37.48(6.0%)**	**0.70(17.72%)**	

4. Graphs and Failure Modes



Stress–strain relationships



Failure mode

Note: M.V. = Mean Value; CoV = Coefficient of Variation; n.a. = Not available; B1–B3 = Specimen width (mm); H1–H3 = Specimen thickness (mm); L = Specimen length (mm); M = Specimen mass (g).

Appendix A.22 - Tensile Test 90° Results: P-VE-W60-24M-W

1. Series Data

Designation	P-VE-W
Resin type	Vinyl ester
Environment	Hygrothermal water immersion at 60°C
Duration	24 months
Test type	Tensile test 90°
Test standard	EN ISO 527-4:1997
Test location	Structures Laboratory, University of Minho
Test date	30/06/2026
Observation	The GFRP specimens were subjected to hygrothermal water immersion at 60°C for 24 months and tested immediately after conditioning

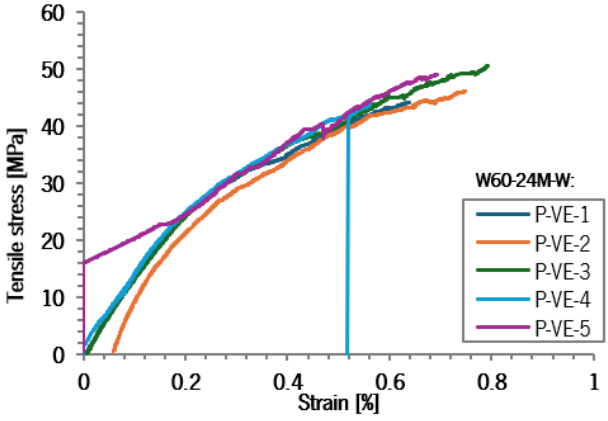
2. Specimen Dimensions

Specimen	H1	H2	H3	B1	B2	B3	L	M
1	8.1	8.1	8.0	20.1	20.2	20.1	249.0	91.8
2	8.1	8.1	8.0	20.2	20.3	20.1	249.0	91.7
3	8.1	8.1	8.1	20.1	20.2	20.2	249.0	91.7
4	8.3	8.1	8.5	20.1	20.1	20.1	249.0	91.9
5	8.0	8.1	8.1	20.1	20.1	20.1	249.0	92.3
6								
Mean Value	**8.1**	**8.1**	**8.2**	**20.1**	**20.1**	**20.1**	**249.0**	**91.9**

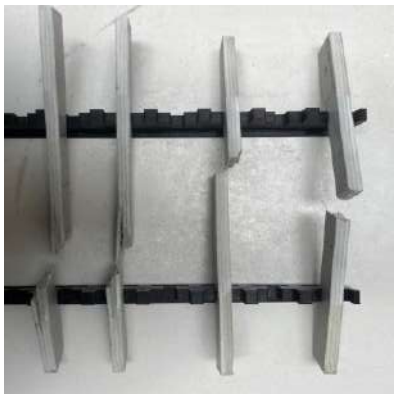
3. Main Results

Specimen	E [GPa]	f_{tu} [MPa]	ε_{tu} [%]	Failure Mode
1	10.70	43.97	0.64	AGM (1)
2	13.16	46.84	0.87	LGM
3	10.84	50.48	0.79	LGM
4	10.40	44.00	0.56	LGM
5	4.82	48.94	0.69	LGM
Mean Value (CoV)	**8.99(9.4%)**	**37.48(6.0%)**	**0.70(17.72%)**	

4. Graphs and Failure Modes



Stress–strain relationships



Failure mode

Note: M.V. = Mean Value; CoV = Coefficient of Variation; n.a. = Not available; B1–B3 = Specimen width (mm); H1–H3 = Specimen thickness (mm); L = Specimen length (mm); M = Specimen mass (g).

Appendix A.23 - In-plane shear test Results: P-UP-REF

1. Series Data

Designation	P-UP-REF
Resin type	Unsaturated polyester
Environment	Unconditioned reference specimens stored under laboratory conditions
Duration	N/A
Test type	In-plane shear test
Test standard	ASTM D5379/D5379M:2012
Test location	Structures Laboratory, University of Minho
Test date	24/04/2026
Observation	The GFRP specimens were tested in the unaged condition and served as the reference series for comparison with the conditioned specimens.

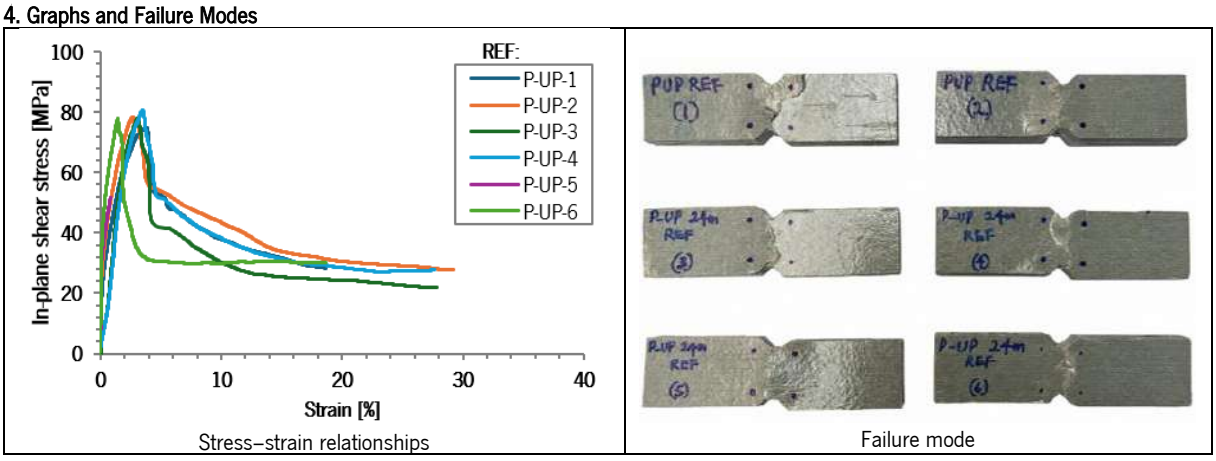
2. Specimen Dimensions

Specimen	H	B	L	M
1	7.9	13.6	76.0	22.0
2	7.9	13.5	75.5	22.1
3	7.9	13.4	76.0	21.9
4	7.9	13.5	76.0	21.9
5	7.8	13.7	75.5	22.0
6	7.9	13.5	75.5	21.8
Mean Value	**7.9**	**13.5**	**75.8**	**21.9**

3. Main Results

Specimen	G [GPa]	τ_{max} [MPa]	$\gamma_{\tau,max}$ [%]	Failure Mode
1	3.52	74.79	3.83	M(hv)GN
2	3.80	78.14	2.68	VGN
3	2.01	77.92	3.10	VGN
4	2.03	80.49	3.49	M(hv)GN
5	3.09	76.71	2.55	VGN
Mean Value (CoV)	**2.89(28.8%)**	**77.61(2.7%)**	**3.13(17.2%)**	

4. Graphs and Failure Modes



Stress–strain relationships

Failure mode

Note: M.V. = Mean Value; CoV = Coefficient of Variation; n.a. = Not available; B1–B3 = Specimen width (mm); H1–H3 = Specimen thickness (mm); L = Specimen length (mm); M = Specimen mass (g).

Appendix A.24 - In-plane shear test Results: P-VE-REF

1. Series Data

Designation	P-VE-REF
Resin type	Vinyl ester
Environment	Unconditioned reference specimens stored under laboratory conditions
Duration	N/A
Test type	In-plane shear test
Test standard	ASTM D5379/D5379M:2012
Test location	Structures Laboratory, University of Minho
Test date	29/04/2026
Observation	The GFRP specimens were tested in the unaged condition and served as the reference series for comparison with the conditioned specimens.

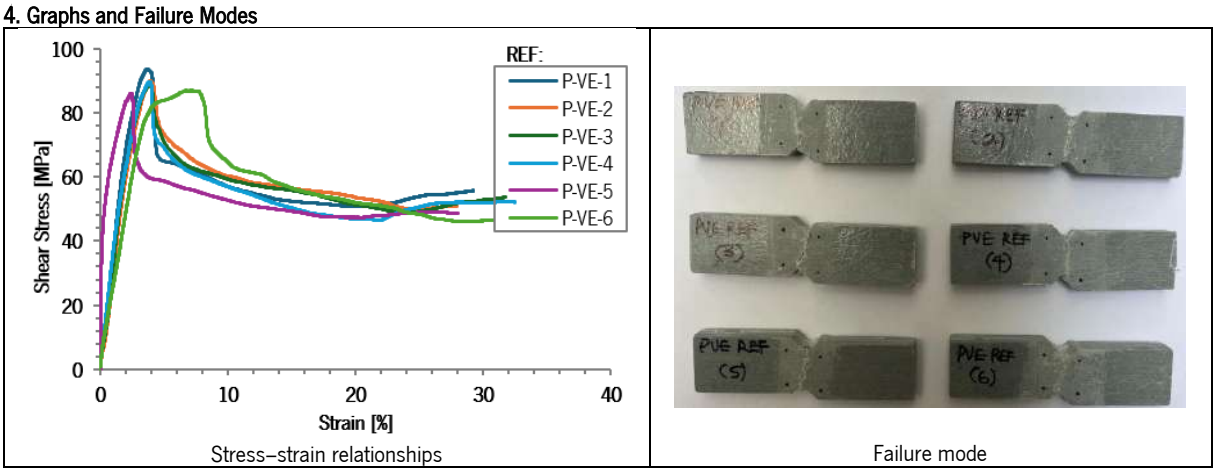
2. Specimen Dimensions

Specimen	H	B	L	M
1	7.9	13.6	76.0	22.3
2	7.9	13.5	75.5	21.7
3	7.9	13.4	76.0	22.1
4	7.9	13.5	76.0	22.6
5	7.8	13.7	75.5	21.7
6	7.9	13.5	75.5	22.2
Mean Value	**7.9**	**13.5**	**75.8**	**22.1**

3. Main Results

Specimen	G [GPa]	τ_{max} [MPa]	$\gamma_{\tau,max}$ [%]	Failure Mode
1	2.58	93.73	3.64	VGN
2	2.10	89.92	3.92	VGN
3	2.30	88.60	3.89	VGN
4	3.46	89.68	3.84	VGN
5	4.49	86.05	2.41	VGN
6	2.44	86.16	6.73	VGN
Mean Value (CoV)	**2.90(31.5%)**	**89.16(3.1%)**	**4.07(34.94%)**	

4. Graphs and Failure Modes



Stress–strain relationships | Failure mode

Note: M.V. = Mean Value; CoV = Coefficient of Variation; n.a. = Not available; B1–B3 = Specimen width (mm); H1–H3 = Specimen thickness (mm); L = Specimen length (mm); M = Specimen mass (g).

Appendix A.25 - In-plane shear test Results: P-UP-W60-24M-D

1. Series Data

Designation	P-UP-D
Resin type	Unsaturated polyester
Environment	Hygrothermal water immersion at 60°C, followed by drying under laboratory conditions
Duration	24 months
Test type	In-plane shear test
Test standard	ASTM D5379/D5379M:2012
Test location	Structures Laboratory, University of Minho
Test date	29/09/2026
Observation	The GFRP specimens were immersed in water at 60°C for 24 months, dried under laboratory conditions, and then tested

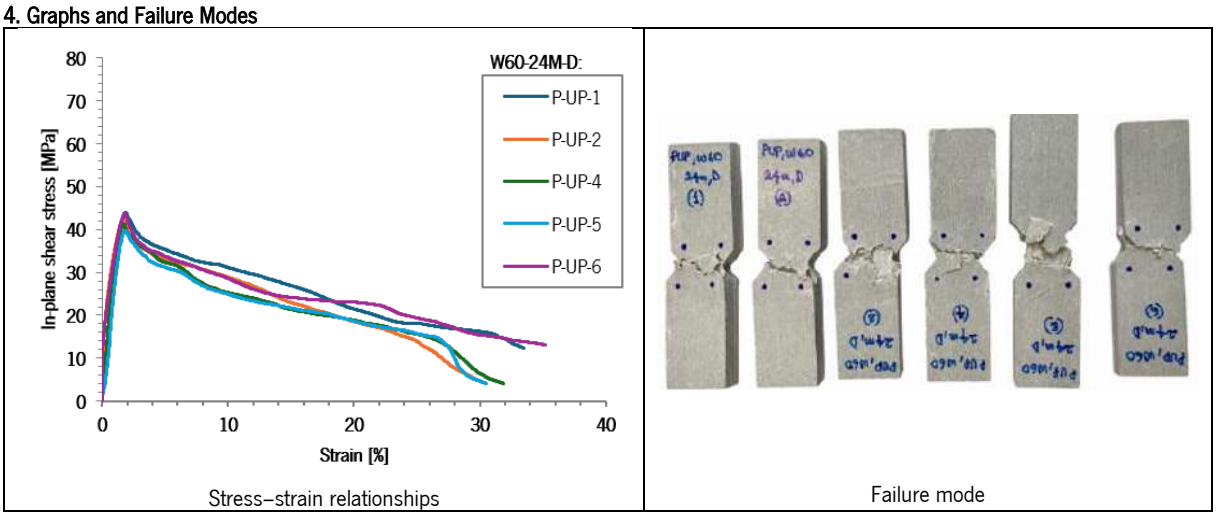
2. Specimen Dimensions

Specimen	H	B	L	M
1	7.8	13.2	76.0	21.3
2	7.9	13.0	75.5	21.3
3	7.8	13.4	76.0	21.3
4	7.9	13.2	76.0	21.3
5	7.8	13.3	75.5	21.4
6	7.8	13.2	75.5	21.2
Mean Value	**7.8**	**13.2**	**75.8**	**21.3**

3. Main Results

Specimen	G [GPa]	τ_{max} [MPa]	$\gamma_{\tau,max}$ [%]	Failure Mode
1	2.8	43.91	1.93	M(hv)GN
2	3.03	41.92	1.72	VGN
3	n. a	n. a	n. a	M(hv)GN
4	3.21	41.32	1.59	M(hv)GN
5	2.23	39.67	1.82	M(hv)GN
6	2.45	43.65	1.77	VGN
Mean Value (CoV)	**2.74(14.7%)**	**42.09(4.15%)**	**1.77(7.06%)**	

4. Graphs and Failure Modes



Stress–strain relationships

Failure mode

Note: M.V. = Mean Value; CoV = Coefficient of Variation; n.a. = Not available; B1–B3 = Specimen width (mm); H1–H3 = Specimen thickness (mm); L = Specimen length (mm); M = Specimen mass (g).

Appendix A.26 - In-plane shear test Results: P-VE-W60-24M-D

1. Series Data

Designation	P-VE-D
Resin type	Vinyl ester
Environment	Hygrothermal water immersion at 60°C, followed by drying under laboratory conditions
Duration	24 months
Test type	In-plane shear test
Test standard	ASTM D5379/D5379M:2012
Test location	Structures Laboratory, University of Minho
Test date	30/06/2026
Observation	The GFRP specimens were immersed in water at 60°C for 24 months, dried under laboratory conditions, and then tested

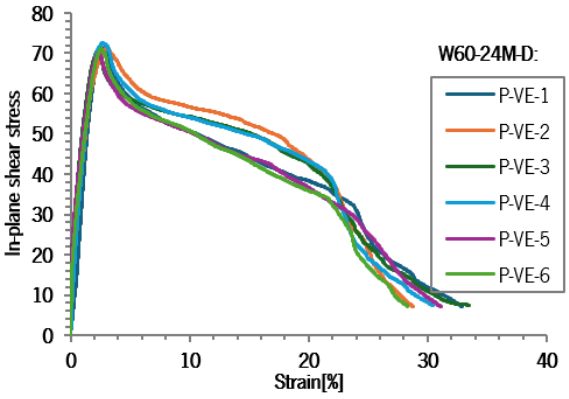
2. Specimen Dimensions

Specimen	H	B	L	M
1	8.0	13.0	75.5	22.3
2	7.9	12.9	75.5	21.5
3	8.0	13.0	76.0	22.2
4	8.0	12.9	75.9	22.0
5	8.0	13.3	75.5	21.8
6	8.0	13.1	75.5	21.8
Mean Value	**8.0**	**13.0**	**75.7**	**21.9**

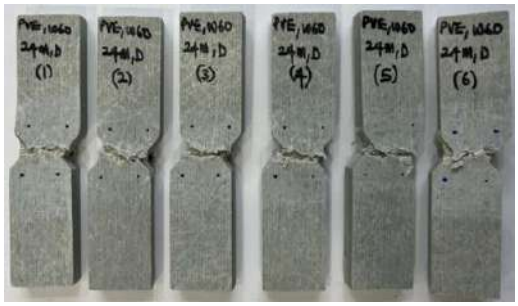
3. Main Results

Specimen	G [GPa]	τ_{max} [MPa]	$\gamma_{\tau,max}$ [%]	Failure Mode
1	2.92	71.50	2.86	VGN
2	4.37	71.26	3.03	VGN
3	3.74	70.56	2.20	VGN
4	4.51	72.65	2.74	VGN
5	3.65	70.01	2.30	VGN
6	3.58	**71.08**	2.51	VGN
Mean Value (CoV)	**3.8(15.3%)**	**71.18(1.3%)**	**2.62(11.9%)**	

4. Graphs and Failure Modes



Stress–strain relationships



Failure mode

Note: M.V. = Mean Value; CoV = Coefficient of Variation; n.a. = Not available; B1–B3 = Specimen width (mm); H1–H3 = Specimen thickness (mm); L = Specimen length (mm); M = Specimen mass (g).

Appendix A.27 - In-plane shear test Results: P-UP-W60-24M-W

1. Series Data

Designation	P-UP-W
Resin type	Unsaturated polyester
Environment	Hygrothermal water immersion at 60°C
Duration	24 months
Test type	In-plane shear test
Test standard	ASTM D5379/D5379M:2012
Test location	Structures Laboratory, University of Minho
Test date	30/04/2026
Observation	The GFRP specimens were subjected to hygrothermal water immersion at 60°C for 24 months and tested immediately after conditioning

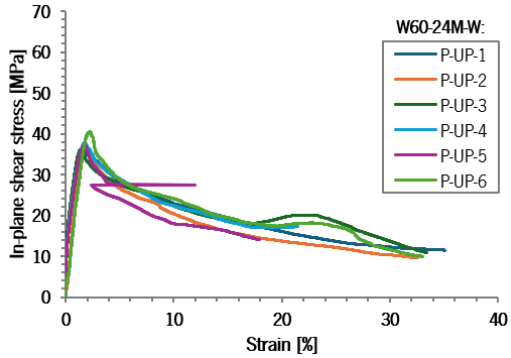
2. Specimen Dimensions

Specimen	H	B	L	M
1	7.9	13.1	75.5	21.9
2	7.8	13.0	75.5	21.4
3	7.9	13.3	76.0	22.1
4	7.9	13.1	75.9	21.5
5	8.0	13.0	75.5	21.6
6	7.9	13.2	75.9	22.0
Mean Value	**7.9**	**13.1**	**75.7**	**21.8**

3. Main Results

Specimen	G [GPa]	τ_{max} [MPa]	$\gamma_{\tau,max}$ [%]	Failure Mode
1	2.58	36.17	1.46	VGN
2	2.90	37.60	1.84	M(hv)GN
3	2.36	36.42	1.54	VGN
4	2.38	37.73	1.72	VGN
5	2.17	37.11	1.74	VGN
6	2.14	40.41	2.24	VGN
Mean Value (CoV)	**2.42(11.7%)**	**37.58(4.0%)**	**1.76(15.7%)**	

4. Graphs and Failure Modes



Stress–strain relationships



Failure mode

Note: M.V. = Mean Value; CoV = Coefficient of Variation; n.a. = Not available; B1–B3 = Specimen width (mm); H1–H3 = Specimen thickness (mm); L = Specimen length (mm); M = Specimen mass (g).

Appendix A.28 - In-plane shear test Results: P-VE-W60-24M-W

1. Series Data

Designation	P-VE-W
Resin type	Vinyl ester
Environment	Hygrothermal water immersion at 60°C
Duration	24 months
Test type	In-plane shear test
Test standard	ASTM D5379/D5379M:2012
Test location	Structures Laboratory, University of Minho
Test date	30/06/2026
Observation	The GFRP specimens were subjected to hygrothermal water immersion at 60°C for 24 months and tested immediately after conditioning

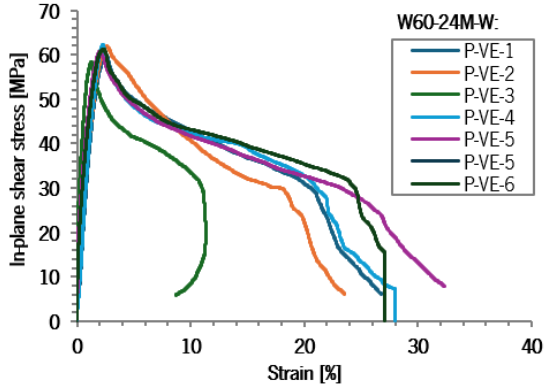
2. Specimen Dimensions

Specimen	H	B	L	M
1	7.9	13.3	75.5	22.0
2	7.9	12.9	75.5	22.0
3	8.0	13.2	76.0	22.6
4	7.9	13.1	75.9	22.1
5	8.1	12.9	75.5	22.8
6	8.0	13.0	75.9	22.4
Mean Value	**8.0**	**13.1**	**75.7**	**22.3**

3. Main Results

Specimen	G [GPa]	τ_{max} [MPa]	$\gamma_{\tau,max}$ [%]	Failure Mode
1	3.75	59.60	2.45	VGN
2	4.14	61.91	2.65	VGN
3	4.48	58.40	1.27	M(hv)GN
4	3.96	62.28	2.28	VGN
5	3.50	60.75	1.98	VGN
6	3.86	61.26	2.28	VGN
Mean Value (CoV)	**3.95(8.53%)**	**60.70(2.42%)**	**1.76(15.7%)**	

4. Graphs and Failure Modes



Stress–strain relationships



Failure mode

Note: M.V. = Mean Value; CoV = Coefficient of Variation; n.a. = Not available; B1–B3 = Specimen width (mm); H1–H3 = Specimen thickness (mm); L = Specimen length (mm); M = Specimen mass (g).

Appendix A.29 - Compression test Results: P-UP-REF

1. Series Data

Designation	P-UP-REF
Resin type	Unsaturated polyester
Environment	Unconditioned reference specimens stored under laboratory conditions
Duration	N/A
Test type	Compression test
Test standard	ISO 14126:1999
Test location	Structures Laboratory, University of Minho
Test date	15/06/2026
Observation	The GFRP specimens were tested in the unaged condition and served as the reference series for comparison with the conditioned specimens.

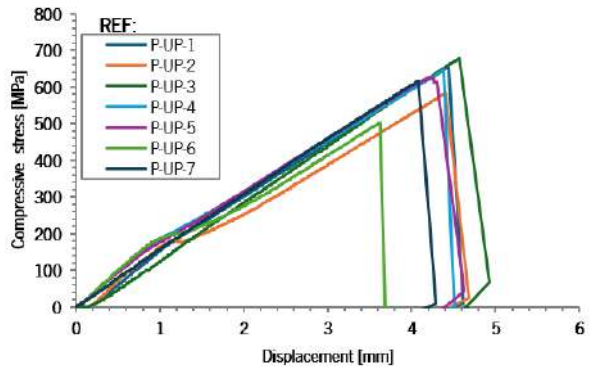
2. Specimen Dimensions

Specimen	H1	H2	B1	B2	L	M
1	8.0	8.0	25.2	25.1	152.5	56.68
2	8.0	8.0	25.2	25.2	153.0	56.4
3	8.0	8.0	25.2	25.2	152.5	56.4
4	7.9	7.9	25.1	25.2	152.5	56.3
5	8.0	8.0	25.1	25.1	152.5	56.1
6	7.9	7.9	25.2	25.3	153.0	56.1
7	8.0	7.9	25.2	25.1	152.5	56.2
Mean Value	**7.9**	**7.9**	**25.2**	**25.2**	**152.6**	**56.3**

3. Main Results

Specimen	F_{max} [kN]	σ_{max} [MPa]	$\delta_{f,max}$[mm]	Failure Mode
1	131.94	654.64	4.44	Complex Fracture
2	117.73	583.06	4.41	Complex Fracture
3	137.08	677.27	4.57	Complex Fracture
4	130.29	645.70	4.39	Complex Fracture
5	127.65	626.73	4.25	Complex Fracture
6	101.89	502.75	3.65	Complex Fracture
7	124.11	615.91	4.08	Complex Fracture
Mean Value (CoV)	**124.38(9.37%)**	**615.15(9.4%)**	**4.25(7.49%)**	

4. Graphs and Failure Modes



Stress–strain relationships



Failure mode

Note: M.V. = Mean Value; CoV = Coefficient of Variation; n.a. = Not available; B1–B3 = Specimen width (mm); H1–H3 = Specimen thickness (mm); L = Specimen length (mm); M = Specimen mass (g).

Appendix A.30 - Compression test Results: P-VE-REF

1. Series Data

Designation	P-VE-REF
Resin type	Vinyl ester
Environment	Unconditioned reference specimens stored under laboratory conditions
Duration	N/A
Test type	Compression test
Test standard	ISO 14126:1999
Test location	Structures Laboratory, University of Minho
Test date	16/06/2026
Observation	The GFRP specimens were tested in the unaged condition and served as the reference series for comparison with the conditioned specimens.

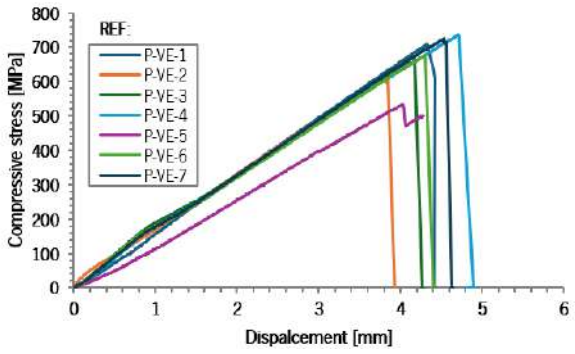
2. Specimen Dimensions

Specimen	H1	H2	B1	B2	L	M
1	7.9	7.9	25.2	25.1	152.5	56.68
2	8.0	7.9	25.2	25.2	153.0	56.4
3	8.0	7.9	25.2	25.2	152.5	56.4
4	7.9	7.9	25.1	25.2	152.5	56.3
5	7.9	8.0	25.1	25.1	152.5	56.1
6	8.0	8.0	25.2	25.3	153.0	56.1
7	7.9	7.9	25.2	25.1	152.5	56.2
Mean Value	**7.9**	**7.9**	**25.2**	**25.2**	**152.6**	**56.3**

3. Main Results

Specimen	F_{max} [kN]	σ_{max} [MPa]	$\delta_{f,max}$[mm]	Failure Mode
1	142.95	709.24	4.33	Complex Fracture
2	122.69	607.63	3.80	Complex Fracture
3	136.00	671.95	4.18	Complex Fracture
4	148.56	736.26	4.70	Complex Fracture
5	108.62	533.29	4.03	Complex Fracture
6	137.14	676.68	4.30	Complex Fracture
7	146.07	724.88	4.54	Complex Fracture
Mean Value (CoV)	**134.57(9.8%)**	**665.70(10.0%)**	**4.27(6.6%)**	

4. Graphs and Failure Modes



Stress–strain relationships



Failure mode

Note: M.V. = Mean Value; CoV = Coefficient of Variation; n.a. = Not available; B1–B3 = Specimen width (mm); H1–H3 = Specimen thickness (mm); L = Specimen length (mm); M = Specimen mass (g)

Appendix A.31 - Compression test Results: P-UP-W60-24M-D

1. Series Data

Designation	P-UP-D
Resin type	Unsaturated polyester
Environment	Hygrothermal water immersion at 60°C, followed by drying under laboratory conditions
Duration	24 months
Test type	Compression test
Test standard	ISO 14126:1999
Test location	Structures Laboratory, University of Minho
Test date	25/05/2026
Observation	The GFRP specimens were immersed in water at 60°C for 24 months, dried under laboratory conditions, and then tested

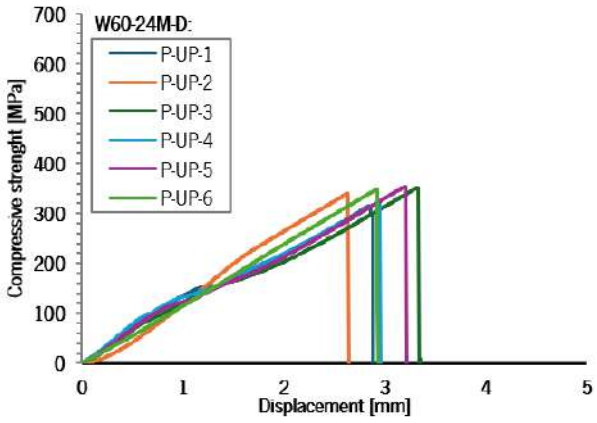
2. Specimen Dimensions

Specimen	H1	H2		B1	B1		L	M
1	7.8	7.9		25.2	25.2		152.5	54.91
2	7.9	7.9		25.2	25.2		152.5	55.0
3	7.9	7.9		25.1	25.2		152.9	54.6
4	7.8	7.8		25.1	25.1		153.0	55.0
5	7.9	7.9		25.2	25.2		152.5	55.4
6	7.9	7.9		25.1	25.2		153.0	54.0
7	7.9	7.8		25.2	25.2		153.0	54.7
Mean Value	**7.9**	**7.9**		**25.2**	**25.2**		**152.8**	**54.8**

3. Main Results

Specimen	F_{max} [kN]	σ_{max} [MPa]	$\delta_{f,max}$[mm]	Failure Mode
1	62.41	316.21	2.86	Complex Fracture
2	67.77	340.63	2.64	Complex Fracture
3	69.85	352.52	3.33	Complex Fracture
4	63.67	324.21	2.95	Complex Fracture
5	69.89	352.86	3.2	Complex Fracture
6	68.95	348.84	2.93	Complex Fracture
Mean Value (CoV)	**67.09(4.9%)**	**339.21(4.6%)**	**2.98(8.3%)**	

4. Graphs and Failure Modes



Stress–strain relationships



Failure mode

Note: M.V. = Mean Value; CoV = Coefficient of Variation; n.a. = Not available; B1–B3 = Specimen width (mm); H1–H3 = Specimen thickness (mm); L = Specimen length (mm); M = Specimen mass (g).

Appendix A.32 - Compression test Results P-VE-W60-24M-D

1. Series Data

Designation	P-VE-D
Resin type	Vinyl ester
Environment	Hygrothermal water immersion at 60°C, followed by drying under laboratory conditions
Duration	24 months
Test type	Compression test
Test standard	ISO 14126:1999
Test location	Structures Laboratory, University of Minho
Test date	17/06/2026
Observation	The GFRP specimens were immersed in water at 60°C for 24 months, dried under laboratory conditions, and then tested

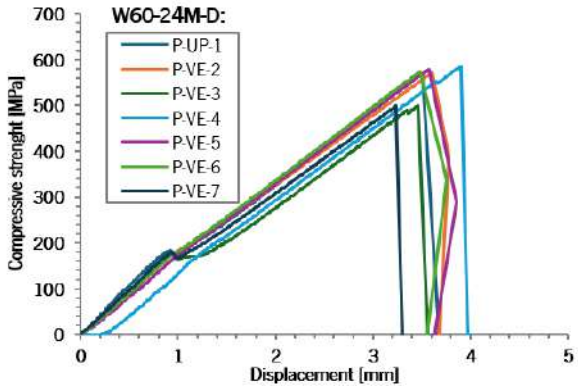
2. Specimen Dimensions

Specimen	H1	H2		B1	B2		L	M
1	8.0	8.0		25.2	25.1		152.5	57.59
2	8.0	8.0		25.1	25.1		153.0	56.5
3	8.0	8.0		25.2	25.1		153.0	56.9
4	8.0	8.0		25.1	25.1		153.0	57.1
5	8.0	8.0		25.1	25.1		153.0	57.3
6	8.0	8.0		25.1	25.2		153.0	57.8
7	7.9	8.0		25.1	25.1		152.5	56.3
Mean Value	**8.0**	**8.0**		**25.1**	**25.1**		**152.9**	**57.1**

3. Main Results

Specimen	F_{max} [kN]	σ_{max} [MPa]	$\delta_{f,max}$[mm]	Failure Mode
1	112.52	570.07	3.51	Complex Fracture
2	113.9	572.48	3.61	Complex Fracture
3	99.01	499.69	3.46	Complex Fracture
4	114.77	584.41	3.9	Complex Fracture
5	114.68	578.97	3.57	Complex Fracture
6	113.4	573.66	3.48	Complex Fracture
7	98.68	498.79	3.23	Complex Fracture
Mean Value (CoV)	**109.56(6.7%)**	**554.01(6.8%)**	**3.54(5.7%)**	

4. Graphs and Failure Modes



Stress–strain relationships



Failure mode

Note: M.V. = Mean Value; CoV = Coefficient of Variation; n.a. = Not available; B1–B3 = Specimen width (mm); H1–H3 = Specimen thickness (mm); L = Specimen length (mm); M = Specimen mass (g).

Appendix A.33 - Compression test Results: P-UP-W60-24M-W

1. Series Data

Designation	P-UP-W
Resin type	Unsaturated polyester
Environment	Hygrothermal water immersion at 60°C
Duration	24 months
Test type	Compression test
Test standard	ISO 14126:1999
Test location	Structures Laboratory, University of Minho
Test date	13/04/2026
Observation	The GFRP specimens were subjected to hygrothermal water immersion at 60°C for 24 months and tested immediately after conditioning

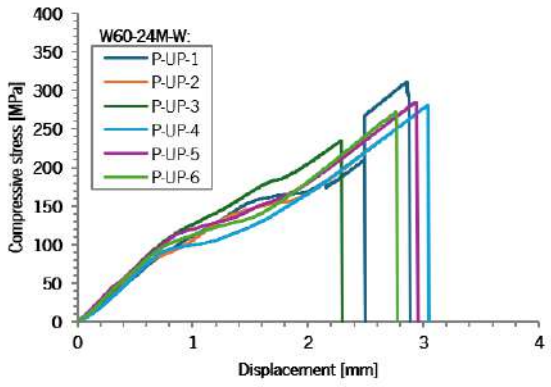
2. Specimen Dimensions

Specimen	H1	H1		B1	B1		L	M
1	8.0	8.0		25.2	25.1		152.5	56.68
2	8.0	8.0		25.2	25.2		153.0	56.4
3	8.0	8.0		25.2	25.2		152.5	56.4
4	7.9	7.9		25.1	25.2		152.5	56.3
5	8.0	8.0		25.1	25.1		152.5	56.1
6	7.9	7.9		25.2	25.3		153.0	56.1
7	8.0	7.9		25.2	25.1		152.5	56.2
Mean Value	**7.9**	**7.9**		**25.2**	**25.2**		**152.6**	**56.3**

3. Main Results

Specimen	F_{max} [kN]	σ_{max} [MPa]	$\delta_{f,max}$[mm]	Failure Mode
1	62.41	311.11	2.86	Complex Fracture
2	67.41	236.31	3.49	Complex Fracture
3	47.2	235.39	2.29	Complex Fracture
4	56.06	280.98	3.04	Complex Fracture
5	56.95	284.97	2.93	Complex Fracture
6	54.03	271.81	2.76	Complex Fracture
Mean Value (CoV)	**57.3(12.2%)**	**270.09(10.9%)**	**2.9(13.5%)**	

4. Graphs and Failure Modes



Stress–strain relationships



Failure mode

Note: M.V. = Mean Value; CoV = Coefficient of Variation; n.a. = Not available; B1–B3 = Specimen width (mm); H1–H3 = Specimen thickness (mm); L = Specimen length (mm); M = Specimen mass (g).

Appendix A.34 - Compression test Results P-VE-W60-24M-W

1. Series Data

Designation	P-VE-W
Resin type	Vinyl ester
Environment	Hygrothermal water immersion at 60°C
Duration	24 months
Test type	Compression test
Test standard	ISO 14126:1999
Test location	Structures Laboratory, University of Minho
Test date	27/05/2026
Observation	The GFRP specimens were subjected to hygrothermal water immersion at 60°C for 24 months and tested immediately after conditioning

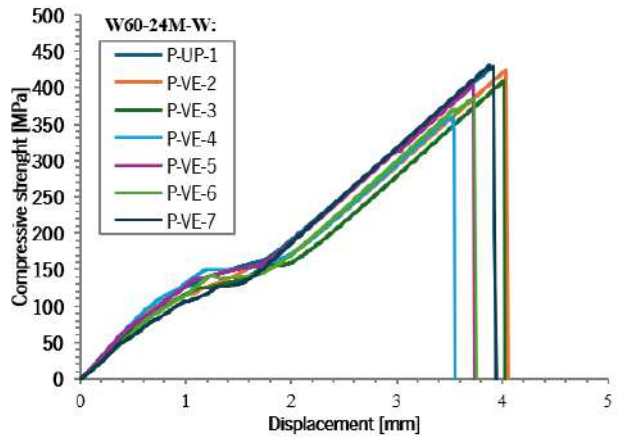
2. Specimen Dimensions

Specimen	H1	H2		B1	B2		L	M
1	8.1	8.0		25.1	25.1		152.5	57.21
2	8.1	8.1		25.1	25.0		153.0	57.8
3	8.0	8.0		25.1	25.1		152.5	57.4
4	8.0	8.0		25.1	25.0		152.5	58.1
5	8.1	8.1		25.1	25.0		152.5	58.6
6	8.1	8.1		25.0	25.0		153.0	58.1
7	8.1	8.1		25.1	2.0		152.5	58.2
Mean Value	**8.1**	**8.0**		**25.1**	**21.8**		**152.6**	**57.9**

3. Main Results

Specimen	F_{max} [kN]	σ_{max} [MPa]	$\delta_{f,max}$[mm]	Failure Mode
1	86.79	429.71	3.92	Complex Fracture
2	85.76	424.75	4.04	Complex Fracture
3	81.74	409.07	4.01	Complex Fracture
4	72.43	359.77	3.53	Complex Fracture
5	81.55	402.41	3.72	Complex Fracture
6	78.04	386.36	3.73	Complex Fracture
7	87.04	430.12	3.87	Complex Fracture
Mean Value (CoV)	**81.91(6.5%)**	**406.03(6.4%)**	**3.83(4.8%)**	

4. Graphs and Failure Modes



Stress–strain relationships



Failure mode

Note: M.V. = Mean Value; CoV = Coefficient of Variation; n.a. = Not available; B1–B3 = Specimen width (mm); H1–H3 = Specimen thickness (mm); L = Specimen length (mm); M = Specimen mass (g).